July 2017

On Axon-Axon Interaction via Currents and Fields

Aman Chawla
University of South Florida, aman.chawla@gmail.com

On Axon-Axon Interaction via Currents and Fields

by

Aman Chawla

A dissertation submitted in partial fulfillment
of the requirements for the degree of
Doctor of Philosophy
Department of Electrical Engineering
College of Engineering
University of South Florida

Major Professor: Salvatore D. Morgera, Ph.D.
Wilfrido Moreno, Ph.D.
Ghanim Ullah, Ph.D.
Mark Jaroszeski, Ph.D.
Arthur D. Snider, Ph.D.

Date of Approval:
June 20, 2017

Keywords:
synchronization, coupling, ephaptic, neurons, bioelectricity

DEDICATION

This dissertation is dedicated to Learning.

ACKNOWLEDGEMENT

This dissertation would not have been possible without the commitment of my major professor, Prof. Salvatore D. Morgera and my coadvisor Prof. Arthur D. Snider. Their constant motivating interest in the research work as well as their expertise, have enabled this work. They and my committee members have been friends in this multi-year journey through the ups and downs of a research program. Their vision, their insight, their guidance, patience and timely inputs have shaped this dissertation into the one that you hold in your hands. Prof. Christopher Passaglia, who is a reader for this dissertation, has, in particular, taken a keen interest in this dissertation and its conclusions. I would also like to take this opportunity to thank the wonderful staff at both the College of Engineering as well as the Department of Electrical Engineering - Ms. Catherine Burton, Ms. Cherie Dilley, Ms. Jessica Procko as well as Ms. Irene Spunde. Their timely help for all the necessary administrative tasks has enabled my smooth sailing through this PhD program.

TABLE OF CONTENTS

LIST OF TABLES

LIST OF FIGURES

ABSTRACT

In this dissertation, we investigate coupling between axons in a tract, when the tract has an arbitrary cross-section, with the coupling being mediated by currents as well as electric fields. Under the current mediated setting, we develop a new master equation which captures the relative axonal geometry, specifically, the axon inclinations θ_i and the inter-axon distances W_{ip} and perform a number of simulations. We observe synchronization in our simulations of axons with differing diameters and separation-dependent coupling delays in the case of non-trivial tract geometries. For the field-mediated interaction setting, we determine the electric near-field of a firing axon's node of Ranvier - its strength and direction - by a volume conduction approach as well as a more microscopic, dipole-based approach. We obtain field strengths of about $10^5 V/m$ at a few hundred micron distance from the source at the node. With the field levels having been found significant enough to cause 100 mV voltage drops across 1 micron-diameter axons, we develop an alternate, field-mediated model for synchronization between axons based on the dipole fields generated during action potential propagation. This model shows that synchronization between action potentials on differing axons depends on the phases of the synchronizing action potentials and not merely their separation. Since synchronization takes place in both settings, but currents are generated by fields, when constrained to a specific direction, we find that the field picture is a generalization of the presently prevalent current mediated picture for interaction between axons.

PROLOGUE

> "He becomes the one ocean, he becomes the sole seer! This, Your Majesty, is the world of brahman." So did Yajnavalkya instruct him. "This is his highest goal! This is his highest attainment! This is his highest world! This is his highest bliss! On just a fraction of this bliss do other creatures live."[1][1]

The human nervous system is one of the most complicated functioning systems in the known universe. Man has attempted to understand the *stars*, the very structure of spacetime and the nature of matter itself. This has been and is being accomplished with the help of this most unassuming biological system. All of human progress is traceable to the human brain. We won't take sides in the debate on the relationship between mind and brain, but it is easy to see that the stars of the astrophysicist must be projected in his or her mind for him or her to study them.

In this dissertation we seek to understand a fraction of a part of the nervous system - the axon tract. We try to understand its mathematical and biophysical properties. We place it in a three dimensional context and examine the inter-relationships between the axons in a tract.

This quick overview of a fraction of a fraction of the marvelous mammalian or human brain, will provide the reader with some appreciation of the complexities of this system. It will also enable him or her to marvel at him or herself, for brain activity is a window to the mind [2]. If these two points were both accomplished, it would have been well worth the effort of the author.

[1] This quotation from Brihadaranyaka Upanishad (4.3.32) compares the seer or the observer to a vast ocean and thus hints at the mysteries hidden within the brain.

CHAPTER 1 INTRODUCTION

1.1 The Clinical Motivation

Multiple sclerosis and other diseases of the nervous system such as autism spectrum disorder, involve malfunction of nervous tissue, primarily neurons and glial cells [3]. Multiple sclerosis has a wide-ranging impact ranging from the patient, to the caregiver and ultimately to society as a whole. Studies have revealed that the caregiver is influenced by the patients cognitive impairment over and above the disability due to neurological symptoms [4]. This serves to highlight how imperative it is to quickly and completely analyze the disease, develop and simulate a rigorous model, and provide clinicians with the predictive power and understanding gained from accurate modeling and simulation.

Moreover, it is not a simple case of malfunctioning of individual, isolated cells, but there may be collective aspects to the problem. That is, collectively, the cells in question fail to perform as expected. Further, as indicated above, there may also be heterogenous aspects to the problem wherein the malfunction involves a heterogenous set of cells - namely, the glial cells, and oligodendrocytes, in addition to neuronal axons. The glial cells and oligodendrocytes come into the picture since they form the myelin sheath which deteriorates, leading to cross-talk or cross-interaction among collections of axons. The impact of this cross-talk is not understood as being either clearly assistive or clearly pernicious. This is one of the questions that we wish to tackle.

The collective and heterogenous character of the disease calls for investigations along two mutually influencing, yet distinct lines. The hetergenous character, namely the deterioration due to glial cells unsuccessfully myelinating the axons, is best studied by models of the axon as a cable placed in a resistive extracellular space. The cable model is suited to include regions of myelination

called internodes, thereby bringing the glial cells indirectly into the picture. An example of such a study is [5].

The collective character is best studied by modeling the axon as a generator of electric fields (albeit quasistatic ones, not fully dynamic) that then influence neighboring axons across the intercellular space. We can assume that the fields are generated solely at the nodes of Ranvier of the axon and their influence is also felt solely at nodal positions of neighboring axons. These endogenous fields have been studied in addition to the impact of externally applied fields in recent works [6].

Finally, the mutual influence between these two lines of work is straightforward to postulate, for the electric fields generated by an axon's nodes, might serve to induce currents at the nodes of other axons which would then go on to cause an interaction with the other axons' internal resistive current flow in their respective cable models. However, simulation and testing of this idea has not been undertaken in the literature. This is a second question which we wish to tackle in this dissertation.

1.2 Preliminaries

We utilize the remainder of this chapter to introduce the reader to some of the key concepts needed for a study of this dissertation.

1.2.1 Key Concepts

The first concept we will need is quasistatic electrodynamics. As the name suggests, when charge is in motion with respect to time, we have a case of electrodynamics. Moving charges radiate electromagnetic fields. Stationary charges simply create static electric fields. The quasistatic situation is somewhere in between these two cases.

In the quasi static case, the charges may actually be in motion, but at each time instant, we can treat the charge as being stationary. We then compute the field created by that stationary charge. To get the overall picture, one then sequentializes the pictures obtained from each time

instant. Mathematically, in the quasi static case, the current's variation with time and space can be factored cleanly into a product of the time variation and the spatial variation [7].

In our context, we will model the current produced by a node of Ranvier as a quasi static distribution. The source of this current is the ions moving in and out of the ion channels which are present in large numbers on any node. As the channel opens, ions move down the electrochemical gradient and from one side of the membrane to the other and this motion ceases when the channel closes.

The time variation is therefore captured by this opening-closing profile whereas the spatial variation needs to be captured by another function of space. The product of these two gives the spacetime evolution of the nodal ionic current.

The second concept needed pertains to the cable equation. The cable equation is a partial differential equation, which gives the spacetime variation of a quantity such as the voltage which is associated with every position along a cable. The derivation is quite straightforward in the electrical case. We consider a section of a cable and model it as a capacitor in parallel with a conductance. The cable equation then gives the time varying potential difference across the capacitor for this section of the cable. Several such sections are then interconnected with resistances and the currents flowing between these sections and through these resistances are then used to give the potential 'drops' between the sections. In this way we get a governing spacetime 'cable' equation.

The last concept relates to computer simulation. The first two parts of this dissertation will involve simulation of the neurological network's physical layer[1] in MATLAB. MATLAB is a versatile scientific programming language and allows the graphical display of simulation results. We will use MATLAB for carrying out basic procedures such as solving integrals and solving a certain set of Crank-Nicolson discretized matrix equations.

[1]The layer which consists of the physical medium or channel of communication

1.2.2 Limitations of Our Studies

We first discuss the limitations as related to quasistatic electrodynamics. In the fourth chapter of this dissertation, we do not do a fully electrodynamic formulation, nor a quantum electrodynamic formulation. Both of these formulations may be applicable in some regime or the other to our ion channel models for the node of Ranvier. We simply do a quasistatic electrodynamic formulation. This therefore constitutes a limitation of our work here which can be addressed in future extensions.

Now we discuss the limitations pertaining to the cable equation. In the second chapter of the dissertation, where we use the standard Hodgkin-Huxley cable equation to model an axon as a whole, we are circumscribed by the limitations of this equation. This equation is fully deterministic while events at the ionic level may have a random character to them. This may be addressed in future extensions by replacing this equation by stochastic partial differential equations for axon function.

Finally, there are some limitations pertaining to computer simulation. In the second and third chapters of this dissertation where we have employed computer (MATLAB) simulation, we can do much better. We can always improve the accuracy, efficiency and stability of our simulations. This is therefore also left to future work.

The nervous system is a highly complex and dense system with many things going on at the same time. To parse this system, to understand every detail as well as get the big picture right, it is necessary to take a two pronged approach. The top down direction is the function-purpose perspective - what do the various parts of the nervous system do when functioning together? The bottom up approach is the structural perspective. How are these parts composed? And what do they inturn compose? This bottom up perspective can help to understand the physical layer of the nervous system. Understanding of both the data layer[2] as well as the physical layer might be important to develop a complete understanding of the nervous system, which is essentially a natural communication network.

[2]The layer which contains the actual information or bits communicated

There are several analogies between neurological networks and telecommunications networks. For example, both involve information transmission as well as processing; both involve coding and both are large-sized networks. Nevertheless, the neurological network has some unique properties such as extremely high connectivity per unit volume; lateral connectivity (within axon tracts) as well as longitudinal connectivity (between one neuron and the next), etc. The analogies and the unique properties together make it fascinating to comparatively study these two networks. We next take a brief look at the literature relevant to this dissertation.

1.3 Review of the Literature

The pioneering work by Hodgkin and Huxley on the squid giant axon set the stage for all future developments in the field of axon conduction. In 1942, Arvanitaki [8] proposed the use of the term "ephapse" and, consequently, ephaptic. His work contains the experimental results of studying the interaction between two axons placed side by side. This seminal work introduces some of the key concepts such as looking at the electric potential gradients in the zone of interaction between the two ephaptically coupled axons, which to this date has not been simulated.

According to Markin [9], who focuses on resistive potential drops as mediating the interaction between coupled axons, the main difficulty in producing an analytical solution to the problem of interaction between two fibers is the intractability of analytically solving the Hodgkin Huxley [10] equations for the ionic currents. He gets around this problem by proposing a simplifying model for the ionic current. He then uses this model to derive a set of governing equations based on a simple resistive-capacitive (R-C) network representing two interacting fibers, interacting by means of ion current flow in and out of the shared extracellular space.

Markin then goes on to examine the solutions to this model and finds, in the case when there is a spike on only the first fiber, that there are two possible values of impulse velocity, one stable and the other unstable, with stability being defined in relation to persistence of the impulse at that velocity. He also examines the case in which a spike on the first fiber excites a spike on the second one. This case occurs only when the second fiber has a diminished threshold for action

potential initiation. In companion papers [11, 12] Markin considers the collective conduction of spikes as well as their interaction in bundles of fibers.

The same problem of the analytical intractability of the Hodgkin Huxley equations is encountered by Eilbeck, Scott and Luzader [13]. They address the problem by using the FitzHugh-Nagumo set of equations instead of the Hodgkin Huxley equations and solving that system by a so-called perturbation analysis. They also perform simulations on the coupling of identical fibers. This work is primarily analytical, focusing only on two fibers. Furthermore, they don't consider the geometrical arrangement of many fibers in a tract. This therefore distinguishes their work from the work that will be presented in this dissertation.

Reutskiy, Rossoni and Tirozzi (RRT) [5] modify the Franekenhaueser Huxley [14] set of equations, extend them to incorporate ephaptic coupling via an assumption on the electrical isolation of the tract, which is also present in Markin's papers. They do not provide an analytical solution, but present the results of computer simulations. Their work, which provides a fiducial point for our present dissertation, incorporates large sized tracts with many fibers, all identical, with no reference to their geometrical arrangement.

In the present decade, one of the most comprehensive reviews of ephaptic coupling is the paper by Anastassiou and Koch. They conjecture that ephaptic coupling might rely on a feedback mechanism between the extracellular electric field and the intracellular activity that generates it in the first place [6]. Providing further motivation for our work, they emphatically state that

> "How . . . ephaptic effects are mediated and manifested in the brain remains a mystery. . . . argue that it is both possible and worthwhile to vigorously pursue such research as it has significant implications on . . . understanding of brain processing . . .."

Their paper includes a comprehensive survey of the literature and comprises both experimental and computational work. We refer the reader to the references in this work for further background on ephaptic coupling.

As an example, the reference [15], takes a look at the impact of externally applied inhomogeneous fields on axons in a tract, placed in a specific geometrical arrangement. This paper

however, does not have a formulation for ephaptic coupling similar to ours. Specifically, the extracellular voltage based coupling that we study in this dissertation, is not studied by these authors.

CHAPTER 2 EPHAPTIC GEOMETRY

In this chapter[1] we will expound on the first major thrust of this work, the extracellular voltage mediated coupling between axons. To begin with, we give an overview of the physiological setting in which our work will take place.

2.1 Physiological Review

To serve as a data communication and processing device, a neuron may be divided into several functional parts, of which the axon [16] is of fundamental interest to us. The axon is primarily a signal communication channel - it takes signals from the cell body or soma of the neuron to the distal terminal boutons, where these signals exit the neuron, available for influencing other neurons. This is the traditional view of the role of the axon. This chapter is however concerned with ephaptic conduction by axons, in which other axons in the transversal plane can be influenced by and influence the axon under consideration, thereby forming a joint transversal-longitudinal communication system.

We will now study the detailed biological structure of an axon. The detailed structure of an axon is shown in Figure 2.1. There are four regions of primary interest - the axon hillock, the node of Ranvier, the myelinated internode and the terminal bouton. The axon hillock is where processed signals from the cell body or soma of the neuron enter the axon. The processed signal coming from the soma and entering the axon hillock may or may not trigger a signal propagation down the axon, depending on whether or not it crosses the stimulation threshold. This stimulation threshold is a key physiological property of an axon. The axon hillock or its immediate, axon-

[1]This chapter is based in part on a submission to IEEE/ACM Transactions on Bioinformatics and Computational Biology, under review as of May 13, 2017.

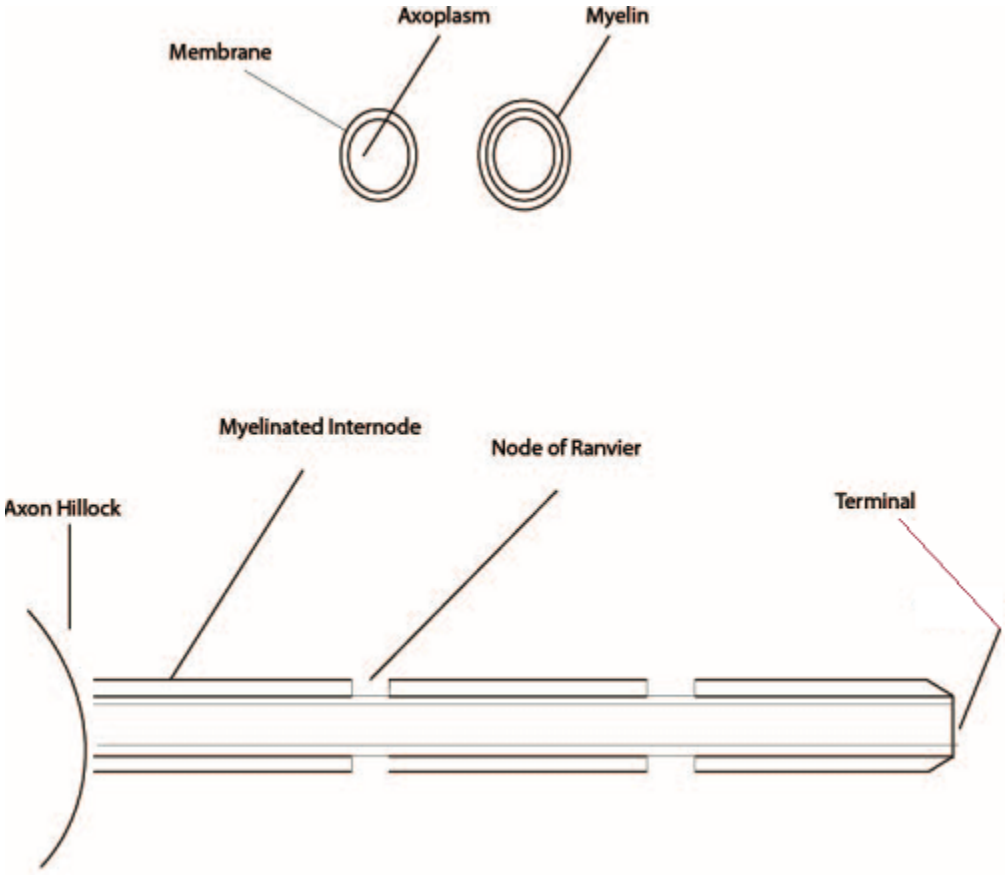

Figure 2.1: Geometrical rendering of the essential parts of an axon. Top panel, left to right: Nodal cross section; internodal cross-section. Bottom panel: Longitudinal section of an axon.

facing neighborhood, is also the place where, in experimental studies, the stimulating current is injected into the axon.

As we move along the axon longitudinally, we encounter specialized, periodically placed regions called nodes of Ranvier. At the nodes of Ranvier, ion channels and ion pumps are present that allow movement of chemical ions to and from the extracellular medium. Between two nodes of Ranvier is a zone called an internode, which is wrapped by oligodendrocytes in the central nervous system (or Schwann cells in the peripheral nervous system [16]) forming what is known as a myelin sheath. This largely insulating sheath, blocks off any ion channels that may otherwise be present in this region and so there is very little possibility of chemical movement between intra and extracellular space in this region. An axon contains several nodes of Ranvier. As we reach the longitudinal-terminal point of this alternating sequence of node and inter-node, the zone between

nodes, we end up in a terminal zone called a bouton which is non-myelinated and contains ion channels which open out into the extracellular space, the synaptic cleft or the neuro-muscular junction, as the case may be.

Next we look at the axon cross section at the node of Ranvier. As illustrated in Fig. 2.1, we have the lipid bilayer which constitutes the axon membrane and holds specialized molecules that form ion channels as well as ion pumps. An ion channel is a device which has a voltage sensor and a gate that allows one-way flow of a specific ionic species between intra and extra cellular regions. An ion pump is constituted so as to actively transport particular ionic species between intra and extra cellular spaces. There are other components that are embedded in the membrane, serving other functions. Within the boundary provided by the lipid bilayer, we have the intracellular medium which contains the neuron's cytoplasm, also known as the axoplasm. Coming to the internodal cross section, we see a further structure at the outermost periphery, the myelin sheath. As stated before, this insulating sheath prevents ion exchange between the intra- and extra-cellular regions.

The intracellular and extracellular regions are rich in various ionic species, the main ones being K+ ions and Na+ ions. These ionic species appear in commonly found concentration gradients across the cell membrane. The set of values for their concentrations that we will use throughout our work are: external concentrations of 114.5 milliMolar (mM) and 2.5 mM for Na+ and K+, respectively, and internal concentrations of 13.74 mM and 120 mM for Na+ and K+, respectively.

These concentration gradients set up electrochemical forces that operate across the membrane. When the membrane becomes porous to a particular ion species at a node of Ranvier, ions flow down the electrochemical gradient for that particular species. This changes the potential difference and chemical concentration of that ion across the membrane which in turn affects the electrochemical forces in operation and modifies or stops the flow of that species across the membrane. This is the basic mechanism underlying ion flow across the membrane. The law or equation which governs this is the Nernst equation for a single ion. When several ionic species are present the equilibrium electric potential is given by the Goldman-Hodgkin-Katz equation [17].

2.1.1 Properties of Ion Channels

Ion channels such as the voltage gated Na+ channel and the voltage gated K+ channel are present at the nodes of Ranvier. The voltage gated Na+ channel has a sensor and a gate which causes the opening of the channel when the intracellular voltage (with respect to the extracellular voltage) reaches a certain voltage range. When the channel is open, it is selectively open only to the passage of Na+ ions from outside the cell to inside [18, 19].

There is an intricate relationship between what are known as the microscopic gating variables (m, n, h, p) at an ion channel and the macroscopic current that flows through the ion channel. This relationship was carefully reconstructed by Hodgkin and Huxley [10] and later improved upon by Frankenhauser [20]. It is semi-empirical, based on experimental data from the squid giant axon, as well as data-fitting [21]. The potassium current is given as

$$P_K \cdot n^2 \cdot Z_K \tag{2.1}$$

and the sodium current as

$$P_{Na} \cdot m^2 \cdot h \cdot Z_{Na} \tag{2.2}$$

where P_K and P_{Na} are constant coefficients, m, n and h are the gating variables, and Z_K and Z_{Na} are voltage and concentration dependent variables [2]. Thus, the present voltage and values for the equilibrium ionic concentrations play a role in determining the ionic current that will flow across the membrane.

The next two Figs., 2.2 and 2.3, show the four gating variables as they change with time at two different nodes in response to a stimulus at the first node. The equations which govern these variables are as follows:

$$\frac{dq}{dt} = Q \cdot [\alpha_q(1 - q) - \beta_q q] \tag{2.3}$$

[2]The gating variable p is involved in a similar equation which we exclude for simplicity of exposition, but is part of our simulation.

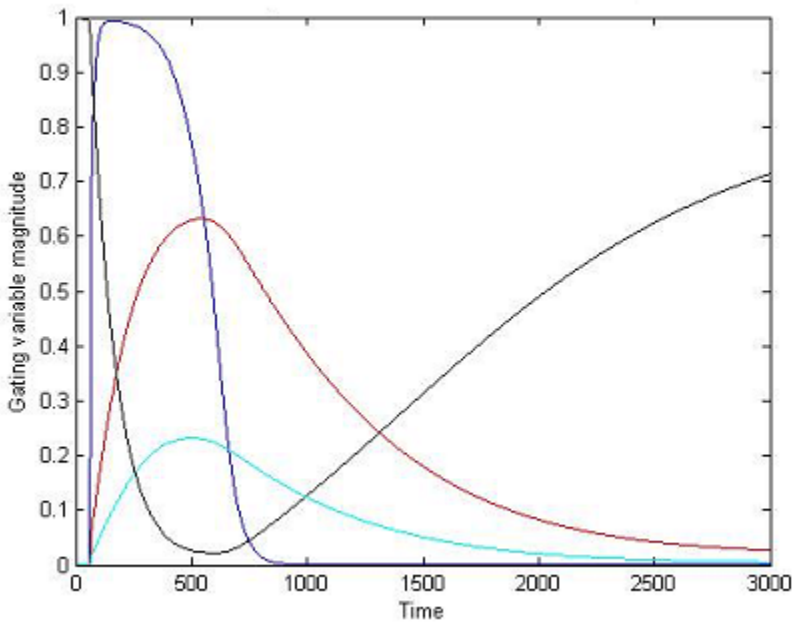

Figure 2.2: Gating variables m (blue), n (red), h (black), p (cyan) with time at the injected node. The curves compare well with the Hodgkin-Huxley data. The abscissa is time in units of the time step size (delta t) used in the simulation.

where Q is a temperature dependent constant, q stands in for the variables m, n, h, p and α_q and β_q are transmembrane voltage dependent variables.

The two figures following these, Figs. 2.4 and 2.5, show the two key ionic currents, the sodium (Na+) ionic current and the potassium (K+) ionic current, as they change with time at two different nodes in response to a stimulus at the initial node of the axon. It is clear from these two figures that the sodium current is primarily outward (positive) while the potassium current is primarily inward. As mentioned earlier in this section, the direction of the current flow for a particular ionic species depends mainly upon the concentration gradients and resulting electrochemcial forces acting on that particular ionic species. For further details, we refer the reader to chapter four in [19].

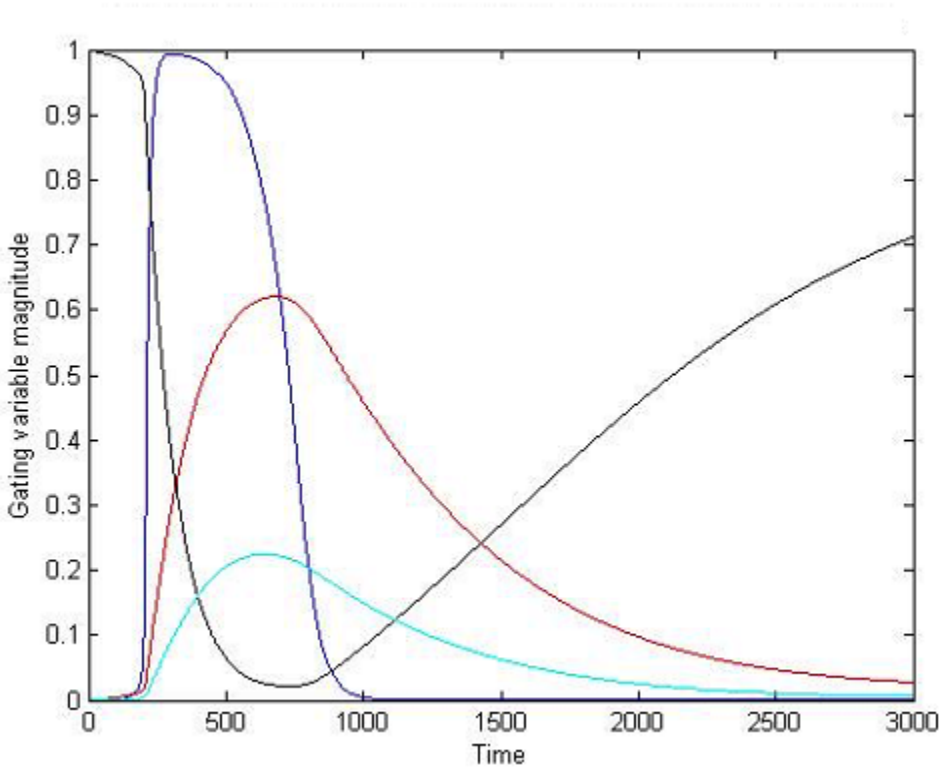

Figure 2.3: Gating variables m (blue), n (red), h (black), p (cyan) with time at the downstream node, node 30. The nodes are placed at a separation of 10 spatial segments along the axon. The curves of the previous figure are now shifted rightward in time, indicating the time it takes for the action potential to hop from the stimulated node to node 30. The abscissa is time in units of the time step size (delta t) used in the simulation.

2.2 Additional Physiological Details

The voltage gated sodium channel is embedded in the cell membrane of the node of Ranvier of the neuron, although it is also expressed in paranodal[3] regions of the internode. As the name indicates, this channel has a voltage sensor and gate. Under resting conditions, i.e. the transmembrane voltage being at its resting value, this gate is closed, making the channel impermeable to the movement of sodium ions through it.

Due to an intracellular depolarization (excess of positive charge), the gate undergoes a conformational change and 'opens' to the flow of sodium ions. When the depolarization is no

[3]This is the region of the internode that adjoins a node of Ranvier. There are thus two paranodal regions in each internodal segment since there may be flanking nodes of Ranvier on either side of the internodal segment.

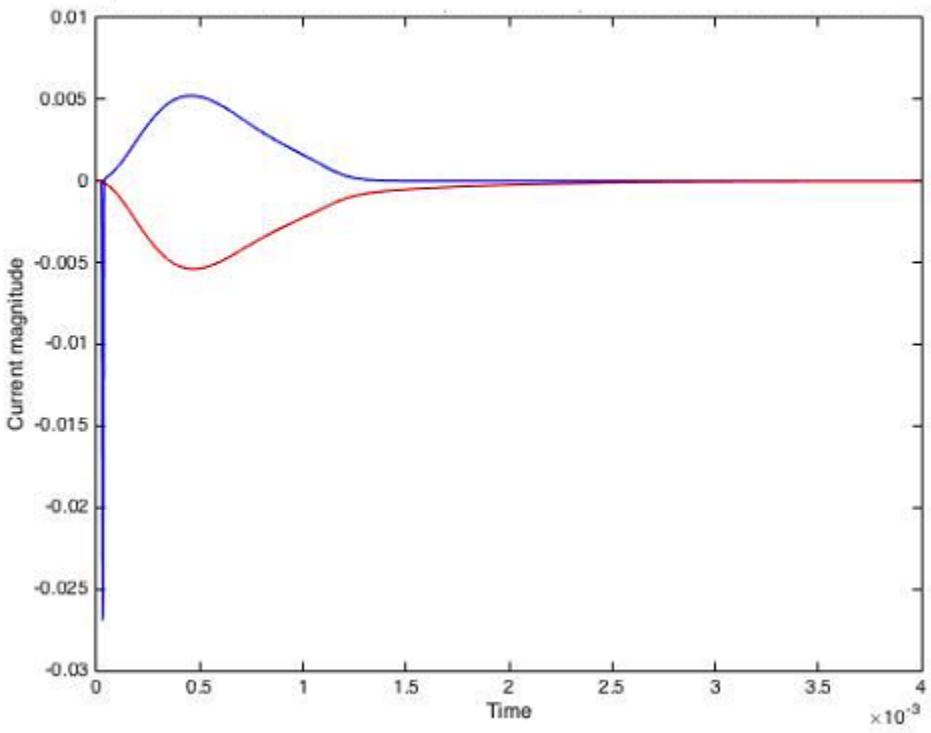

Figure 2.4: Current magnitude in Amps/centimeter-squared for sodium (blue) and potassium (red) at the position of injection. The x-axis is time in seconds.

longer present, the gate 'closes'. Fig. 2.6, from [22], shows the current flow through a patch of voltage gated sodium channels when a depolarization step is applied across the cell membrane. The current is on the order of a couple of pico-Amperes. A node of Ranvier has longitudinal dimensions of the order of 3 to 7 microns or more [23]. This is where there is the primary concentration of ion channels. Studies have shown a sodium channel density of about 10,000 per square micrometer at the nodes of Ranvier [24].

The myelinated axon is a concatenation of non-myelinated nodal and myelinated internodal regions. The total axonal length is of the order of 1 mm to 1 meter [16]. Smooth axons differ primarily in that there is no myelin sheath.

Axons may come together to form collections. We will not distinguish between nerves and bundles. The optic nerve of *Anurans* for example contains on the order of half a million axons, both myelinated as well as unmyelinated ones [25] put together, without the formation of bundles.

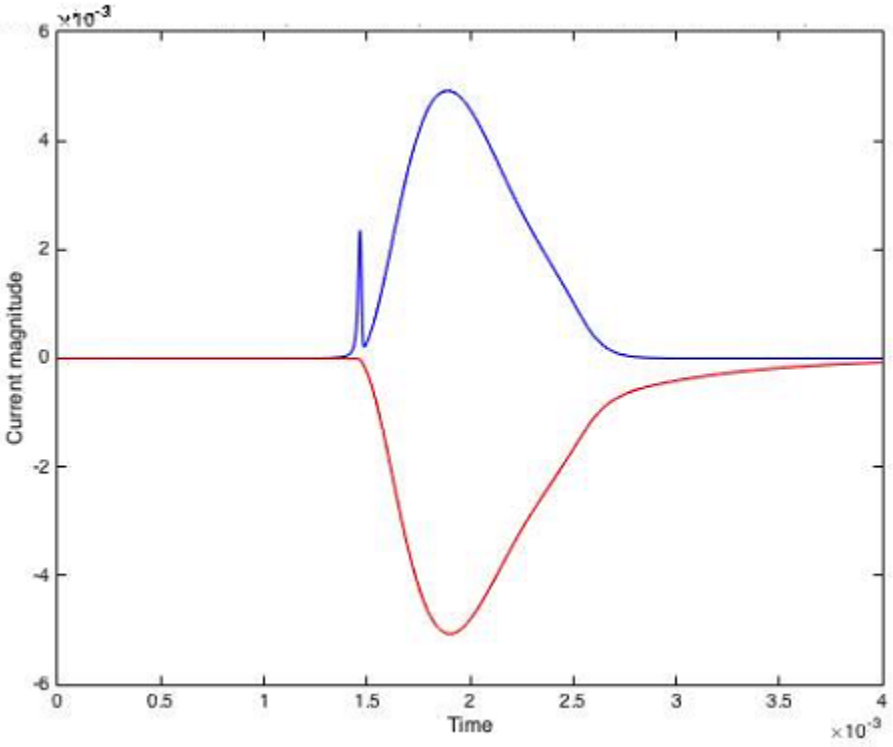

Figure 2.5: Current magnitude in Amps/centimeter-squared for sodium (blue) and potassium (red) downstream from the position of injection. The x-axis is time in seconds.

2.3 The Need for Realistic Models of Axon Tracts

Our study is motivated by the need to deepen understanding of the nervous system, in general, and neurological disorders, such as multiple sclerosis and autism spectrum disorder, in particular. In this chapter we focus on the phenomenon of ephaptic coupling. This phenomenon is chosen since it could have relevance for a number of neurological disorders.

We seek to understand how critical elements of the nervous system act as networks to process information. For this, a thorough understanding of the physical layer[4] of the nervous system network is essential. In particular, questions such as the following need to be considered:

- What are the capacities of the optic nerves and spinal cord?
- What is an appropriate way to model a tract of axons - is it a multiple input multiple output

[4]The layer which consists of the physical medium or channel of communication

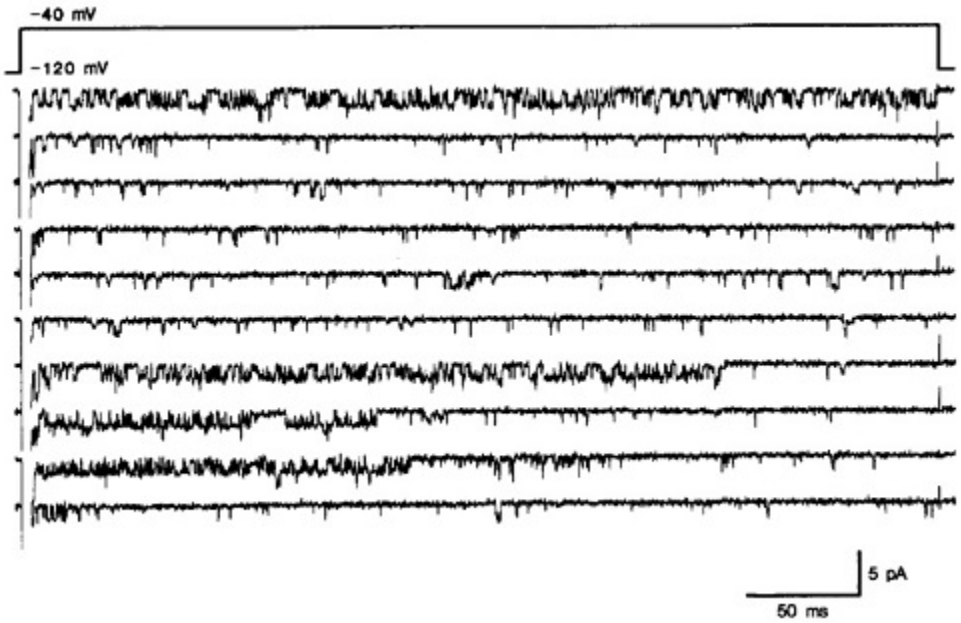

Figure 2.6: Late currents through Na+ channels. Courtesy RUPress. [22] doi:10.1085/jgp.87.2.305; Used with permission. The y-axis is in pico Amperes and the x-axis is in milliseconds.

(MIMO) communication system?

- Does signaling take place in ways other than via chemical synapses and if so, how should it be modeled?
- Does noise play a role in nervous communication systems?
- If so, is there a role for coding on the data layer[5] of the nervous network?
- How are neurons able to talk to one another over vast multi-hop distances?

Understanding and answering these questions is the goal of those that work at the intersection of neuroscience and electrical engineering. In this chapter, we will not attempt to answer all of these questions. Rather, we will focus on the physical layer and a very specific phenomenon - the phenomenon of ephaptic interaction. This phenomenon, and the synchronization it can entrain, is chosen since it could help to answer some of the above questions and have relevance for a number of neurological disorders.

[5]The layer which contains the actual information or bits communicated

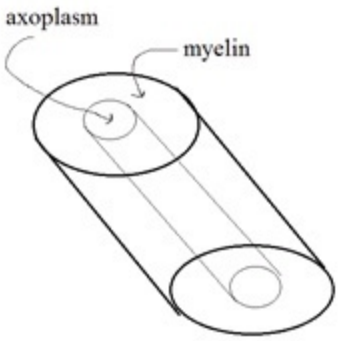

Figure 2.7: Axon with myelin sheath. Inner area $= \pi r_{inner}^2$; sheath area $= \pi(r_{outer}^2 - r_{inner}^2)$

For example, multiple sclerosis is a significantly prevalent disorder of the nervous system with no effective treatment. While there is some understanding of the mechanism underlying the disease, the exact impact of demyelination on the operation of the nervous system is not known. There have been several studies on modeling nervous conduction under diseased conditions [5, 26], but no known study has incorporated the geometrical arrangement of axons in a tract into the model and simulations, which we do here. This is important since multiple sclerosis leads to demyelination plaques in areas such as the brain, optic nerve and spinal cord, where nerve fibers are tightly bundled in tracts. Here the packing is not necessarily homogeneous or uniform, and we cannot simply reduce the intricacy of the system to a single dimension.

2.4 Derivation of Generalized Model for Interaction between Axons

Figure 2.8 specifies the geometric parameters for a tract of axons, encased in a right cylinder aligned with the z axis. The ith axon itself consists of sections of right circular cylinders of axoplasm fiber, surrounded by myelin sleeves, connecting the Ranvier nodes (Figure 2.7). The axons can have a variety of cross section areas, material parameters, and misalignments with the tract axis. Note that each point on the ith axon has a "local coordinate" given by its distance s_i along the axon, and a "universal coordinate" $z = s_i \cos\theta_i$. Derivatives are related by the chain rule

$$\frac{\partial}{\partial s_i} = \cos\theta_i \frac{\partial}{\partial z}.$$

Table 2.1: List of principal symbols and their meanings used in Chapters 2 and 3.

Symbol	Meaning
C	myelin capacitance per unit length
G	conductance per unit length (axoplasm, myelin, extracellular)
V	Transmembrane potential drop
θ_i	Inclination of axon i with respect to tract axis
s_i	Spatial position along an inclined axon
r	(inner, outer)myelin sheath radius
z	Spatial position along the tract axis
$\mathbf{r}$	Position vector of a point in the tract
$\phi(\mathbf{r})$	Electric potential at a point $\mathbf{r}$ of the tract
$\phi_{ext}(z,t)$	Extracellular potential at a spatial height z along the tract axis
$\phi_i(s_i,t)$	Intracellular potential of axon i at a spatial distance s_i along the axon
$\mathbf{r}_i$	Location of the base of axon i
$\mathbf{n}_i$	Unit vector along axon i
I	current (axoplasm, myelin, extracellular, injected or ionic)
A	cross-sectiona area (axoplasm, myelin, extracellular)
σ	conductivity (axoplasm, myelin, extracellular)
δ	Spatial separation between pulses on fibers 1 and 2
$v^{(1)}(\delta), v^{(2)}(\delta)$	Impulse velocity on fiber 1,2 as a function of spatial separation δ

Table 2.1 (continued).

Symbol	Meaning
$v_0, v_1^{(1)}, v_1^{(2)}$	First term and second terms in the expansion of $v^{(1)}$ and $v^{(2)}$
α, η, a^*	Coupling and threshold parameters
β	Geometrical parameter for two fibers' synchronization analysis
$u^{(1)}, u^{(2)}$	Dimensionless uncoupled velocity of fiber 1,2
u_0	Threshold constant with units of velocity
$u_c, u_c^{'}$	Dimensionless coupled velocity, at non-zero and zero interpulse separation
$u_3(\delta)$	Velocity change ratio scaled by u_0, dependent on spatial separation δ
$c(\beta)$	β dependent ordinate-intercept in the equation for u_c
$\lambda(\beta)$	β dependent interpolation parameter

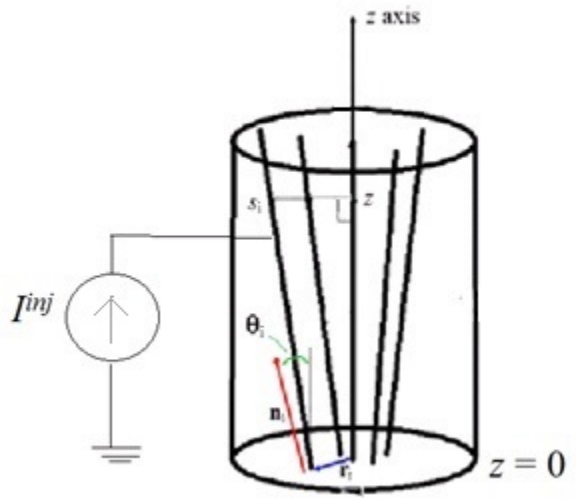

Figure 2.8: Relationship between tract axis and angle of inclination. $z = s_i \cos\theta_i$

The electric potential throughout the tract is denoted $\phi(\mathbf{r})$. Our model invokes simplifying assumptions that spawn two different regional formulations for ϕ.

1. In Reutskiy's words [[5], p.3], "each transverse section of the extracellular space is isopotential"; that is, in the extracellular space $\phi(\mathbf{r}, t)$ is a function only of z:

$$\phi(\mathbf{r}, t) = \phi_{ext}(z, t).$$

   $\phi_{ext}(z, t)$ depends, of course, on the electrical effects produced inside all the axons. It is the mechanism for the ephaptic coupling between them.

2. Inside the ith axon fiber, ϕ varies only along the fiber length:

$$\phi(\mathbf{r}, t) = \phi_i(s_i, t)(\mathbf{r} = \mathbf{r}_i + s_i\mathbf{n}_i).$$

Ion currents obeying the Hodgkin-Huxley equations are generated at the Ranvier nodes, and the voltage propagation along the fiber is modeled by the well known cable equation [10], [5], [27]. It is derived by observing that the change in (longitudinal) current I, over a differential length

ds, must be accounted for by incoming transversal currents through the myelin sheath (capacitive, ohmic and ionic or injected):

$$I(s+ds) - I(s) = -Cds\frac{\partial v}{\partial t} - G^{my}dsV + I^{inj}ds \tag{2.4}$$

or,

$$\frac{\partial I}{\partial s} = -C\frac{\partial V}{\partial t} - G^{my}V + I^{inj}, \tag{2.5}$$

where $V(s,t) \equiv \phi(s,t) - \phi_{ext}(z \equiv s\cos\theta, t)$ is the voltage drop across the myelin sheath, $C = \frac{2\pi\epsilon_{my}}{\ln\frac{r_{out}}{r_{in}}}$, $G^{my} = \frac{2\pi\sigma_{my}}{\ln\frac{r_{out}}{r_{in}}}$, and $I^{inj}(s,t)$ denotes any injected current. We ignore longitudinal myelin currents. For clarity we have temporarily suppressed the subscripts that associate the physical and geometric parameters with particular axons.

Since I is driven by the gradient of the potential, $I = -G^{ax}\frac{\partial\phi}{\partial s}$, ($G^{ax} = \sigma_{ax}\pi r_{in}^2$) and the cable equation takes the familiar form

$$\begin{aligned} C\frac{\partial V}{\partial t} &= G^{ax}\frac{\partial^2\phi}{\partial s^2} - G^{my}V + I^{inj} \\ &\equiv G^{ax}\cos^2\theta\frac{\partial^2[V+\phi_{ext}]}{\partial z^2} - G^{my}V + I^{inj}. \end{aligned} \tag{2.6}$$

The occurrence of the extracellular potential in this equation gives rise to ephaptic coupling. We have a cable equation for each axon voltage V_i; we need an equation for $\phi_{ext}(z,t)$. But, in fact, the extracellular region itself can be modeled as a cable, wherein longitudinal variation in its current $I_{ext}(z,t)$ is accounted for by the total transversal currents from the axons:

$$\begin{aligned} I_{ext}(z+dz) - I_{ext}(z) &= \sum_{axons,p} C_p ds_p\frac{\partial V_p}{\partial t} + G_p^{my}ds_pV_p - I_p^{inj}ds_p \\ &\equiv -\sum_{axons,p}\frac{\partial I_p}{\partial s_p}ds_p. \end{aligned} \tag{2.7}$$

This implies,

$$\begin{aligned} \frac{\partial I_{ext}}{\partial z} &= -\sum_{axons,p} \frac{\partial I_p}{\partial s_p}\frac{ds_p}{dz} \\ &= -\sum_{axons,p} \frac{\partial I_p}{\partial z}. \end{aligned} \tag{2.8}$$

That is,

$$I_{ext} + \sum_{axons,p} I_p = \text{constant}. \tag{2.9}$$

Expressed in terms of the potential, (2.9) says

$$\begin{aligned} -G^{ext}\frac{\partial^2 \phi_{ext}}{\partial z^2} &- \sum_{axons,p} G_p^{ax}\frac{\partial}{\partial z}\frac{\partial \phi_p}{\partial s_p} \\ &= 0 \\ &= -G^{ext}\frac{\partial^2 \phi_{ext}}{\partial z^2} - \sum_{axons,p} G_p^{ax}\cos\theta_p \frac{\partial^2 \phi_p}{\partial z^2} \end{aligned} \tag{2.10}$$

where $G^{ext} = \sigma_{ext} A_{ext}$. Expressing the axon potentials as $\phi_p = V_p + \phi_{ext}$, we obtain an equation for the extracellular potential

$$\begin{aligned} -G^{ext}\frac{\partial^2 \phi_{ext}}{\partial z^2} &- \sum_{axons,p} G_p^{ax}\cos\theta_p \frac{\partial^2 \phi_{ext}}{\partial z^2} \\ &- \sum_{axons,p} G_p^{ax}\cos\theta_p \frac{\partial^2 V_p}{\partial z^2} \\ &= 0 \end{aligned}$$

or $\frac{\partial^2 \phi_{ext}}{\partial z^2} =$

$$\frac{-\sum_{axons,p} G_p^{ax}\cos\theta_p \frac{\partial^2 V_p}{\partial z^2}}{\left[G^{ext} + \sum_{axons,p} G_p^{ax}\cos\theta_p\right]}.$$

We substitute for $\frac{\partial^2 \phi_{ext}}{\partial z^2}$ in the axon cable equations (2.6) to derive the generalized ephaptic equation

$$\begin{aligned} C_i \frac{\partial V_i}{\partial t} &= G_i^{ax} \cos^2 \theta_i \left(\frac{\partial^2 V_i}{\partial z^2} - \sum_{axons,p} K_p \frac{\partial^2 V_p}{\partial z^2} \right) \\ &- G_i^{my} V_i + I_i^{inj} \end{aligned} \tag{2.11}$$

where

$$K_p = \frac{G_p^{ax} \cos \theta_p}{G_{ext} + \sum_{axons,p} G_p^{ax} \cos \theta_p}.$$

This equation reduces to that of Reutskiy [5] if the misalignment effects (θ_i) are ignored and the axons are all identical. It further reduces to that of Hodgkin and Huxley [10] for the case of a single axon.

It is important to note that some workers have been troubled by Reutskiy's postulate that the net longitudinal current flux across any transversal plane must be *zero*: $I_{ext}(z) + \sum_{axons} I_p(z) = 0$. In fact, the postulate is false. One can impose a uniform longitudinal electric field E along the tract, decreasing every potential by a term proportional to z ($\phi_p^{'} = \phi_p - Ez$, $\phi_{ext}^{'} = \phi_{ext} - Ez$); the cable equations (2.6) and (2.10) will still be satisfied, and there will be a nonzero current flux (independent of z). Reutskiy, however, only employed the *derivative* of this condition (2.8) in his derivation, so it is consistent with the present analysis.

The term $K_p \frac{\partial^2 V_p}{\partial z^2}$ quantifies how the contribution to the extracellular potential by the pth axon influences the voltage in the ith axon. Intuitively, we feel that a more sophisticated model of the extracellular potential would predict an attenuation of this effect as the distance between the two axons increases. In the absence of such a model, we phenomenologically propose that a factor W_{ip} be inserted into the equation (2.11), diminishing with separation between axons i and p:

$$\begin{aligned} C_i \frac{\partial V_i}{\partial t} &= G_i^{ax} \cos^2 \theta_i \left[\frac{\partial^2 V_i}{\partial z^2} - \sum_{axons,p} W_{ip} K_p \frac{\partial^2 V_p}{\partial z^2} \right] \\ &- G_i^{my} V_i + I_i^{inj}. \end{aligned} \tag{2.12}$$

Section 2.5 reports simulations that were performed incorporating the innovations described here.

2.5 Simulation

2.5.1 Tract Injury: Generalized Ephaptic Equation Simulation

To illustrate the power and importance of our formulation, in this subsection we consider the case of a compressive injury (lateral compression in a cross-sectional plane) to a tract containing three parallel axons resulting in a change in the angular inclinations of the axons to the tract axis, by thirty degrees each, but no change in the mean separation between the axons (i.e. no change in the W_{ip} matrix). The axons are placed in a non-equilateral arrangement with the W_{ip} matrix entries being:

$$\begin{bmatrix} 1 & 0.892 & 0.99 \\ 0.892 & 1 & 0.9001 \\ 0.99 & 0.9001 & 1 \end{bmatrix} \tag{2.13}$$

We simulate the phenomenological version of the generalized ephaptic equation (2.12) for this case. The simulation result is shown in Figs. 2.9, 2.10 and 2.11. The figures show the output when a different axon is stimulated in each case.

Next, for the post-injury case, we simulate the same equation for the case of three symmetrically inclined axons ($\theta_i = 30$) and W_{ip} being unchanged. The simulation result is shown in Figs. 2.12, 2.13 and 2.14. The figures show the output when a single, different axon is stimulated in each case. From these six figures, we can clearly see that the injury has a dramatic impact on the ephaptic coupling. Before injury, when axon 1 is stimulated, axons 2 and 3 both fire. However, after injury, only axon 3 fires in response. Similarly, when axon 2 is stimulated before injury, axons 1 and 3 would also fire, but after injury they do not respond. Likewise, when axon 3 is stimulated, before injury 1 and 2 both fire, whereas after injury 2 does not respond.

Thus we see that the injury has tended to cut-off axon 2's communication with the other two axons. This changes not only the configuration but also the functionality of the axon interaction network.

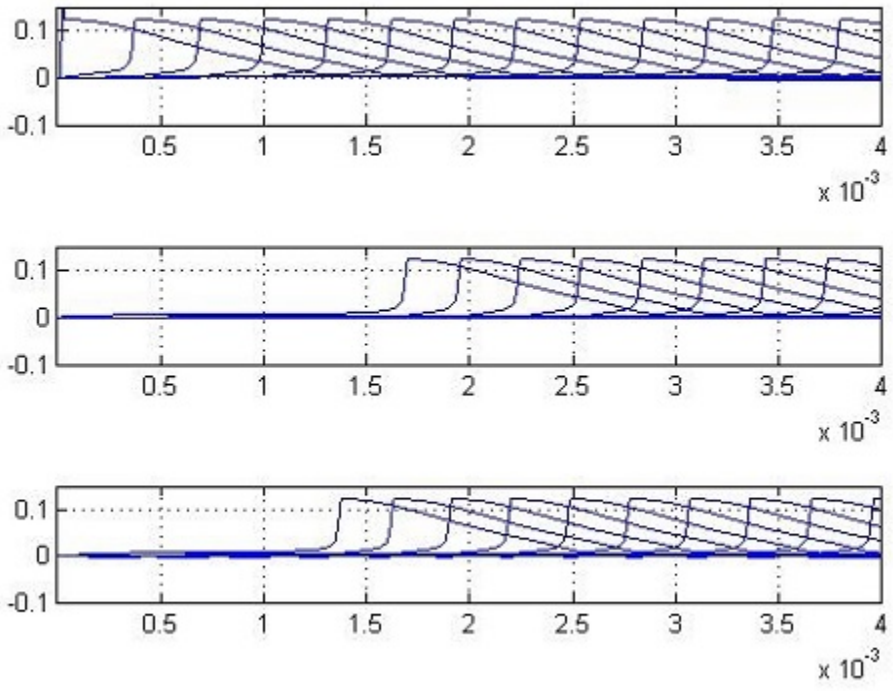

Figure 2.9: Three axons are considered with a W-matrix which incorporates non trivial inter-axonal distances and inclinations of 0 degrees from the tract axis, axon 1 being stimulated. The y-axis is in Volts and the x-axis is in seconds.

2.5.2 Synchronization: Simulation of Axons having Differing Diameters

Although synchronization can be studied for the case of three axons, we come back to a simpler case, that of two parallel axons and in this subsection study *synchronization* between the impulses launched on them. Since there are only two parallel axons, the full power of the generalized ephaptic equation is not needed and we can simply use the special case without W_{ip} and with $\theta_i = 0$.

The case of synchronization between axons having different diameters has not been simulated to our knowledge. It is well known that conduction velocity increases as axon diameter increases [28]. The analysis presented in the book [29] reviews how the velocities on fibers with different diameters synchronize with time. That analysis is summarized in Chapter 3. This presentation forms the motivation to simulate the case where the fibers being coupled have different

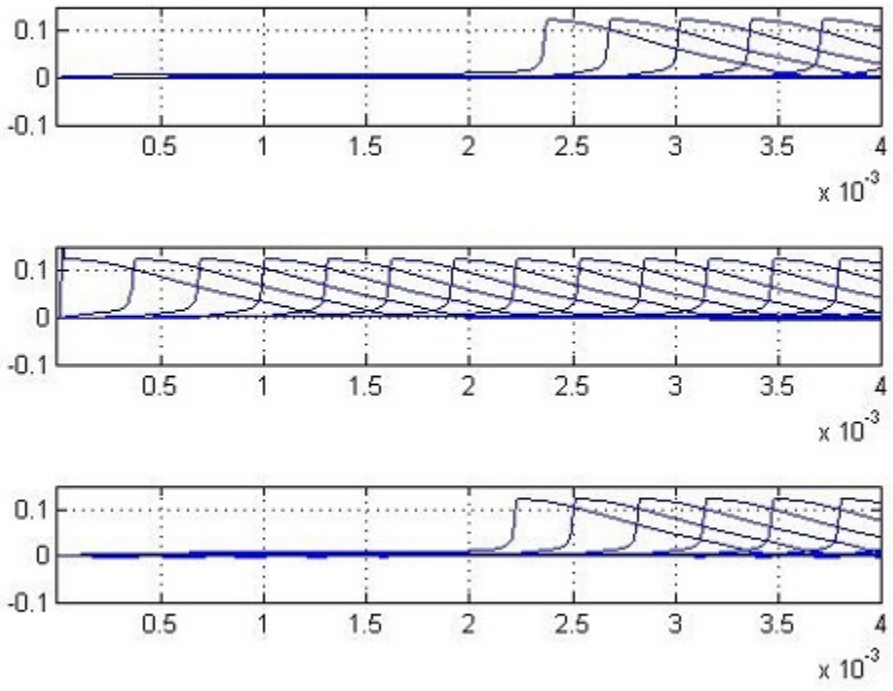

Figure 2.10: Three axons are considered with a W-matrix which incorporates non-trivial inter-axonal distances and inclinations of 0 degrees from the tract axis, axon 2 being stimulated. The y-axis is in Volts and the x-axis is in seconds.

diameters. We note that a tract may contain a range of axonal diameters. See, for example, Fig. 2.15 [30].

To study the impact of different diameters, and eventually obtain Figs. 2.18 and 2.19, we computed C_{my},G_{ax}, and G_{my} for different-sized axons. The results obtained for the case of two different diameters are shown in Figs. 2.17 and 2.16. A null value of extracellular resistance is used in Fig. 2.17, leading to a null coupling term [5].

The figures clearly demonstrate that the action potentials on the unstimulated fiber which are initially lagging behind those on the stimulated fiber, speed up to catch up with the former. These simulation results agree with the analysis in [29] which indicates that the lagging pulse speeds up to catch up to the leading pulse. A more extensive set of simulation runs would be required to completely characterize what happens in different situations when fiber diameters differ. Because this is a nonlinear phenomenon, it might not be possible to exhaust all the possibilities by

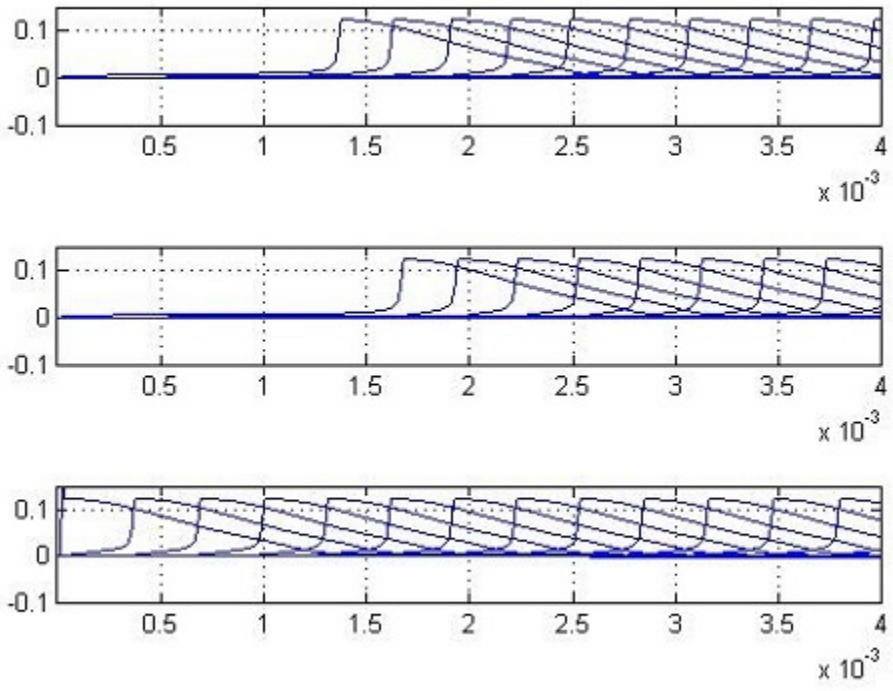

Figure 2.11: Three axons are considered with a W-matrix which incorporates non-trivial inter-axonal distances and inclinations of 0 degrees from the tract axis, axon 3 being stimulated. The y-axis is in Volts and the x-axis is in seconds.

simulation runs. However, the following two figures, Fig. 2.19 and 2.18, are a fair way to capture the essence of what is happening in synchronization. They show the spatial sum of the action potentials on two axons, standing alone (Fig. 2.18) and when coupled and synchronizing (Fig. 2.19). A beat-like phenomenon and eventual synchronization is clearly visible in Fig. 2.19.

2.6 Conclusions and Future Work Directions

In this chapter, we developed a new method for incorporating the geometrical arrangement of axons in a tract into the known cable equation models. This led to a generalized equation of which the known equations such as the Hodgkin-Huxley equation and the Reutskiy equation are special cases. The equation can be written in both nodal and internodal versions. One can then combine the nodal and internodal versions in alternate fashion, as per the distribution of the nodes

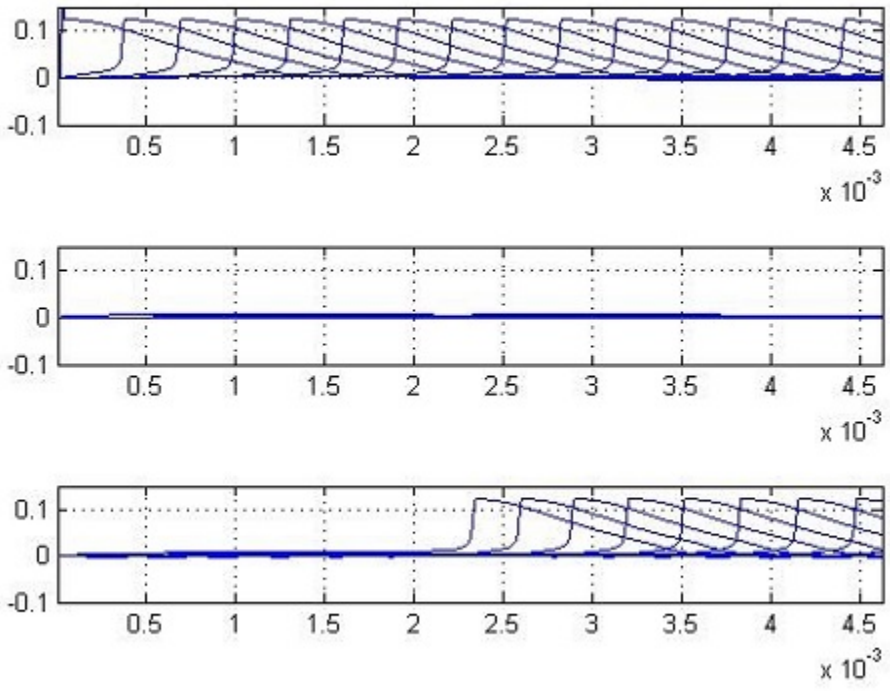

Figure 2.12: Three axons are considered with a W-matrix which incorporates non trivial interaxonal distances and inclinations of 30 degrees from the tract axis, axon 1 being stimulated. The x-axis is in seconds, the y-axis in Volts.

of Ranvier along the axon lengths. The axons were further allowed to have differeing diameters, differing myelin conductances as well as axoplasm conductances and capacitances.

In a realistic tract of axons, one can determine, by clinical measurements, the precise interaxonal distances at each plane of cross-section along the tract axis. As an example, the rodent cortico-spinal tract has been measured clinically. It has been found that an estimated 15 to 40 (average 25) axons of less than one micron in diameter appear in a cross-sectional area of 25 square microns [31]. This highlights the importance of our work to clinicians, for modeling and simulating such a tract.

The work can be extended in a few directions. First of all, we should be able to study multiple sclerosis directly, by incorporating demyelination, specifically focal demyelination, into our program. Focal demyelination is the condition wherein the region around a node gets progressively demyelinated. This might be incorporated by replacing the internodal segments around a node by

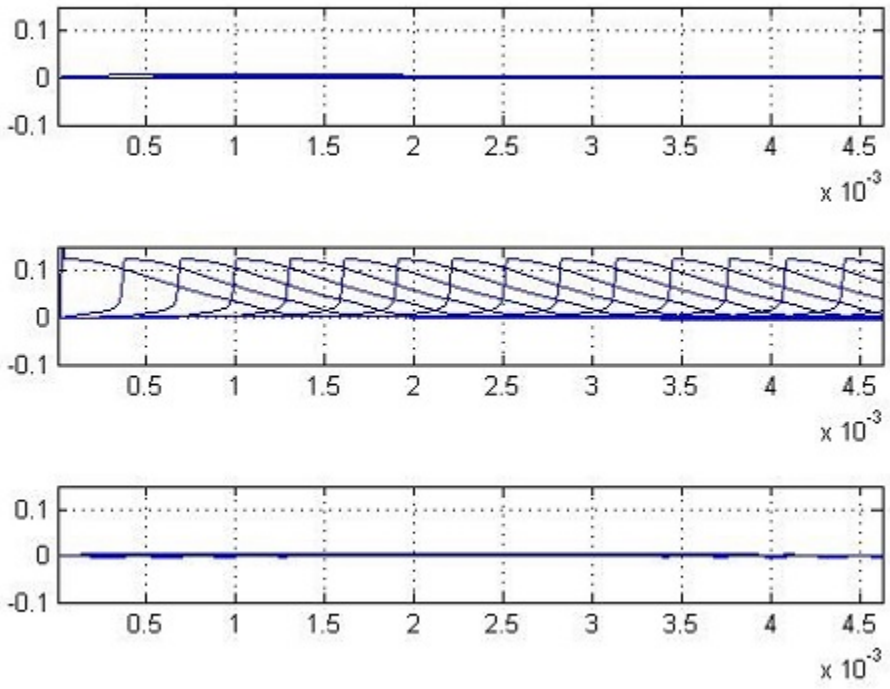

Figure 2.13: Three axons are considered with a W-matrix which incorporates non-trivial inter-axonal distances and inclinations of 30 degrees from the tract axis, axon 2 being stimulated. The x-axis is in seconds, the y-axis in Volts.

node-like segments in the program we developed to simulate the generalized ephaptic equation.

Secondly, we can consider studying the spread of local ephaptic rhythms into global ones via simulation. This can be done by taking a tract with a large number N of axons, say $N = 1000$, and stimulating only a few of them, close to the axis of the tract. The goal then would be to study how fast the ephaptic effect leads to a spread of this stimulation. That is, how soon do the neighbors of the stimulated set get coupled in and begin firing their own action potentials. Another question that can be addressed is whether the whole tract eventually begins to fire or not, and what are the threshold conditions and geometric constraints for this happening.

Finally, we can study the impact of noisy current injections on the input side to a tract, by randomly stimulating the input side. This would constitute an interesting study of academic interest and not just possible clinical impact. Preliminary investigations indicate that noise may be added and that this is equivalent to noisy current injections. If we next treat the axon tract as a data

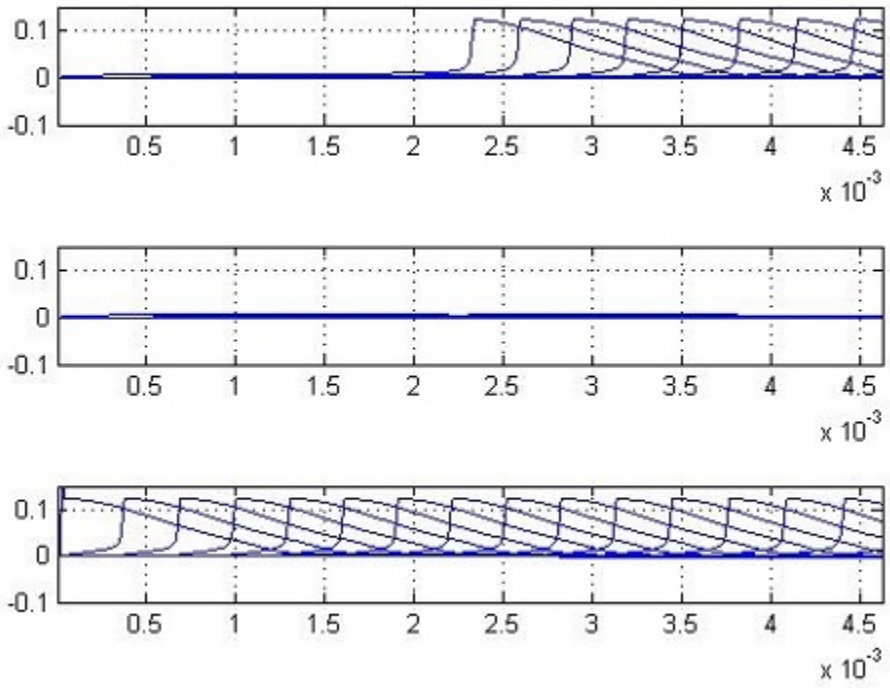

Figure 2.14: Three axons are considered with a W-matrix which incorporates non-trivial inter-axonal distances and inclinations of 30 degrees from the tract axis, axon 3 being stimulated. The x-axis is in seconds, the y-axis in Volts.

storage device or channel in time, then this setup likely results in a form of discrete time additive noise channel with perfect feedback. The capacity of a number of such channels is known in the information theory literature and therefore we may be able to compute the storage capacity of the axon tract.

Further, we can incorporate applied electric fields as additional current injections and study their impact on the synchronous firing of axons in the tract. To conclude, the theory and program[6] that has been built as a part of this investigation have many potential extensions and can be useful to neurophysiologists as well as those studying fundamental communication and storage limits of the nervous system.

[6]See Appendix A.4.

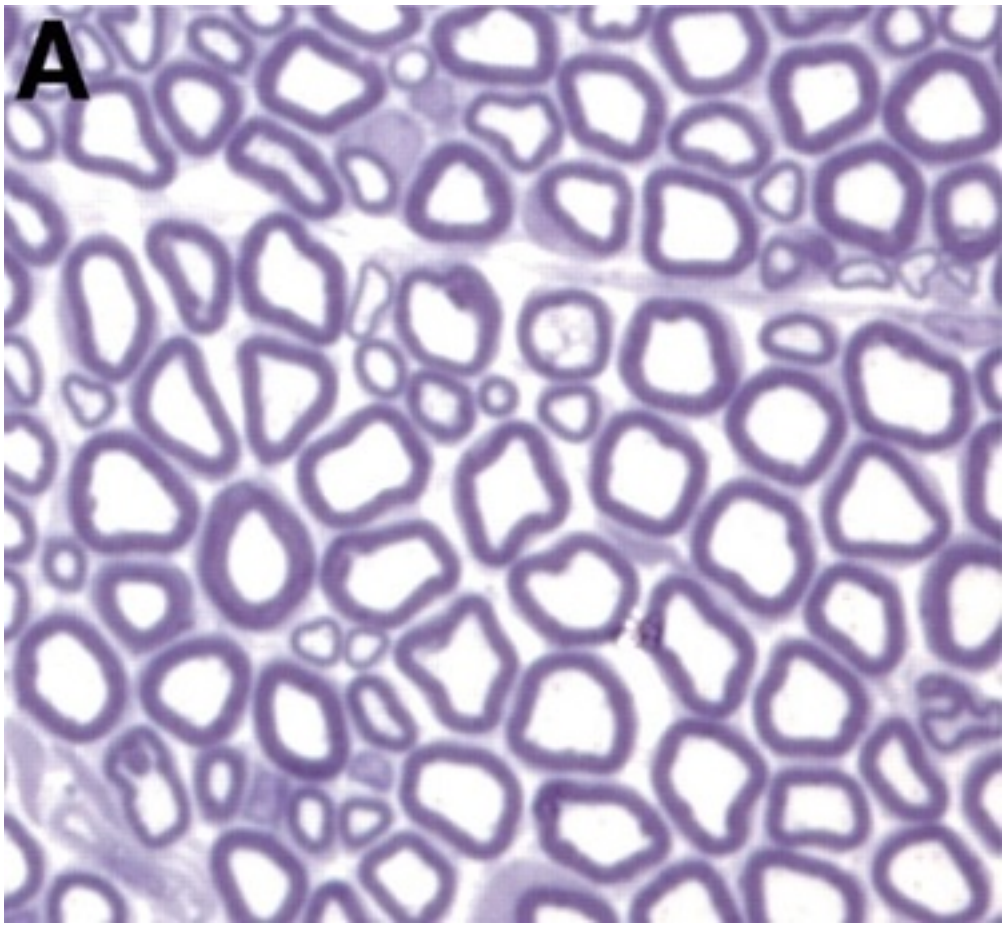

Figure 2.15: Non homogeneous distribution of axons of various diameters in a tract. Reproduced/adapted with permission of the journal Development [30].

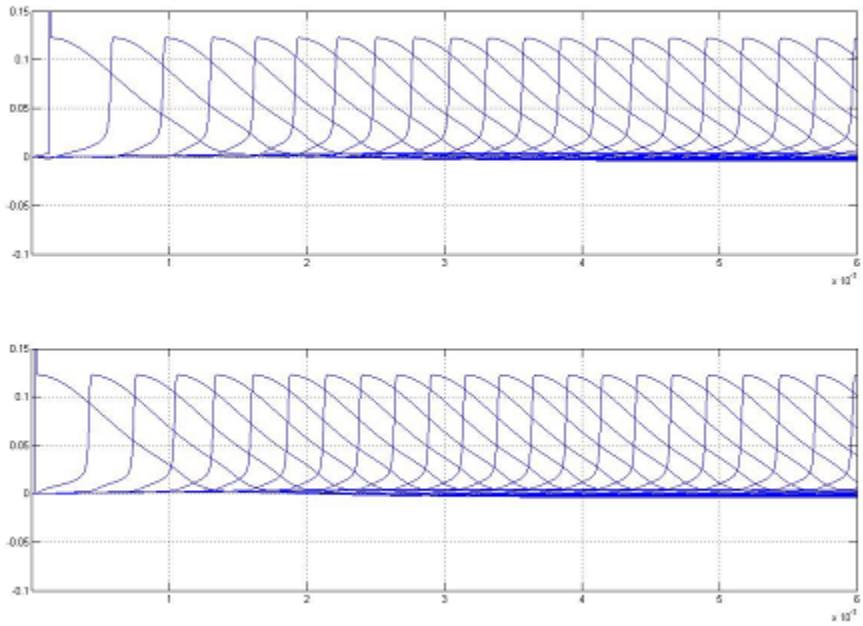

Figure 2.16: Two axons are considered, the second with 10 percent larger diameter than the first one. A smaller value of extracellular resistance is used to show the coupled and synchronizing propagation on the two fibers. The second one here is stimulated before the first one. The x-axis is time in seconds, the y-axis is in volts.

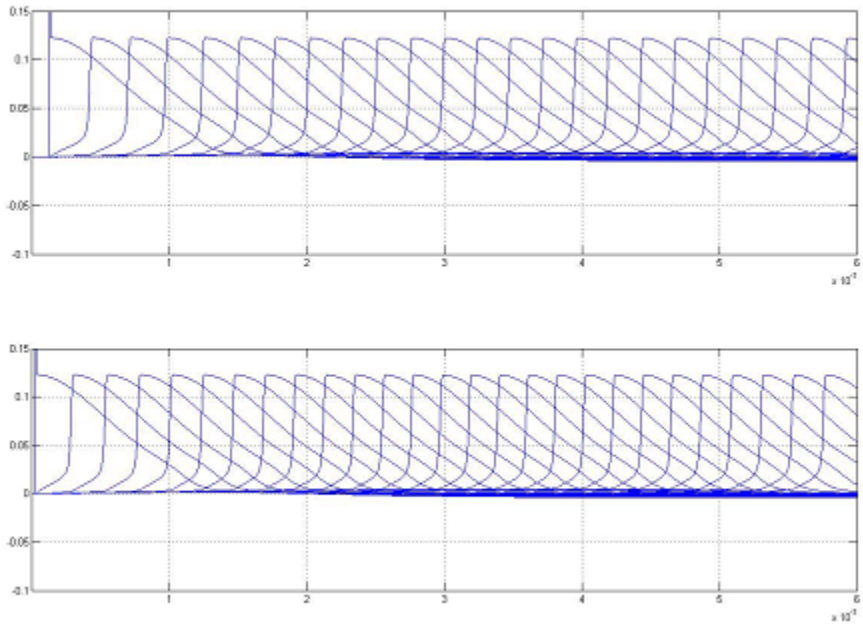

Figure 2.17: Two axons are considered, the second with 10 percent larger diameter than the first one. A null value of extracellular resistance is used to show the propagation under lack of coupling for the sake of comparison with the previous figure. The second axon here is stimulated before the first one. The x-axis is time in seconds, the y-axis is in volts.

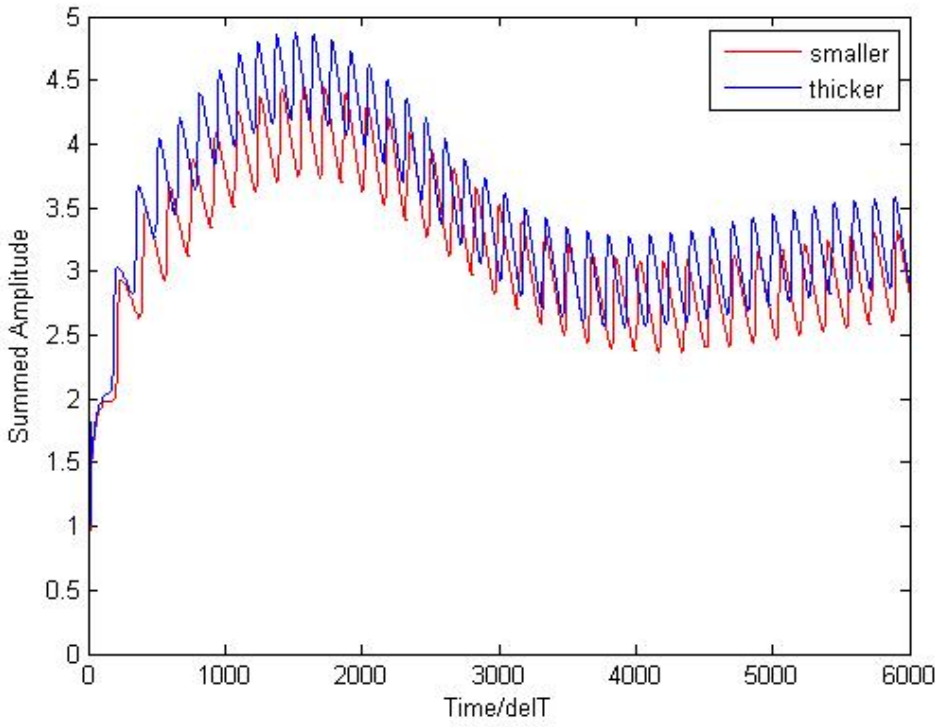

Figure 2.18: Curves showing summed voltages of two axons' nodes. To obtain these two curves, we simulated twice. Both simulations were for the case $N = 1$, but the axon diameters were varied, one being 10 percent larger than the other. In each simulation, the voltage profiles of all the nodes were summed. This yielded the two curves. The x-axis is in delta-T time units, where delta-T is the time step size, the y-axis is in volts.

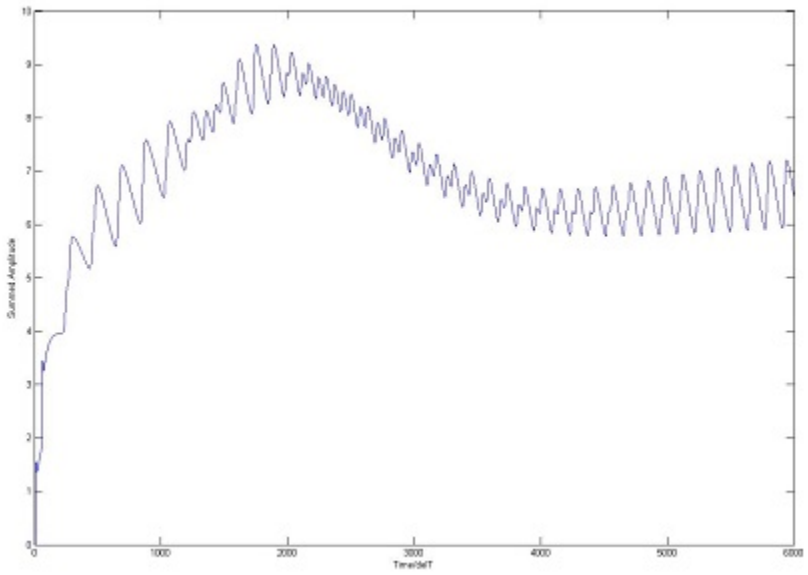

Figure 2.19: Signatures of neuronal harmony, showing perfect phase synchronization. Beats and phase synchronization when action potentials on two axons with differing diameters synchronize. To obtain this curve, we simulated the case $N = 2$, with coupling, between axons of two different diameters, differing by 10 percent. The voltage profiles at each node were summed with each other to obtain the curve. On the curve, the left side shows the onset of the 'beats' envelope. The right end shows the eventual perfect phase synchronization. The x-axis is in delta-T time units, where delta-T is the time step size, the y-axis is in volts.

CHAPTER 3 EPHAPTIC SYNCHRONIZATION

In this chapter[1] we give a simple presentation of the phenomenon of ephaptic synchronization as studied in the dissertation of Luzader. This gives the reader theory to go with the computer synchronization experiments reported in the previous chapter.

> . . . it is possible for pulses on two fibers to become coupled together and propagate with a velocity that may be different from either of the uncoupled velocities.[2]

From the electrical standpoint, the fundamental signal in the axon is the action potential. When two or more axons are placed adjacent to each other, the membrane potentials on the two axons begin to interact with one another via the extracellular space. This is known as the ephaptic interaction. It leads to synchronization of the action potentials propagating down different fibers, fibers having differing conduction velocities.

Nonlinear partial differential equations govern the ephaptic interaction and these have been studied for a long time. The ephaptic interaction itself has been explained and we have not much novelty to contribute in this chapter. For our purposes, it is sufficient to acquire an understanding of how conduction velocity changes with ephaptic coupling.

Based on the work by Katz and Schmitt who performed a variety of experiments on a pair of naturally adjacent, unmyelinated fibers from the limb nerve of a crab [29], Scott states that

> If impulses are launched at about the same time on two parallel fibers with independent impulse speeds that do not differ by more than about 10 percent, these impulses

[1] This chapter was also part of a submission to IEEE/ACM Transactions on Computational Biology and Bioinformatics. The symbols used here are defined in the previous chapter.

[2] Page 151 of Luzader's 1979 dissertation [32].

become "locked together," or synchronized. In other words, they are observed to move at exactly the same speed.

He further states,

> Both of these interaction effects are strengthened by increasing the ionic resistivity of the external medium.

Thus there is experimental evidence for synchronization. Furthermore, the literature also contains reported evidence for ephaptic coupling between myelinated fibers [33]. We turn to the analysis.

There is more than one model analyzing ephaptic coupling, but the common feature of these models is that there exist certain stable points (certain values of distance of separation between the impulses on the coupled fibers) such that if the separation increases at these stable points, so that the impulse on a fiber, say number 2, is slightly ahead of the impulse on fiber 1, then the velocity of the impulse on fiber 1 becomes larger than the velocity of the impulse on fiber 2, so that the leading pulse gets 'caught' and they lock again.

This dynamics can be modeled by the differential equation

$$\frac{d\delta}{dt} = -\left[v_1^{(1)}(\delta) - v_1^{(2)}(\delta)\right] \tag{3.1}$$

Here, δ is the distance by which an impulse on fiber 2 leads an impulse on fiber 1. The impulse velocities on the two fibers are given by:

$$\begin{aligned} v^{(1)} &= v_0 + \alpha v_1^{(1)} \\ v^{(2)} &= v_0 + \alpha v_1^{(2)} \end{aligned} \tag{3.2}$$

which represents an expansion in the coupling parameter α where terms of higher order in α have been neglected. This is based on the FitzHugh-Nagumo model of coupling [29].

Clearly, from equation (3.1), the zeros of the right hand side would decide when $\delta(t)$ is constant, i.e. a stable point. The function on the right hand side is shown in Figure 8.5 (b) in [29].

This mechanism is quite intricate and we need not go into the details. However, based on the dissertation of Luzader [32], we have that if we have two fibers of radii r_1 and r_2, we can define a parameter β [3]

$$\beta = \frac{1 - \frac{r_1}{r_2}}{1 + \frac{r_1}{r_2}} \tag{3.3}$$

such that their (dimensionless) uncoupled velocities are

$$u^{(1)} = u_0\sqrt{1-\beta} \tag{3.4}$$

and

$$u^{(2)} = u_0\sqrt{1+\beta}, \tag{3.5}$$

respectively, and their coupled velocity is given by

$$u_c = u_0\left(1 - \frac{\beta}{2} + \eta\frac{u_3(\delta)}{u_0}\right) \tag{3.6}$$

where η is the coupling parameter [4] and $\frac{u_3(\delta)}{u_0}$ is a velocity change ratio for the η-coupling that depends on the distance of separation between the two pulses, with the pulse on fiber two being ahead of the pulse on fiber one by the amount δ, and u_0 is given by

$$u_0 = \frac{1 - 2\cdot a^*}{\sqrt{a^*\cdot(1-a^*)}} \tag{3.7}$$

where a^* is a threshold parameter. For $\delta = 0$ we have that $\frac{u_3(0)}{u_0} = 0$ meaning that when the separation is zero, the coupled velocity is given by

$$u_c^{'} = u_0\left(1 - \frac{\beta}{2}\right), \tag{3.8}$$

[3] Assume that $r_1 \leqslant r_2$ always. This ensures a positive β.

[4] α is another coupling but the η coupling dominates physiologically when both are present. See page 238 in the dissertation of Luzader.

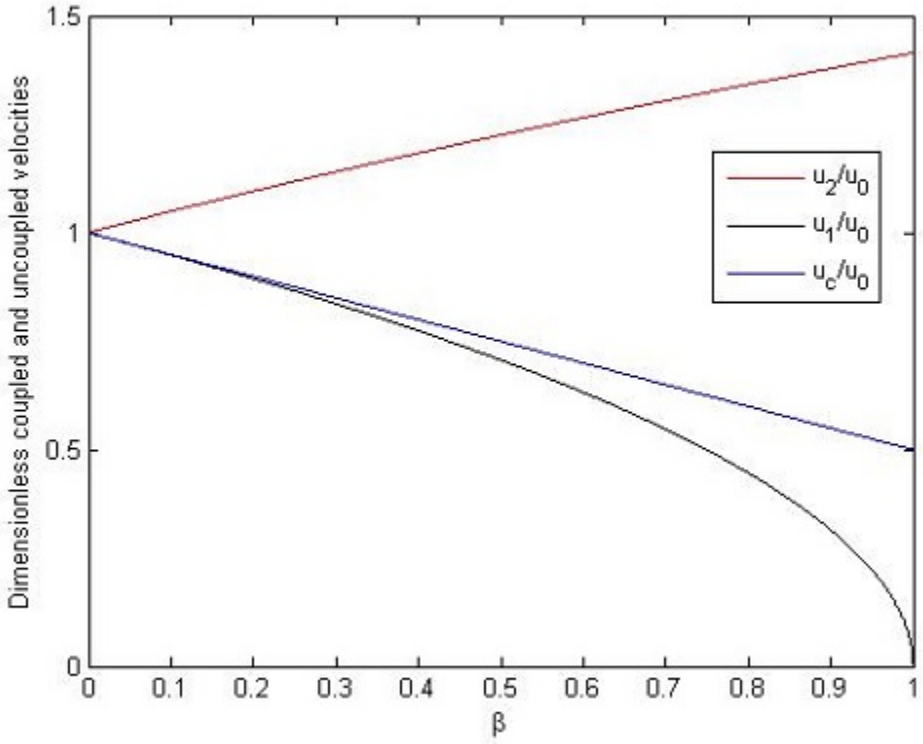

Figure 3.1: Coupled and uncoupled velocities as a function of bundle structure parameter.

i.e. it doesn't depend on the coupling parameter η. In this case, we have the relationship

$$u^{(1)} \leqslant u_c^{'} \leqslant u^{(2)}. \tag{3.9}$$

Figure 3.1, shows this relationship in detail for different values of β.

Next, we fix β and plot the velocity change ratio as a function of the separation δ. We get figure 3.2 as the result. We observe that for values of δ around the origin, $\frac{u_3(\delta)}{u_0}$ is approximately a straight line through the origin (for $\beta = 0$) with a 45 degree slope. In other words, this term is equal to δ when δ is small. Utilizing this observation in equation (3.6), we get

$$u_c = u_0 \left(1 - \frac{\beta}{2} + \eta\delta\right),\ \delta \approx 0 \tag{3.10}$$

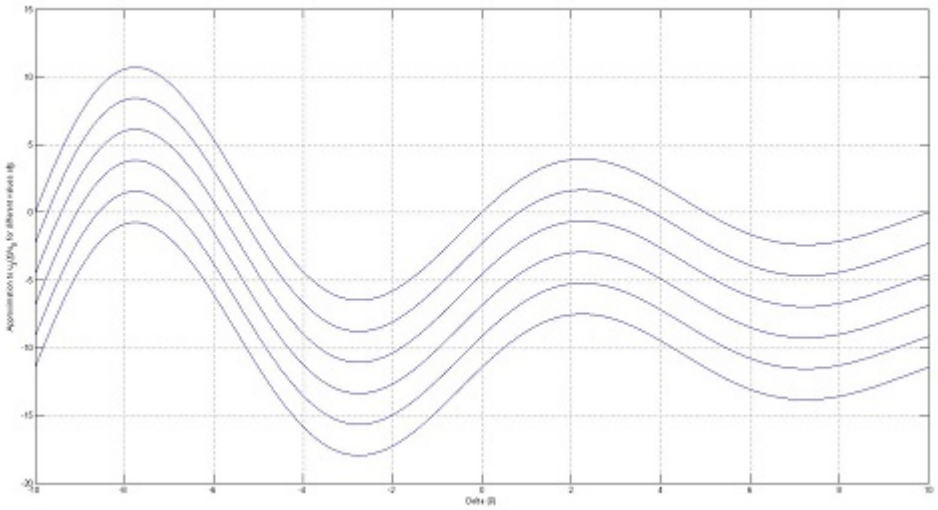

Figure 3.2: Approximation to velocity ratio for different values of beta. For different values of β, ranging from 0 (top curve) to 0.5 (bottom curve) we have plotted an approximation to the ratio of $u_3(\delta)$ to u_0 by a product of a decaying exponential and a sinusoid. Figures 6.4-1, 6.4-2 and 6.4-3 in [32] verify the linear relation for $\delta << 1$. The x-axis is δ.

and for $\beta > 0$ we get

$$u_c = u_0 \left(1 - \frac{\beta}{2} + \eta\delta + c(\beta)\right),\ \delta \approx 0 \tag{3.11}$$

where $c(\beta) < 0$, $c(\beta) \propto \beta$, is a β dependent ordinate-intercept. Thus we can write,

$$u_c = u_0 \left(1 - \left(\frac{1}{2} + k\right)\beta + \eta\delta\right),\ \delta \approx 0 \tag{3.12}$$

where $k > 0$ is a constant of proportionality. Straightforward algebraic manipulations show that

$$\delta \in \left(\frac{\beta k}{\eta}, \frac{\beta(k+1)}{\eta}\right) \tag{3.13}$$

for

$$u^{(1)} \leqslant u_c \leqslant u^{(2)} \tag{3.14}$$

to be valid for appropriate values of β and k, and any value of η. Equation (3.13) is a condition on the separation between the two pulses such that they couple to a velocity between their two

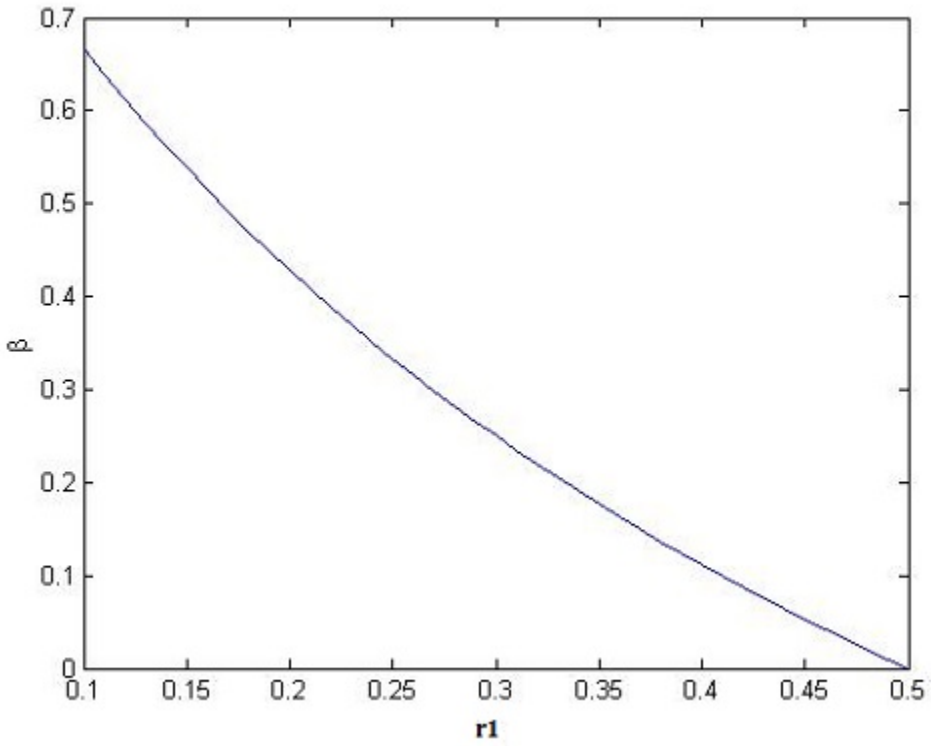

Figure 3.3: Variation of beta. β versus r_1 for fixed r_2.

uncoupled velocities.

To appreciate the relation of β to the structure of the bundle, we have shown in the next Fig. 3.3, a plot of (3.3) versus r_1 for fixed $r_2 = 0.5$. Manipulating further, the coupled velocity may be rewritten as

$$\frac{u_c^{'}}{u_0} = \left[(1 - \lambda(\beta)) * \frac{u^{(2)}}{u_0} + \lambda(\beta) * \frac{u^{(1)}}{u_0} \right] \tag{3.15}$$

where

$$\lambda(\beta) = \frac{u_c + u^{(2)}}{u^{(1)} - u^{(2)}} \tag{3.16}$$

and $0 \leqslant b \leqslant 1$ for small $\beta \approx 0$, turning it into a combination of the uncoupled velocities[5]. This is the mechanism of velocity coupling in detail. This interpolation-of-velocities form of the coupled velocity is an assumption in previous work [34]. Thus we conclude that the theory of [32] and [35] supports the beat-like phenomena that were observed in the previous chapter. The beats represent

[5] $\beta \approx 0$ means the two fibers do not differ much in their physical dimensions.

the period of active computation of the coupled velocity by the nervous system. We next move on to electric field mediated synchronization between axons in a tract.

CHAPTER 4 TOWARDS ENDOGENOUS E-FIELD MEDIATED COUPLING

Having read Chapters 2 and 3, the reader would have become convinced that velocity synchronization in axons of differing diameters is a phenomenon that can be understood via an equation for the ephaptic coupling of axons when the extracellular medium is reduced to a cable model itself Eq. (2.7). This process of equating the extracellular current and the sum of intracellular currents is due to charge conservation or Kirchoffs node-sum rule applied to this model, and applies at every node of the extracellular resistance bearing wire, denoted here by M.

How can we understand more deeply this very mechanism when the axons involved have differing diameters and therefore different conduction velocities? If the two action potentials are moving forward at different speeds, the current injected into the extracellular wire M by the one that is ahead (say the faster one) will need to sum with the current injected into the previous node of the extracellular wire by the one that is lagging. Whereas, it will actually, as per our equation (2.9), sum with a zero injection from the lagging axon, unless there is significant overlap between the two action potentials. If it sums with a zero injection, there will be no synchronization. But if it sums with a small but nonzero injection, there will be the possibility of the depolarization caused by the faster axons action potential leading to a speeding up of the slower one and thereby to synchronization. This was illustrated in Fig. 2.16.

Now we come to the case of Fig. 2.17 which assumed zero extracellular resistance. In the case of perfect alignment, but differing diameters, if one action potential is leading, it will inject at a different spatial position than the lagging action potential. But since the extracellular wire has no resistance, the two injections could sum up as in Eq. (2.9) at the present time. However, a wire with no resistance is like a perfect conductor and so the electric field everywhere within it must be zero. Thus there cannot be any spatial variation of the extracellular potential, which means that the

spatial derivative of the extracellular potential would be zero and hence when we plug back into Eq. (2.6), we would not get any coupling between the axons! This was the case captured in Fig. 2.17.

In both these cases we did not consider misalignment effects. When all the angles of inclinations of the axons are equal to zero, it is the case of perfect (parallel) alignment. For this case, we obtained Figures 2.9, 2.10 and 2.11. We saw that the order in which the axons would be excited when one of their neighbors was stimulated, is governed by the W_{ip} matrix. The column of W_{ip} which has the largest sum of its entries, will get highest priority, the one with the second largest sum will get second priority and the one with the lowest sum will get the lowest priority. The column labels correspond to the axon numbers.

However, when we made all angles thirty degrees, we observed that one of the axons (number 2) did not fire at all in some cases even though the W_{ip} matrix would still give its position in the firing sequence. Why did this axon not fire in these cases? This is because the contributions of the other axons voltages to this axons voltage got diminished by a factor equal to the cosine of the angle of inclination of this axon. Thus Figs. 2.12, 2.13 and 2.14 stand explained.

In this chapter, we will take another angle of approach to this same problem. We will consider the electric field generated by a firing axon. Our first order of business will be to determine the strength of this field. If the field is found to be very weak, it could play no role in axon-axon interaction. If the field is found to be sufficiently strong, we will then consider what its direction is. From a plot of the field vectors emanating from the axon, we will seek to determine whether those vectors can cause significant potential drops across or near the other axon. If so, then we will have a new mechanism for interaction. We will find (in Chapter 6) that these two mechanisms (current and field) may be the same mechanism in the relevant situations.

Let us look here as to why this need not be obviously the case. The reason has to do with Reutskiy et. al.'s derivation in [5]. They assumed an ad-hoc current balance equation and from it derived the ephaptic coupling term. They proposed the assumption that the extracellular potential varies only along the z direction, that is along the length of the axon tract. They further assumed

that the tract was electrically isolated. These two assumptions then allowed them to proceed with their derivation. We used the first assumption in our work of Chapter 2 to get the generalized ephaptic equation Eq. (2.12).

It is clear however, that these two assumptions are very strong assumptions. In a realistic medium the extracellular potential will vary in every direction. Further, the assumption of electrical isolation which allowed them to write the current balance equation is also strong. In a realistic setting, say in a tract with 50 thousand axons, and our location being somewhere in the interior, it should not be of consequence what the boundary regions look like, whether the boundary is electrically isolating or not. To rely upon boundary conditions to derive local effects seems to be a major assumption.

Hence we wonder whether our entire understanding is constrained by these significant assumptions. To relax these assumptions might lead to a broader understanding. It is indeed found to be the case (see Chapter 6). And moreover, when we specialize this broader understanding to the cases considered by Reutksiy, we recover the zone of validity of Reutskiys assumptions and predict the same phenomena as observed by Reutskiy and us, in Chapter 2.

Thus in this chapter we will first determine the e-field magnitude and then do a vector plot of the e-field directions. But before we enter into these details in Sections 4.3 and 4.4, we provide some background on biological electric fields to the reader.

There is a lot of evidence for the interaction between electric fields and cells [36]. Here we will derive expressions for the electric near-field generated by a ring of ion channels on a node of Ranvier of an axon. We also develop computer simulations of this data-driven field[1]. Since cells are affected by fields, there is a great likelihood that endogenous fields[2] also affect cells. This chapter is an effort towards computing such endogenous fields.

[1]The field is based on the presence of action potentials at nodes. Action potentials are present or absent on nodes in accordance with the data being transmitted or carried by the axon. Thus the field is data-driven.

[2]Endogenous fields are fields whose source is the cell itself. This would be in contrast to exogenous where the source of the field is other than the cell under consideration.

4.1 Electrophysiological Introduction

That the nervous system is electrical in its function and nature, was first described by Galvani [37] who did a series of experiments on animal electricity. Since that time, EEG has been discovered and we are now living in an era wherein we are able to measure the averaged electric field activity of large neuronal populations. These measurements are possible by means of electrodes placed on the scalp of the subject. EEG has become an important diagnostic and investigative tool for understanding brain function and malfunction [38].

What are the underlying sources of the fields that are recorded in EEG? This question has plagued neuroscientists for some time. This is a top down question where we start at the highest level - the EEG recordings and seek their underlying source. We can also pose a bottom-up question - what is the form of the electric field generated by individual axons as well as collections of neurons. To answer this latter question is the aim of this chapter.

Prior work such as that of [39], [40], or [41], has simply used cable theory and volume conduction theory in this regard. However we will go beyond such works in Section 4.4 of this chapter and compute also the three-dimensional peak e-field due to sodium activity on an axon with back-to-back action potentials present at the same time on several consecutive nodes of Ranvier when the axon is suspended in free-space.

4.2 Nature of the Current Source at a Single Ion Channel

From [18] we know that as per macroscopic laws, there are roughly 3.1×10^7 ions per second flowing through a typical Na+ channel, which corresponds to a current of about 5 pico-Amperes. This is close to the measured value of 2 pico-Amperes. This also means that a single ion takes about 32.25 nano-seconds to cross a pore. The length of a pore is about 5 Angstroms or 0.5 nano-meters. This leads to a mean velocity through the pore of

$$v_{ion} = \frac{0.5e-9}{32.25e-9} = 15.5e-3 \tag{4.1}$$

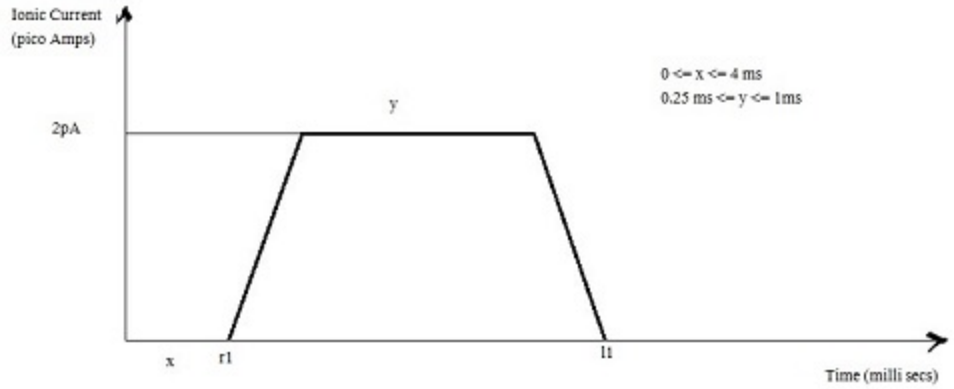

Figure 4.1: A trapezoidal open-close profile with x being the start time and y being the width.

in units of meters per second. This is certainly the non-relativistic regime.

4.3 The Electric Near Field Generated by an Ion Channel Ring

In this section our goal will be to model the opening and closing of a single ion channel with time in response to a voltage step and to compute the electric field that results from this opening-closing profile, shown in Fig. 4.1.

The next equation has the following main features. It is based on the theory presented in Chapter 2.2 of [43]. It models the volume source current density produced by an ion channel ring, in cylindrical coordinates where ρ is the radial distance from the axis of the cylinder, ϕ is the azimuthal angle and z is the distance along the axis of the cylinder. The amplitude I_0 is the magnitude of the current strength at the surface of the node of Ranvier. p is the radial distance from the cylindrical axis where the current magnitude vanishes. r_1 is the starting point in time of the PWM-PPM waveform of the ion channel current profile and l_1 is the termination point in time.

$$I_v(\vec{r'}, t) = I_0 \left(1 - \frac{\rho'}{p}\right) \delta(z') U(t - r_1) \cdot U(l_1 - t) \hat{\rho'} \tag{4.2}$$

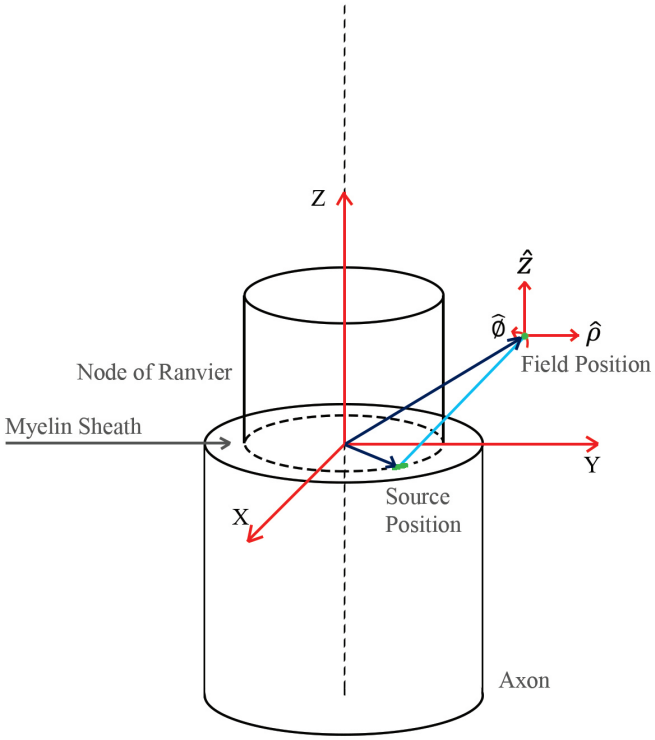

Figure 4.2: Physical setup for computation of the near electric field by an ion channel on a node of Ranvier. Courtesy Soheil Sarmadi, USF EE

Next, to find the electric field associated with this current density, we plug it into

$$\phi_{LFP}(\vec{r},t) = \frac{1}{4\pi\sigma}\int \frac{I_v(\vec{r'},t)}{|\vec{r}-\vec{r'}|}d^3r' \tag{4.3}$$

which gives the local field potential at a position $\vec{r}$ and time t as a volume integral involving the current density of the source and the distance between the source and the field positions. Next,

$$\vec{E} = -\nabla\phi \tag{4.4}$$

gives us the electric field as the negative gradient of the potential computed above. However, all of this is true only for the quasistatic approximation [44, 45]. Thus we get, upon using elementary

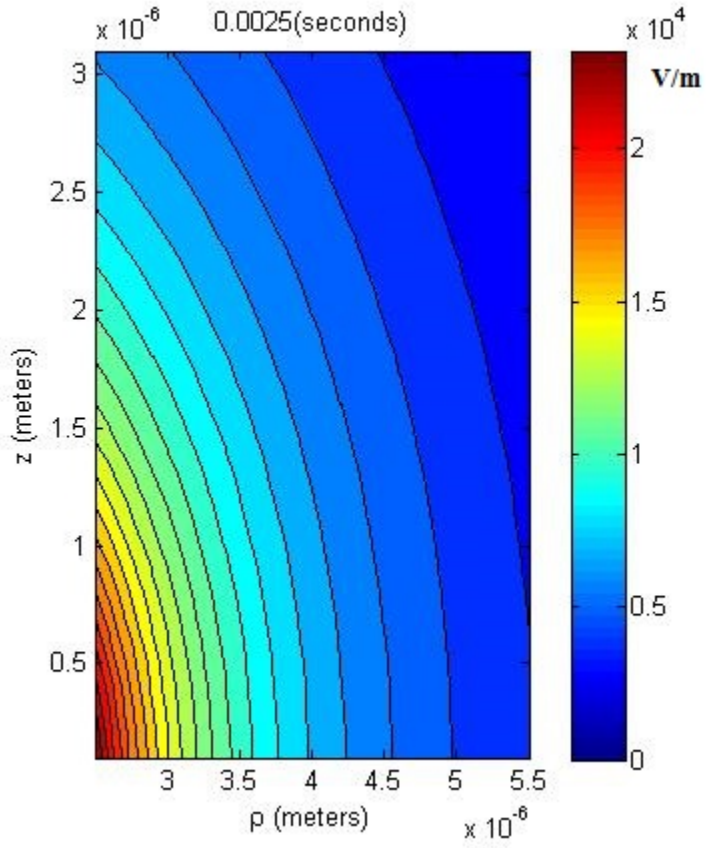

Figure 4.3: Simulation output of the electric near field of a ring of 10 equispaced ion channels on a ring of a node of Ranvier. Simulated using the volume conduction approach outlined in the present section which is based on [42]

vector analysis [46], that,

$$\begin{aligned} \vec{E_{channel}}(\vec{r}) &= \hat{k}\frac{z}{4\pi\sigma}\int \frac{I(\vec{r'})}{|\vec{r}-\vec{r'}|^3}d^3\vec{r'} \\ &+ \hat{e_\rho}\frac{1}{4\pi\sigma}\int \frac{I(\vec{r'})(\rho-\rho'\cos(\phi-\phi'))d^3\vec{r'}}{|\vec{r}-\vec{r'}|^3} \end{aligned} \tag{4.5}$$

Using the equation of a straight line segment, we find

$$\begin{aligned} I(\vec{r'}) &= 0, \text{ for } 0<\rho'<\rho_1^{'} \\ &= \delta(z')\cdot\frac{I_0}{\rho_2^{'}-\rho_1^{'}}(\rho_2^{'}-\rho'), \text{ for } \rho_1^{'}<\rho'<\rho_2^{'} \\ &= 0, \text{ for } \rho'>\rho_2^{'} \end{aligned} \tag{4.6}$$

We also note that

$$\int_{-\infty}^{\infty} 1\delta(z')dz' = 1. \tag{4.7}$$

From vector analysis we know that,

$$|\vec{r} - \vec{r'}| = \sqrt{\rho^2 + (\rho')^2 - 2\rho\rho'\cos(\phi - \phi') + z^2} \tag{4.8}$$

and

$$d^3\vec{r'} = \rho' d\rho' d\phi' dz' \tag{4.9}$$

Using these above results in the first integral, it becomes

$$\frac{I_0}{\rho_2^{'} - \rho_1^{'}} \int_{\phi'=0}^{\Delta\phi'} \int_{\rho'=\rho_1^{'}}^{\rho_2^{'}} \frac{(\rho_2^{'} - \rho')\rho' d\rho' d\phi'}{((\rho')^2 + \rho^2 - 2\rho\rho'\cos(\phi - \phi') + z^2)^{3/2}} \tag{4.10}$$

where $\Delta\phi'$ is the azimuthal thickness of the first ion channel of the ring. This is evaluated using MATLAB for user-input values of ρ, ϕ and z. Following a similar derivation to the one above, the second integral becomes

$$\frac{I_0}{\rho_2^{'} - \rho_1^{'}} \int_{\phi'=0}^{\Delta\phi'} \int_{\rho'=\rho_1^{'}}^{\rho_2^{'}} \frac{(\rho_2^{'} - \rho')(\rho - \rho'\cos(\phi - \phi'))\rho' d\rho' d\phi'}{((\rho')^2 + \rho^2 - 2\rho\rho'\cos(\phi - \phi') + z^2)^{3/2}} \tag{4.11}$$

With these two integrals explicitly in hand, we can simulate the field and its quasistatic time variation by taking the product of the field with the trapezoidal envelope shown in Fig. 4.1.

Let us look at the field magnitude at a distance of about 4 to 5 microns (lets say it is 10^4 V/m based on Fig. 4.3) from the node. This will cause a potential difference of about $10^4 \times 10^{-6} = 10^{-2} = 0.01$ Volts or 10 mV across an axons diameter. This is a significant voltage drop which can push a node over threshold if it is just below threshold. Hence we proceed with another vector based analysis which gives us the directions of the electric field as well.

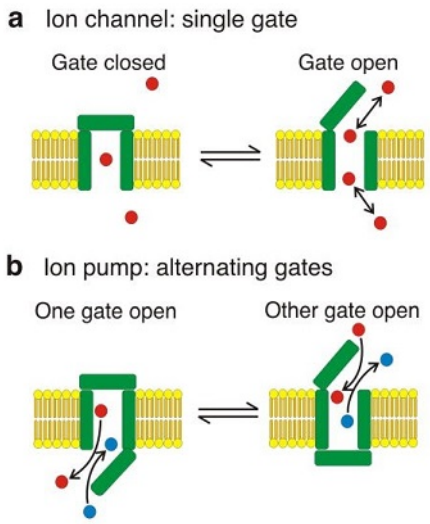

Figure 4.4: Functioning ion channels and ion pumps, part 1. Adapted by permission from Macmillan Publishers Ltd: Nature Reviews Molecular Cell Biology [48], copyright 2009.

4.4 Three Dimensional Axon Fields in Free Space

The volume conduction approach of the previous sections doesn't give much insight into the biophysics of the problem. Therefore, in this section, we adopt an approach in which the node-bearing axon is suspended in free space. Then we seek to determine the time varying electromagnetic fields at a nearby spatial point. In what follows we will assume that we are zoomed in on a node of Ranvier which is injectable as soon as its action potential comes out of the refractory phase. Thus we are looking at back-to-back action potentials. In terms of rate coded communication, this train of spikes communicates a single, highest-possible, rate, while in terms of time coded communication, this train of spikes communicates a sequence of times of arrival. For basic electrodynamics, we follow the development in chapters 10 and 11 of [47].

4.4.1 Biological Setting: Ion Channels and Ion Pumps

Action potential theory is based on ion channels. However pumps are essential to maintain resting membrane potential. They need to be understood for they will play a role in our formulation. The Figs. 4.6 and 4.7 shows a comparison of the functioning of channels and pumps.

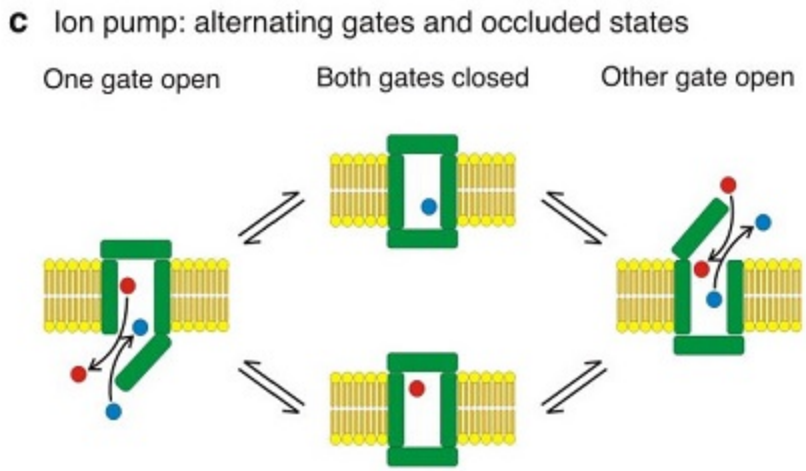

Figure 4.5: Functioning ion channels and ion pumps, part 2. Adapted by permission from Macmillan Publishers Ltd: Nature Reviews Molecular Cell Biology [48], copyright 2009.

4.4.2 Setting up the Timing of the Biophysics

In this subsection we setup the timing and introduce the main quantities that will appear in the subsequent analysis. The section is notationally heavy, but the following table 4.1 introduces all the relevant symbols and their meanings.

We note that even at rest, $q_{out} \neq q_{in}$ since the ion pumps maintain a specific concentration gradient. Let $t^{(1)}$ be the time when charge $q'(t^{(1)})$ is injected, causing depolarization. The following events occur:

1. We have $q_{Net,in}(t^{(1)}) = q_{in}(t^{(1)}) + q'(t^{(1)})$ and, $q_{Net,out}(t^{(1)}) = q_{out}(t^{(1)})$
2. Let the ion channel open due to this depolarization.
3. Let's say a charge $\Delta q''$ flows inward.
4. Thus $q_{Net,in}(t^{(2)}) = q_{in}(t^{(1)}) + q'(t^{(1)}) + \Delta q''$
5. And $q_{Net,out}(t^{(2)}) = q_{out}(t^{(1)}) - \Delta q''$
6. Let at $t^{(2)}$ the channel inactivate so no more charge can flow in.

Table 4.1: List of principal symbols and their meanings used in Chapter 4.

Symbol	Meaning
d	cell membrane thickness at ion channel position
$q_{out}(t)$	charge on the outer side of the ion channel at time t
$q_{in}(t)$	charge on the inner side of the ion channel at time t
$q'(t)$	charge injected at time t
$q_{Net,in}(t)$	net charge, inclusive of any stimulating charge, on the inner side of the ion channel at time t
$q_{Net,out}(t)$	net charge on the outer side of the ion channel at time t
$\Delta q''$	amount of charge that flows in the ion channel
$t^{(0)}, t^{(1)}, t^{(2)}$	time instants
$\Delta\tau$	full width at half maximum of the action potential
ω	angular frequency associated with the action potential
$dc(t)$	dipolar charge as a function of time
$rect$	periodic rectangle function with the parameters as specified in the text.
$\vec{p}(t)$	dipole moment vector as a function of time
$\vec{r'}, \vec{x'}$	position vector of the source
$\vec{r}, \vec{x}$	position vector of the field point
$\hat{r'}$	unit vector pointing from the dipole center to the field point
$\rho(\vec{r}, t)$	charge density at position $\vec{r}$ and time t
$\vec{r'_+}$	position vector of the outer charge concentration of the dipole
$\vec{r'_-}$	position vector of the inner charge concentration of the dipole

Table 4.1 (continued).

Symbol	Meaning
g	radius of dumbell hemispheres shown in Fig. 4.7
s	separation between centers-of-charge of the dumbell's two bells
P, P'	field, source points
f	vertical (along $\hat{z}$ direction) distance of the node from the origin
$V(\vec{r}, t)$	scalar electric potential at position $\vec{r}$, and time t
$\theta, \theta'_+, \theta'_-$	angles defined wrt the z-axis, as in Fig. 4.8
α	vector from the dipole's center to the field point.
$\vec{E_{channel}}(\vec{x})$	Electric field due to the channel at position $\vec{x}$
$\hat{n}$	unit vector pointing from the center of the dipole to the field position
$\vec{E_{ring}}(\vec{x})$	Electric field due to an entire ring of ion channels
$\vec{E_{axon}}(\vec{x'})$	Electric field due to an entire axon
E_{mag}	Magnitude of the electric field due to an entire axon

Thus, $t^{(2)} - t^{(1)} = \frac{\Delta\tau}{2}$. If action potentials are triggered back-to-back, the frequency associated with the action potential is $\omega = \frac{2\pi}{4\Delta\tau}$ radians per second where 4 is empirical. Thus $t^{(2)} - t^{(1)} = \frac{\pi}{4\omega}$ seconds.

There is a Rest $\rightarrow$ Injection $\rightarrow$ Exchange $\rightarrow$ Restoration to Rest cycle which repeats at ω radians per second. This aligns with $t^{(0)} \rightarrow t^{(1)} \rightarrow t^{(2)}$ The external charge cycles through $q_{out}(t^{(1)}) \rightarrow q_{out}(t^{(1)}) \rightarrow q_{out}(t^{(1)}) - \Delta q''$. The internal charge cycles through $q_{in}(t^{(1)}) \rightarrow q_{in}(t^{(1)}) + q'(t^{(1)}) \rightarrow q_{in}(t^{(1)}) + q'(t^{(1)}) + \Delta q''$. There is thus a baseline e-field as well as a dipole field. We will focus on the dipole field and ignore the baseline.

A few remarks are in order:

1. After inactivation there comes deactivation and then the pumps pump to restore to the $t^{(0)}$ configuration by $4\Delta\tau$ seconds.

2. Now another action potential can be initiated since we have accounted for the refractory period.

3. Only in the Exchange phase is there a dipole of charge $\Delta q''$ and separation d.

4. Fig 4.6 shows the time course of the dipolar charge. It has a an implicit rectangular envelope.

This understanding allows us to write for the dipolar charge the expression:

$$dc = \Delta q'' \cos(\frac{\pi}{\Delta\tau}t) \cdot rect \tag{4.12}$$

where $rect$ is the rectangular envelope of the Fig. 4.6. The result is a pulsating dipole:

$$\begin{aligned} \vec{p}(t) &= dc \cdot d\hat{k'} \\ &= \Delta q'' \cdot d \cdot \cos(\frac{\pi}{4\Delta\tau}t) \cdot rect\hat{k'} \end{aligned} \tag{4.13}$$

Since $dc(t)$ never changes sign, the dipole never flips. It merely strengthens and weakens *in situ*. The source is dynamic (non-static) since the charge density at source position is varying with time.

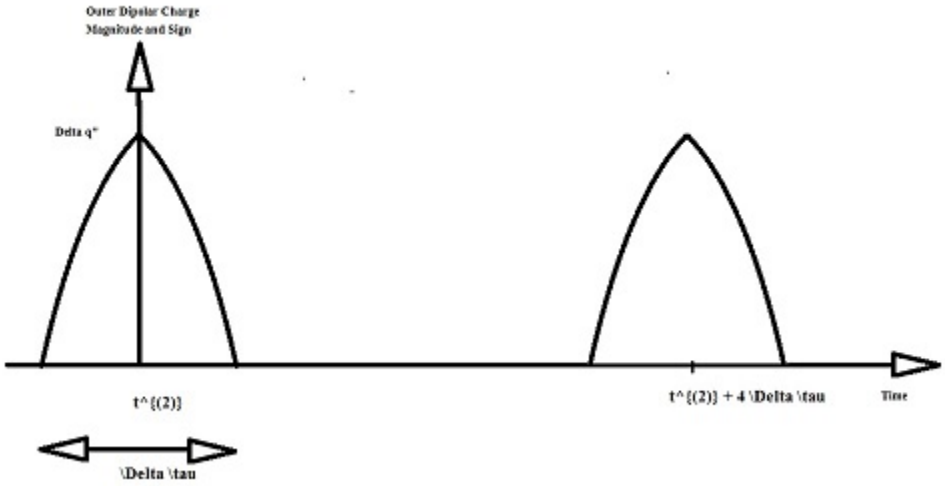

Figure 4.6: Time course of dipolar charge. The x-axis is time and the y-axis is charge.

Specifically,

$$\begin{aligned} \rho(\vec{r_+}, t) &= \frac{dc(t)}{Volume} \\ \rho(\vec{r_-}, t) &= \frac{-dc(t)}{Volume} \end{aligned} \tag{4.14}$$

Let $Volume = \frac{2\pi g^3}{3}$ be hemispherical with radius $g = \frac{lengthofnode}{2}$. g is indicated in Fig. 4.7.

4.4.3 Setting up the Coordinate System

Fig. 4.8 shows the coordinate system. P' is the source position on the nodal surface and P is the field position, the point of observation. f is the vertical distance of the ring of ion channels from the origin. $\vec{r}$ points to the field position and $\vec{r'}$ points to the source position at P'. g is the radius of the hemi-spherical charge-bearing region at the opening of the ion-channel on either side. The ion channel is delineated by the cell membrane to its left and right.

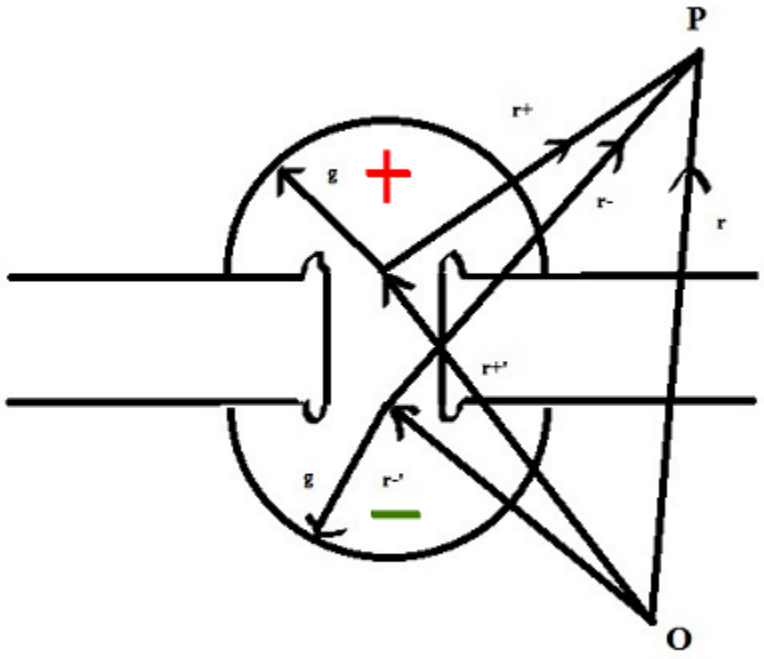

Figure 4.7: Zooming into an ion channel. $r^{+'}$ and $r^{-'}$ mark the position vectors of the outer side and the inner side of the cell membrane, while r is the position vector of the field point. g is the radius of the hemispherical bell containing positive charge on one side and negative charge on the other.

4.4.4 Computation of the Potential in Lorentz Gauge

The common gauges in electromagnetic theory are Coulomb gauge and Lorentz gauge [47]. In Lorentz gauge (see chapters 10 and 11 of [47]), for nonstatic sources, we have:

$$\begin{aligned} V(\vec{r},t) &= \frac{1}{4\pi\epsilon_0}\int \frac{\rho(\vec{r'},t_r)}{r}d\tau' \\ &= \frac{1}{4\pi\epsilon_0}\int \Delta q'' \cos(\frac{\pi}{\Delta\tau}(t-\frac{r_+}{c}))\cdot\frac{rect}{\frac{2}{3}\pi g^3 r_+}d\tau' \\ &- \frac{1}{4\pi\epsilon_0}\int \Delta q'' \cos(\frac{\pi}{\Delta\tau}(t-\frac{r_-}{c}))\cdot\frac{rect}{\frac{2}{3}\pi g^3 r_-}d\tau' \end{aligned} \tag{4.15}$$

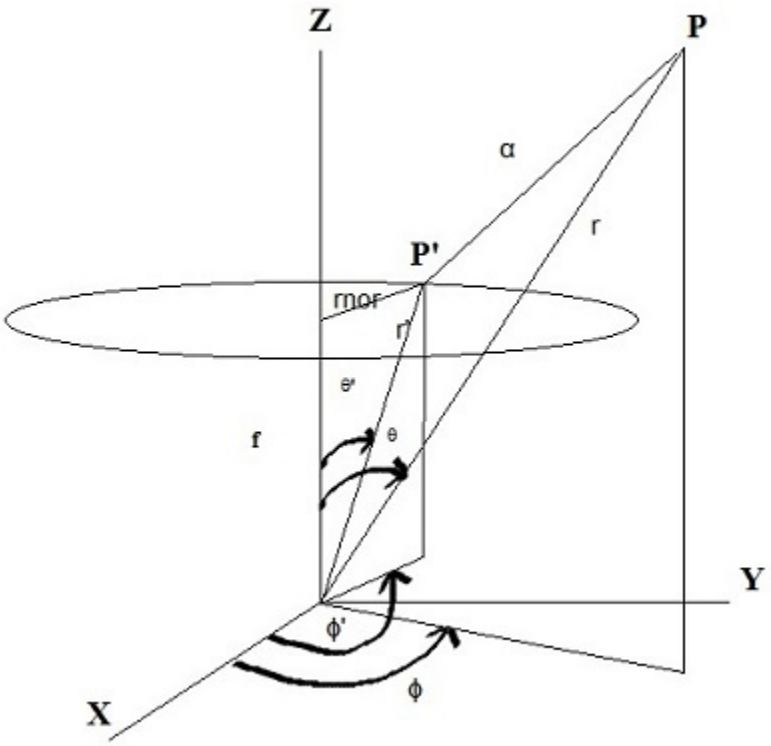

Figure 4.8: The spherical coordinate system.

We will assume that P is far from source so that the $\Delta q''$ is uniformly distributed throughout the hemisphere. Therefore,

$$\begin{aligned} V(\vec{r},t) &= \frac{1}{2\pi\epsilon_0}\cdot(\Delta q''\cos(\frac{\pi}{\Delta\tau}(t-\frac{r_+}{c}))\cdot\frac{rect}{r_+}) \\ &- \frac{1}{2\pi\epsilon_0}\cdot(\Delta q''\cos(\frac{\pi}{\Delta\tau}(t-\frac{r_-}{c}))\cdot\frac{rect}{r_-}) \end{aligned} \tag{4.16}$$

It remains to find r_+ and r_- which are indicated by α in Fig. 4.8. From the Law of Cosines we have:

$$r_+ = \sqrt{r_+'^2 + r^2 - 2rr_+'\cos(\theta-\theta_+')} \tag{4.17}$$

and

$$r_- = \sqrt{r_-'^2 + r^2 - 2rr_-'\cos(\theta-\theta_-')} \tag{4.18}$$

The final potential is:

$$
\begin{aligned}
V(\vec{r},t) &= \frac{\Delta q''}{2\pi\epsilon_0} rect(\frac{2\pi}{4\Delta\tau}, 1, \Delta\tau) \\
&\cdot \frac{(\cos(\frac{\pi}{\Delta\tau}(t - \frac{\sqrt{r_+^{'2} + r^2 - 2r_+^{'} r\cos(\theta - \theta_+^{'})}}{c}))}{\sqrt{r_+^{'2} + r^2 - 2rr_+^{'}\cos(\theta - \theta_+^{'})}} \\
&- \frac{\cos(\frac{\pi}{\Delta\tau}(t - \frac{\sqrt{r_-^{'2} + r^2 - 2r_-^{'} r\cos(\theta - \theta_-^{'})}}{c}))}{\sqrt{r_-^{'2} + r^2 - 2rr_-^{'}\cos(\theta - \theta_-^{'})}})
\end{aligned}
\tag{4.19}
$$

Now let the ring be at a distance f from the origin, along the z axis, so

$$
r_+^{'} = \sqrt{f^2 + (nodalradius + \frac{d}{2})^2} \tag{4.20}
$$

and

$$
r_-^{'} = \sqrt{f^2 + (nodalradius - \frac{d}{2})^2}. \tag{4.21}
$$

Also, $\tan\theta_+^{'} = \frac{nodalradius + \frac{d}{2}}{f}$ and $\tan\theta_-^{'} = \frac{nodalradius - \frac{d}{2}}{f}$. Thus, the potential is completely specified.

4.4.5 Computation of the Fields

At this point we assume that the vector potential will be negligible in its time rate of change and the electric field is to be determined entirely from the spatial gradient of the scalar potential. We thus assume static (not growing and diminishing) dipoles for the ion channel dipoles.

Jackson [49] performs the above computation which we have done for the special case of a biological dipole, and finds also the electric field due to the dipole. We can now switch to his computation since we note that the result we have obtained above 4.19 is akin to the standard dipole formula for the potential. We will therefore use the following formula for the quasistatic field of an ion channel dipole:

$$
\vec{E_{channel}}(\vec{x}) = \frac{3 \cdot \hat{n} \cdot (\vec{p} \cdot \hat{n}) - \vec{p}}{|\vec{x} - \vec{x'}|^3} \tag{4.22}
$$

To apply this formula, we need the dipole moment vector. The magnitude is the dipolar charge $\Delta q''$ times the separation between the charges, d, which is the membrane thickness. The direction would be pointing from the intracellular hemisphere of radius g to the extracellular hemisphere of radius g. The charge $\Delta q''$ may be considered to be concentrated at the center of mass of the hemisphere. This center of mass lies about $\frac{3g}{8}$ above the cell membrane on the outer side and about $\frac{3g}{8}$ meters below the cell membrane on the inner side of the axon. This gives us the separation to be about $s = (d + \frac{3g}{4})$ meters.

As for the direction, we know the position vectors of the center of the dipole to be r' and the height of the dipole to be f along the z-axis. The unit vector giving the direction of the vector from this point to the center of the dipole is therefore

$$\text{unitvector} = \frac{\text{vectdiff}((r', \theta', \phi'), (f, 0, 0))}{\text{magnitude of vectdiff}} \tag{4.23}$$

where vectdiff stands for the vector difference in the position vectors of the two points. Thus, the dipole moment is

$$\vec{p} = \Delta q'' \cdot s \cdot \text{unitvector}$$

Next, we need to know $\hat{n}$ which is a unit vector pointing from the center of the dipole at the center of the cell-membrane and ending at the field point. This would be the vector denoted by α in the figure 4.8. We know,

$$\vec{\alpha} = \vec{r_-} - 0.5 \times (\vec{r'_+} - \vec{r'_-}) \tag{4.24}$$

This yields

$$\hat{n} = \frac{\vec{\alpha}}{||\vec{\alpha}||} \tag{4.25}$$

Further, $\vec{x}$ is the position of the field point, which would be fixed in a given problem. $\vec{x'}$ is the position of the center of the dipole. This is denoted by $\vec{r'_+}$ (for the positive charge-head) and $\vec{r'_-}$ for

the negative charge-head. Thus the position of the center of the dipole is given by

$$\vec{x'} = \vec{r_-^{'}} + \frac{1}{2} \cdot (r_+^{'} - r_-^{'}) \tag{4.26}$$

The net field due to a ring of circumferentially equispaced ion channels is

$$\vec{E}_{ring}(\vec{x}) = \sum_{\phi'} \vec{E}_{channel}(\vec{x}) \tag{4.27}$$

The net field due to an axon with several equispaced rings is

$$\vec{E}_{axon}(\vec{x}) = \sum_{f} \vec{E}_{ring}(\vec{x}) \tag{4.28}$$

In this last equation we note that not all the rings need have action potentials at the same time. Taking this into account makes it a data-driven setup.

4.4.6 Simulation Results

Fig. 4.9 shows the peak electric field strength due to solely sodium channels on four nodes of Ranvier of a single axon. The field decays with distance as expected. The field directions are the superpositions of the fields of several dipoles from all the rings. The anisotropy in the $\pm z$ direction is due to edge effects and partly due to the nature of the plot, being a Cartesian representation of points that are really equispaced only in spherical coordinates. Further, quiver3 of MATLAB scales the arrows to fit the figure.

4.5 Conclusion

In this chapter we determined the magnitude and direction of the electric field generated by an active axon. That the electric field generated by an axon has a periodic structure is clear from Fig. 4.9. But what is the impact of an imposed electric field, whether endogeneous (to the body of the organism) or external, on an axon? Beyond the discussion in this chapter, the reference [51]

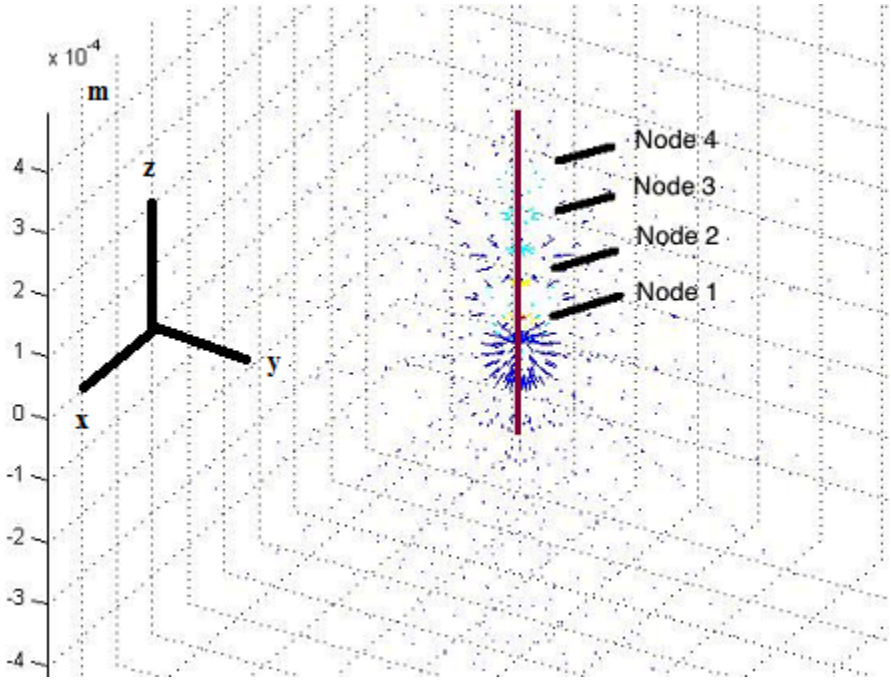

Figure 4.9: Zoomed in electric field due to sodium channels on nodes of Ranvier of an axon with four nodes. Every alternate 'ring' of arrows is close to a nodal position. The color scheme is: a. $E_{mag} < 1e6V/m \rightarrow$ blue. b. $1e6V/m < E_{mag} < 1e7V/m \rightarrow$ cyan. c. $1e7V/m < E_{mag} < 5e7V/m \rightarrow$yellow and d. $E_{mag} > 5e7V/m \rightarrow$ red. The peak magnitude is about $9e8$ Volts per meter, larger than the volume conduction approach values presented in Section 4.3 and in rough agreement with the values provided in [50]. The x, y and z axes are in meters.

shows that transected nerves can regrow rapidly and correctly in the presence of gentle applied electric fields. This suggests a significant interaction between fields and axons. We leave it to future work to study the mechanism that allows a field to induce growth in nerve, but it is clear that this chapter may bear relevance for such a study.

In Chapter 6 we will see the consequences of the results of this chapter, in terms of explaining (field-mediated) synchronization between action potentials on axons having differing diameters. For now, we turn to noisy axon tracts and their capacity.

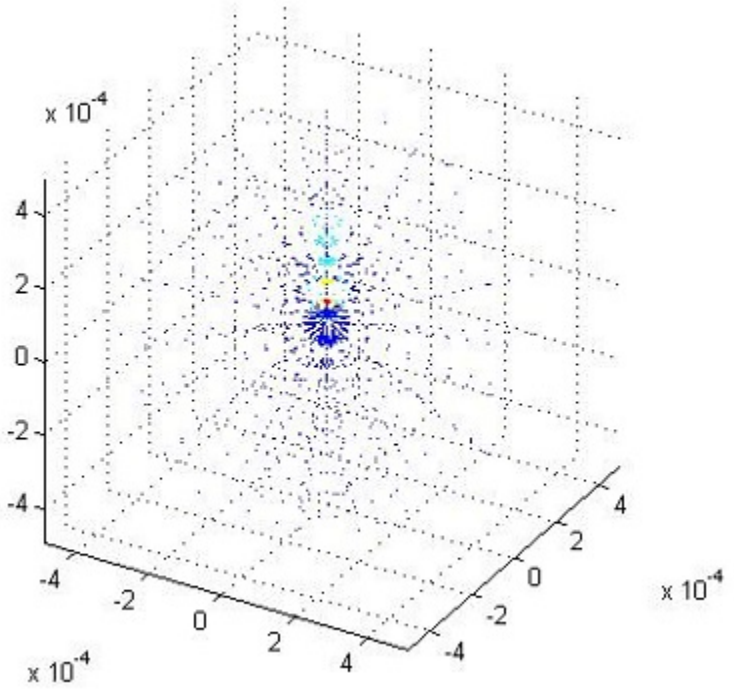

Figure 4.10: Zoomed out electric field due to sodium channels on nodes of Ranvier of an axon with four such nodes. The x, y and z axes are in meters.

CHAPTER 5 AXON TRACT AS A COMMUNICATION CHANNEL

An axon tract is like a multiple input multiple output communication system, in an information theoretic viewpoint. The governing Generalized Ephaptic Equation (2.12) for this tract was derived in Chapter 2 of this dissertation. In this chapter, we will take a look at two additional modifications of this equation which turn this axon tract into a MIMO-like communication system, more precisely a vector Gaussian channel with perfect feedback. This chapter therefore forms a stepping stone for future theoretical work on this channel.

5.1 Modification A

The first modification has to do with the nature of the W_{ip} matrix that appears in the Generalized Ephaptic Equation. Suppose by tomography, one has determined the exact geometrical placement of axons in a tract. This data has then to be incorporated into the Generalized Ephaptic Equation. One way to do this, is to incorporate it in the $W_{ip}-$matrix. However, as it stands, the $W_{ip}-$ matrix currently takes only one distance between each pair of axons. But tomography might yield a complicated set of position dependent distances. To incorporate such a complicated geometry into the equations, all one needs to do is to make the $W_{ip}-$matrix itself position dependent. Thus, letting z be the coordinate along the tract axis, we let the W_{ip}-matrix be $z-$dependent. This means that for every position along the z axis, we have a separate W_{ip} matrix. Practically we would need to segment the $z-$axis and have one W_{ip} matrix per segment which will give the interaxonal distances in that segment. The next segment's W_{ip} matrix will give the interaxonal distances in that segment. Since the change in W_{ip} from segment to segment will be gradual (the axons are smooth though tortuous), $W_{ip}(z)$ is a differentiable matrix function of a single variable. With this

modification in place the Generalized Ephaptic Equation (2.12) becomes:

$$\begin{aligned} C_i \frac{\partial V_i}{\partial t} &= G_i^{ax} \cos^2 \theta_i \left[\frac{\partial^2 V_i}{\partial z^2} - \sum_{axons} W_{ip}(z) K_p \frac{\partial^2 V_p}{\partial z^2} \right] \\ &- G_i^{my} V_i + I_i^{inj}. \end{aligned} \tag{5.1}$$

5.2 Modification B

We go on to note that the ephaptic signals (the second spatial derivatives of the transmembrane voltage) are travelling through the extracellular space. This space possesses various ions moving in various directions. To capture all the random thermal motion of these ions and the resultant 'noise' we introduce a linear, additive, noise term $n(z,t)$ to the 'signal' term. Thus, the Generalized Ephaptic Equation now becomes

$$\begin{aligned} C_i \frac{\partial V_i}{\partial t} &= G_i^{ax} \cos^2 \theta_i \left[\frac{\partial^2 V_i}{\partial z^2} - \sum_{axons} W_{ip} K_p \frac{\partial^2 V_p}{\partial z^2} + n_{ip}(z,t) \right] \\ &- G_i^{my} V_i + I_i^{inj}. \end{aligned} \tag{5.2}$$

This noise term $n_{ip}(z,t)$ may be a simple Gaussian noise process. At each position along the tract axis, there is a time varying stochastic noise process which gets added to each path between the axon under consideration and the other axons. Illustratively, this means that an ephaptic signal which is coming from axon 2 towards axon 1, at a position z_m along the tract axis, gets additively disturbed by a noise variable $n_{12}(z_m, t)$ in a time-varying way.

5.3 The Tract as a Channel

It is clear from the above that the axon tract is quite a non-trivial communication channel which is combining the voltages (or their derivatives) on the various axons, at various positions in a noisy and attenuating way. It is a fascinating question to ask, "What is the communication capacity of such a channel?" To compute this communication capacity, we propose the following approach but don't carry it out for that would be beyond the scope of this dissertation. We will

however, provide the reader with some guiding details in Sections 5.3.1 and 5.3.2. The approach is:

- We look at the Crank Nicolson matrix multiplication step which gives the next state from the current state.
- We take all coefficient matrices to the right hand side by Singular Value Decomposition [52].
- This yields the next state vector in terms of the present state vector and feedback due to the ionic current dependencies.
- This can be then compared to a vector Gaussian channel with perfect feedback.
- The capacities of such channels are known in the information theory literature and so the capacity of the axon tract can be estimated.
- We can thus compute the tract capacity with and without ephaptic coupling by simply modifying the coefficient matrices.

Here this channel is defined in an implicit way with the attenuation and noise being embedded in the governing equation system. Another channel which is defined in this complicated, embedded way is the Poisson or direct detection photon channel. It turns out that this Poisson channel is also useful for modeling neuronal communication systems.

The fundamental limits of communication over the Ephaptic Tract will need to be carefully found out. However, with our simulation of the generalized ephaptic equation in hand, we can introduce these two modifications and run simulations to determine an empirical range of rates that can be handled by a tract. The capacity would then be the least upper bound on these rates such that there is a vanishing probability of communication error. Some of these fascinating questions are left for future work.

5.3.1 Details

In this subsection we give the details of the steps outlined above which lead to the view that the axon tract is a vector Gaussian channel with perfect feedback[1].

First of all, consider the following equation which shows the Crank-Nicolson matrix multiplication step.

$$[A] \cdot \tilde{\tilde{V}} = [B] \cdot \tilde{V} + \tilde{j_{ion}} + \tilde{j_{stim}} \tag{5.3}$$

where A is the LHS matrix of coefficients in the Crank Nicolson discretization procedure output and B is the RHS matrix of coefficients in the Crank Nicolson discretization procedure output. V with two tildes is the set of voltages at the next time step and V with a single tilde is the set of voltages at the present time step. Similarly j_{ion} and j_{stim} have a single tilde and so are the ionic and stimulation currents at the present time step. We can perform a singular value decomposition of A in order to invert it and take it to the other side. This yields:

$$\tilde{\tilde{V}} = [A]^{-1}[B] \cdot \tilde{V} + [A]^{-1}(\tilde{j_{ion}} + \tilde{j_{stim}}) \tag{5.4}$$

Let $K = [A]^{-1}[B]$. In addition we know that the ionic current itself obeys a first order differential equation in time (2.3). The ionic current variable m thus obeys the expression:

$$\tilde{\tilde{m}} = diag(\eta_m \cdot \tilde{V}(1,n), \eta_m \cdot \tilde{V}(2,n), \ldots) \cdot \tilde{m} + \left[\eta_m^{'}(\tilde{V}(1,n)); \eta_m^{'}(\tilde{V}(2,n)); \ldots\right] \tag{5.5}$$

where $T_1 = diag(\eta_m \cdot \tilde{V}(1,n), \eta_m \cdot \tilde{V}(2,n), \ldots)$ and $T_2(n) = \left[\eta_m^{'}(\tilde{V}(1,n)); \eta_m^{'}(\tilde{V}(2,n)); \ldots\right]$. Here η_m and $\eta_m^{'}$ are rather complicated expressions that depend on $\tilde{V}(i,n)$. These can be reconstructed by simply discretizing the differential equation for m. Note that $diag$ is the matrix operation that puts the arguments into a new matrix's diagonal entries. Further, the ionic current is

[1]Note that this section is a very basic outline of the full derivation of Eq. (5.16) which would involve much more book-keeping of the details of all the ionic variables.

of the form

$$j_{ion}(i,n) = (constant) \cdot f(\tilde{V}(i,n)) \cdot m(i,n) + \ldots n(i,n) + \ldots \tag{5.6}$$

where f is a function. Let $R = [A]^{-1} \cdot diag(f(\tilde{V}(1,n)), f(\tilde{V}(2,n), \ldots)$ and $S = T_1$. Then we obtain,

$$\tilde{\tilde{V}} - \tilde{\tilde{m}} = K\tilde{V} + R\tilde{m} + j_{stim} - S \cdot \tilde{m} - \mathbb{I}_L \cdot T_2 \tag{5.7}$$

where $\mathbb{I}_L$ is the identity matrix. Similarly,

$$\tilde{\tilde{V}} + \tilde{\tilde{m}} = K\tilde{V} + R\tilde{m} + j_{stim} + S \cdot \tilde{m} + \mathbb{I}_L \cdot T_2 \tag{5.8}$$

5.3.2 Input-output Relationship

Let's perform an offline computation of the next time step voltages and ionic currents using the above system. In what follows we will do all the computation assuming the ionic current depends solely on the variable m plus some additive noise and knowing that we can always incorporate additively, the other variables n, h and p to get the full ionic current expression. The steps are as follows:

- Step 1: Initialization. We specify $V(i,n)$ for all i and $n = 1$. We also specify $j_{ion}(i,n)$ for all i and $n = 1$.
- Step 2: Input. We specify j_{stim}.
- Step 3: Compute:

$$(\tilde{\tilde{V}} + \tilde{\tilde{m}})(2) = K \cdot \tilde{V}(1) + (R + S) \cdot \tilde{m}(1) + j_{stim} + diag(T_2(1)) \tag{5.9}$$

- Step 4: Compute:

$$(\tilde{\tilde{V}} - \tilde{\tilde{m}})(2) = K \cdot \tilde{V}(1) + (R - S) \cdot \tilde{m}(1) + j_{stim} + diag(T_2(1)) \tag{5.10}$$

- Step 5: From Steps 3 and 4 we can easily recover $\tilde{\tilde{V}}(2)$ and $\tilde{\tilde{m}}(2)$.
- Step 6: Similarly we obtain for all $n > 2$, $\tilde{\tilde{V}}(n)$ and $\tilde{\tilde{m}}(n)$.

Let x_n be the state of the system at time n, consisting of the voltage and the activation variable. Then we have

$$x_0 = \left[\tilde{V}(1), \tilde{m}(1)\right] \tag{5.11}$$

and

$$x_1 = x_0 \begin{bmatrix} K & K \\ R+S & R-S \end{bmatrix} + [j_{stim}, j_{stim}] + [F(x_0(1)), -F(x_0(1))] + [N, N] \tag{5.12}$$

where F is based on T_2 above. Thus $Y_1 = x_1$ is given by the above expression. This is the channel output at time 1. Now the next output is not taken at the next time step, but rather on time step 4. This allows the two intermediate timesteps to be available for computational settling down of the tract. Likewise, after 4, the next output is taken at time 6 and so on.

This mechanism of data flow during the computation is illustrated in Fig. 5.1. Here H is the matrix which is given by:

$$\begin{bmatrix} 1/2 & 1/2 \\ 1/2 & -1/2 \end{bmatrix} \tag{5.13}$$

and Z is given by

$$\begin{bmatrix} K & K \\ R+S & R-S \end{bmatrix} \tag{5.14}$$

I is the identity. The pyramidal top part is another computation that inputs a function of the previous time step's $\tilde{\tilde{V}}$ into both the upper rail and the lower rail of the next time step. If we follow this data-flow diagram of Fig. 5.1, we obtain:

$$Y_2 = x_4 = x_1 \cdot H \cdot Z + [F(1/2(x_1(1) + x_1(2))), F(1/2(x_1(1) + x_1(2)))] + [j_{stim}(2), j_{stim}(2)] \tag{5.15}$$

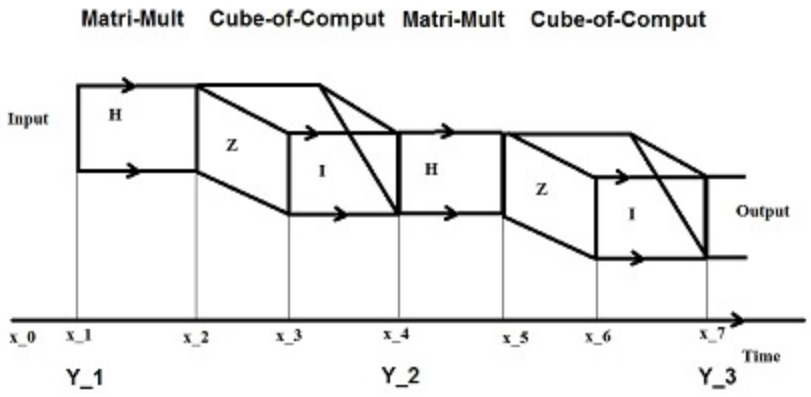

Figure 5.1: Computation process of reaching the output from the input. Matrix multiplication followed by a cube of computation to produce the next output.

In general we obtain that

$$Y_2 = D(Y_1) + x_2 + N_2 \tag{5.16}$$

This is the key result which shows us that the system is acting as a perfect feedback vector Gaussian noise channel. It is called perfect because D is a deterministic function, and Gaussian because we chose to add Gaussian noise to the ephaptic coupling term. Under the assumption of all noise terms having the same distribution, this Gaussian noise term can be added to the ionic current term instead of the ephaptic coupling term. This is a key assumption in the above analysis.

5.4 Initial Noisy Simulations

We have run some initial simulations of the noisy ephaptic master equation (5.2) shown in this chapter. An immediate question which is highlighted by these simulations is whether synchronization is robust to noise, and if so, how much noise? This will not be answered here, but is only a suggested direction for future research.

5.4.1 Two Axons

The two axon case output of Figs. 5.2, 5.3 and 5.4 reminds one of a cellular automaton moving on a two dimensional graph, providing an interesting link between noisy neural processes

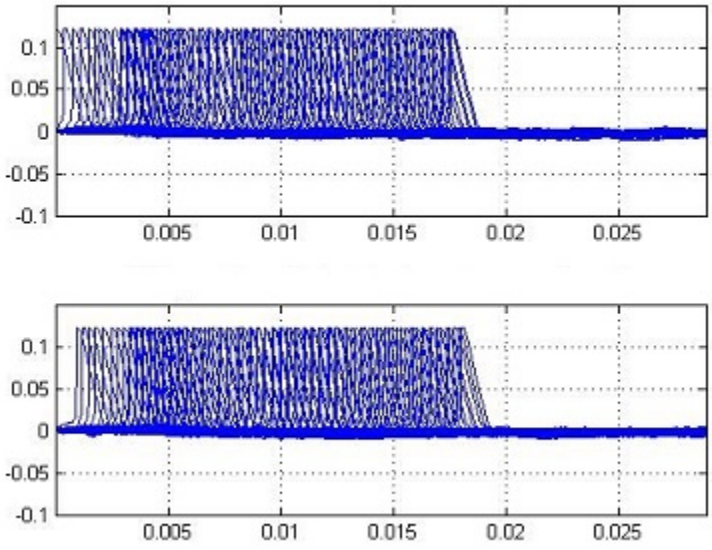

Figure 5.2: Output when one of two axons is stimulated under noisy ephaptic coupling. Voltage (y-axis) in volts vs time (x-axis) in seconds.

and attempts to explain life itself [53]. However one should note that what the output is showing, is that at certain time instances, spatially much separated nodes fire impulses together. This effect is caused by noise crossing threshold at several positions simultaneously. Yet the overall 'track' persists appearing as a connected curve, perhaps because the underlying biophysical medium is common (with a physical-medium-fixed conduction velocity).

5.4.2 Three Axons

Further, under this setting, why restrict to several one-dimensional cables? We can speculate on entire sheets of Hodgkin Huxley membrane which would then have propagation in two dimensions, with different sheets interacting via ephaptic coupling. This would perhaps model cortex well. We would also like to point to the reader that these results should be contrasted with the back-propagation or antidromic propagation effects that have been noted in the literature such as [5]. The following Figs. 5.5, 5.6, 5.7 and 5.8 show the output when an axon tract consisting of three axons is stimulated under noisy ephaptic coupling conditions. Fig. 5.5 shows the time course of action potentials propagating on all three axons. A region of overlap is visible on axon 1. To

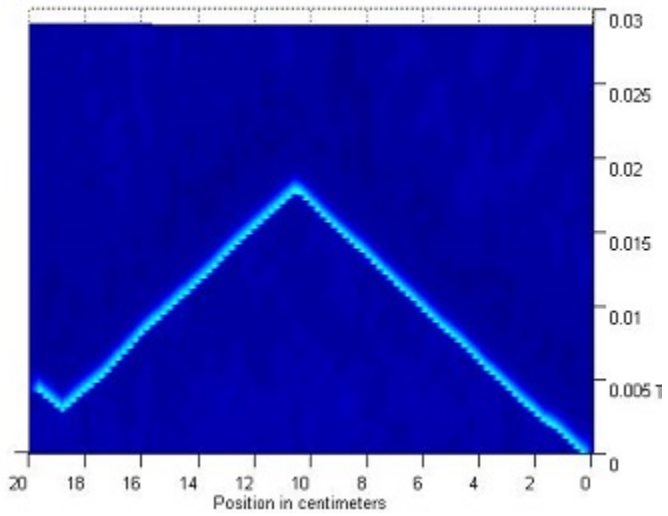

Figure 5.3: Output when the first axon is stimulated, under noisy ephaptic coupling. x-axis is position in centimeters, $y-$axis represents time.

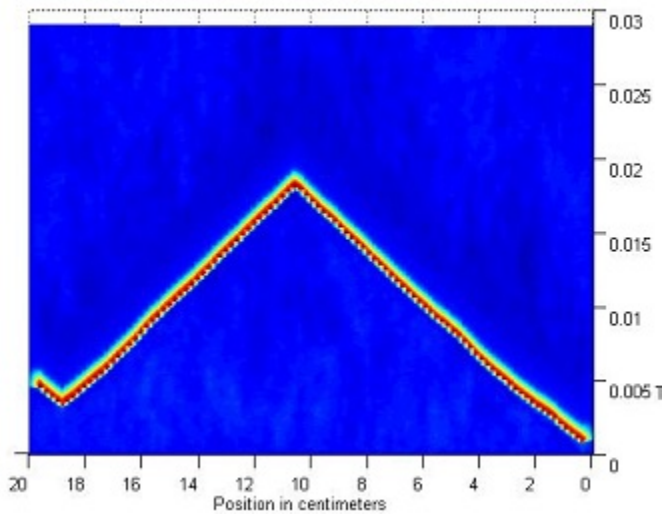

Figure 5.4: The second, unstimulated axon, under noisy ephaptic coupling. x-axis is position in centimeters, $y-$axis represents time.

view this region of overlap in detail we go to Fig. 5.6 which shows a three dimensional perspective that illuminates the presence of an anti-dromic noise-created action potential on axon 1. Figs. 5.7 and 5.8 show a similar three dimensional view for axons 2 and 3. Change in velocity is visible in the figure for axon 3, Fig. 5.8. This is usually the harbinger of synchronization.

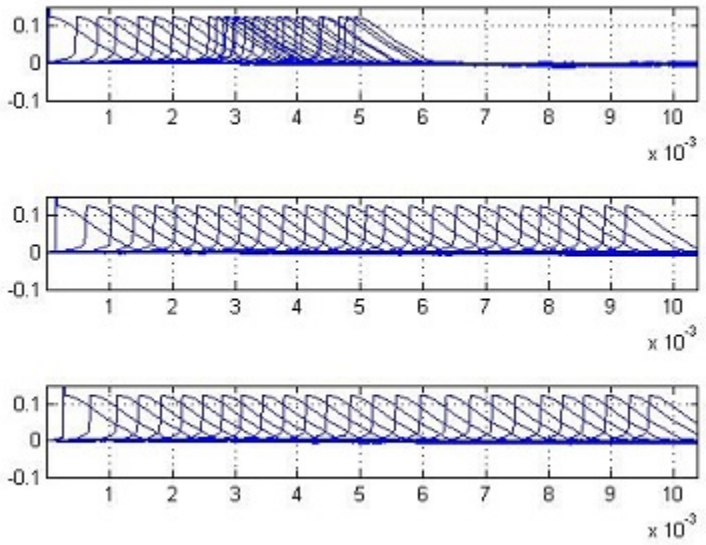

Figure 5.5: Output when all three of three axons are stimulated. Voltage (y-axis)in volts vs time (x-axis) in seconds. Axons are numbered 1, 2 and 3 from top to bottom.

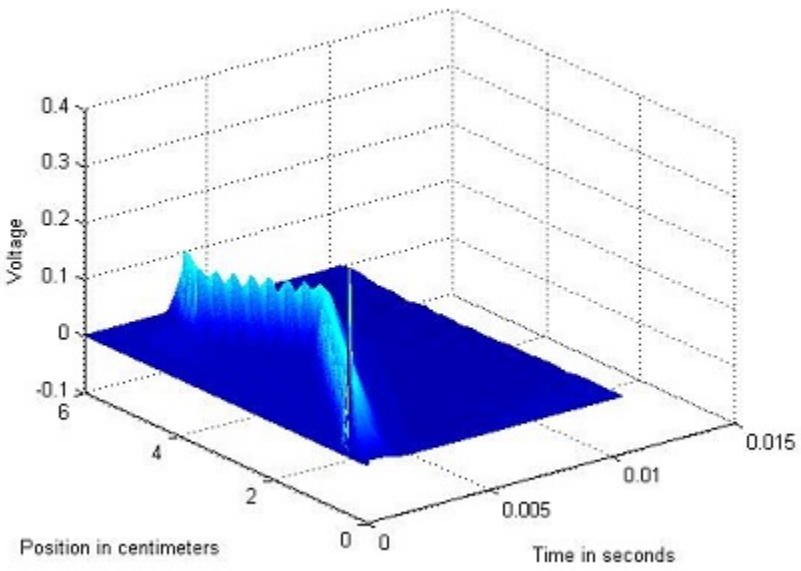

Figure 5.6: Output when axon one out of three axons is stimulated under noisy ephaptic coupling.

5.5 Conclusion

In this chapter we developed a rudimentary sketch of an axon tract as a noisy communication channel. We considered additive Gaussian noise and also compared the tract to an embedded

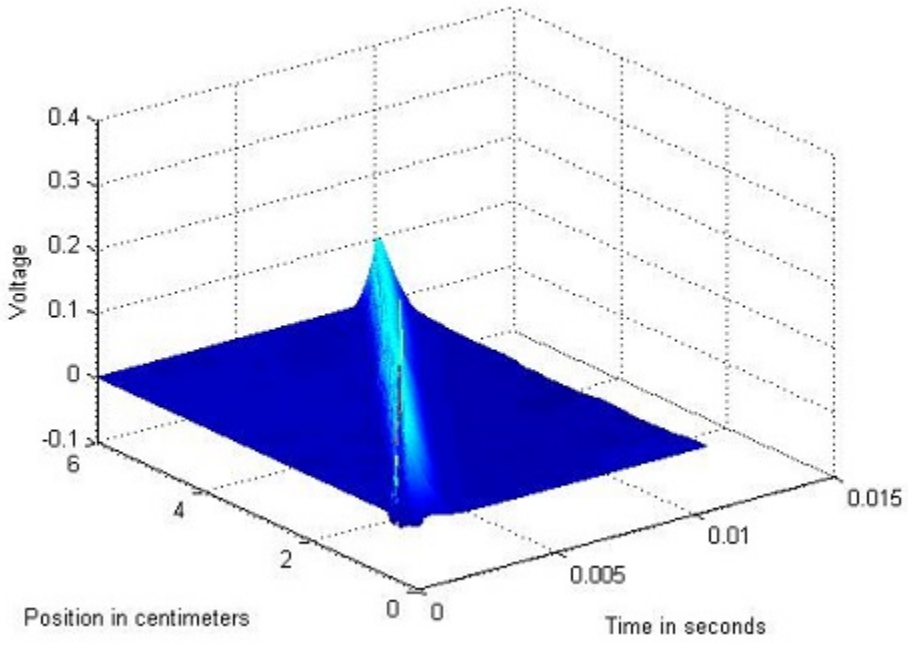

Figure 5.7: Output when axon two of three is stimulated under noisy ephaptic coupling.

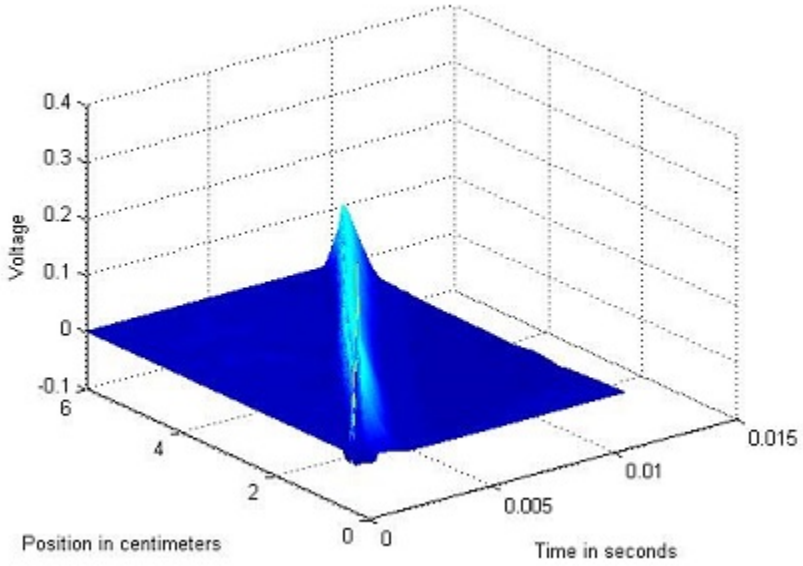

Figure 5.8: Output when axon three of three axons is stimulated under noisy ephaptic coupling.

channel such as the Poisson channel. We found that in discrete time, the tract acts as a vector Gaussian channel with perfect feedback[2]. The capacity analysis of many such channels may already be

[2]Here the channel was viewed as a channel-in-time, i.e., a storage device for data.

found in the information theory literature. For example, [54, 55, 56, 57] are relevant references. Having provided the motivation for treating this channel as a vector Gaussian channel with perfect feedback, we leave the full capacity computation as an important future direction of work. It would also be interesting to decouple Eqn. (5.2) and compare the decoupled capacity with the ephaptic capacity. Whether or not there is a capacity gain from ephaptic coupling can then be resolved. We also performed simulations of the noisy generalized ephaptic master Eqn. (5.2) which illuminated the fascinating phenomenon of random action potential initiations at downstream nodes, and ortho- as well as anti-dromic propagation. Our results indicate that even with noise present, there may be velocity change which can potentially lead to downstream synchronization.

CHAPTER 6 UNIFICATION AND FUTURE WORK

In Chapter 4, we saw the strength and direction of the electric field of a firing axon. In this chapter, we will continue our alternate approach to ephaptic coupling. Our first task in this chapter, therefore, is to see if we can address the question of the velocity synchronization mechanism from a different perspective than the current based perspective investigated in Chapters 2 and 3.

6.1 Joint Consideration of Ephaptic and Field-based Synchronization

The e-field emanating from a node of Ranvier is the negative of the gradient of the electric potential, where the gradient is taken in an arbitrary outward (from the surface of the axon) direction. The ephaptic coupling term, however, involves the gradient of the potential along the axon. In spite of this transversal-longitudinal dichotomy, a unified view of these two phenomena seems possible.

We can say that when we are ignoring transversal effects, such as the case described in [5], then the e-field effect reduces to an along-axon effect. The other way around, when we wish to include a three dimensional view, the along-axon gradient must be augmented by an arbitrary-directional gradient of the potential. This latter is a true three-dimensional unification of both ephaptic coupling and endogenous field effects.

To see this clearly, examine Fig. 6.1. It shows the field directions and rough magnitudes due to an axon with just three nodes. It is apparent that while on certain rings, the field is normal to the axon surface, between the rings the arrows assume other directions as well, with a component parallel to the surface of the axon. It is these latter components that cause ephaptic coupling because when two or more axons with aligned nodes are placed next to each other, the parallel components will add while the normal components likely cancel each other out. Thus, for perfectly

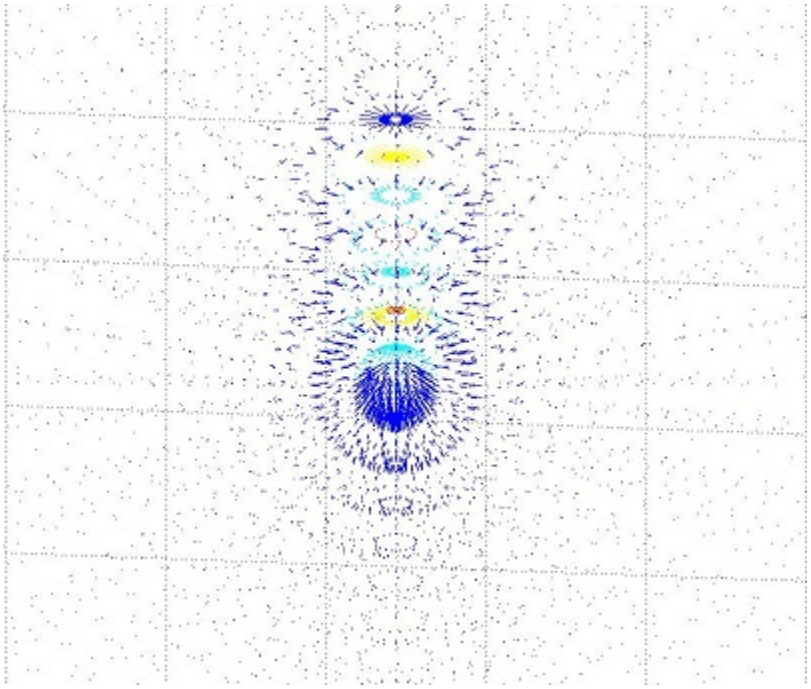

Figure 6.1: The dense electric field around three nodes of an axon.

aligned, parallel axons the Reutskiy ephaptic coupling equation would suffice as it only considers along-axon voltage gradients. However, for more complicated geometries and misalignments of the nodes, we would need a full three dimensional electric field approach.

To derive the unified equation, it is necessary to relax certain assumptions in our derivation of the Generalized Ephaptic Equation that presently do not allow extracellular currents to flow in arbitrary directions and therefore incorporate e-field generated currents. Essentially, we have ignored in our Chapter 2 derivation, the planar equations (i.e. equations corresponding to the $\hat{x}$ and $\hat{y}$ directions). When these are taken into account we would get a true, all-encompassing three dimensional system of equations.

A complete derivation of such a system of equations would involve a heavy dose of differential geometry [58], particularly if we wish to take into account axons that are tortuously wound in a tract. As such, this derivation is beyond the scope of this dissertation and is therefore left to future work.

However, such a unified consideration is important as the following example would suggest. Consider Fig. 4.9 which shows the electric field around an axon. It is seen that the electric field

seems nearly $L/2$-periodic where L is the internodal length. Now if this field were to interact with another axon placed close by, then if the two axons were perfectly misaligned, there ought to be no observable difference from when they are perfectly aligned. This is because in both cases, the other axon will have its nodes aligned with a crest or trough of the electric field of the first axon. The other axon would be perpendicular to the field direction due to the first axon and so this will have a maximal effect on its transmembrane potential [59]. Thus it may be that the studies of Scott, Binczak and Luzader [60] on the effect of nodal misalignment, which are based solely on current-mediated interaction, will have to be revised in the light of this field-mediated effect.

In this way, we see that the insights gained from the field mediated interaction can illuminate theories built upon purely current mediated interaction, showing that they are a superset of the current mediated theories. Thus any effort towards studying field mediated interaction and showing it as a generalization of current mediated interaction is worthwhile, illuminating, and potentially unifying.

6.2 Origin of Synchronization

Fig. 6.2 shows axon 1 with a smaller diameter and axon 2 with a larger diameter, placed next to each other. The action potential on axon 1 is leading. This figure is a time snapshot, with position axis going from right to left instead of left to right. At the time of the snapshot, node 3 on axon 1 is just beginning to depolarize (initiation of AP) and the action potential is at node 2 of axon 2 and is beginning to depolarize there as well.

The field directions are sketched. They indicate an inward (into the node 3 of axon 1) field emanating from axon 1 and also, an inward (into node 2 of axon 2) field from axon 2. This is because during depolarization the field is due to the flow of Na+ ions inward which leads to an inward pointing extracellular field while during repolarization, this field weakens out and the K+ field kicks in which has an outward pointing extracellular field direction.

Thus the action potential of axon 1 is generating downward field lines at the position of node 3 of axon 2, and the action potential of axon 2 is generating downward field lines too at this

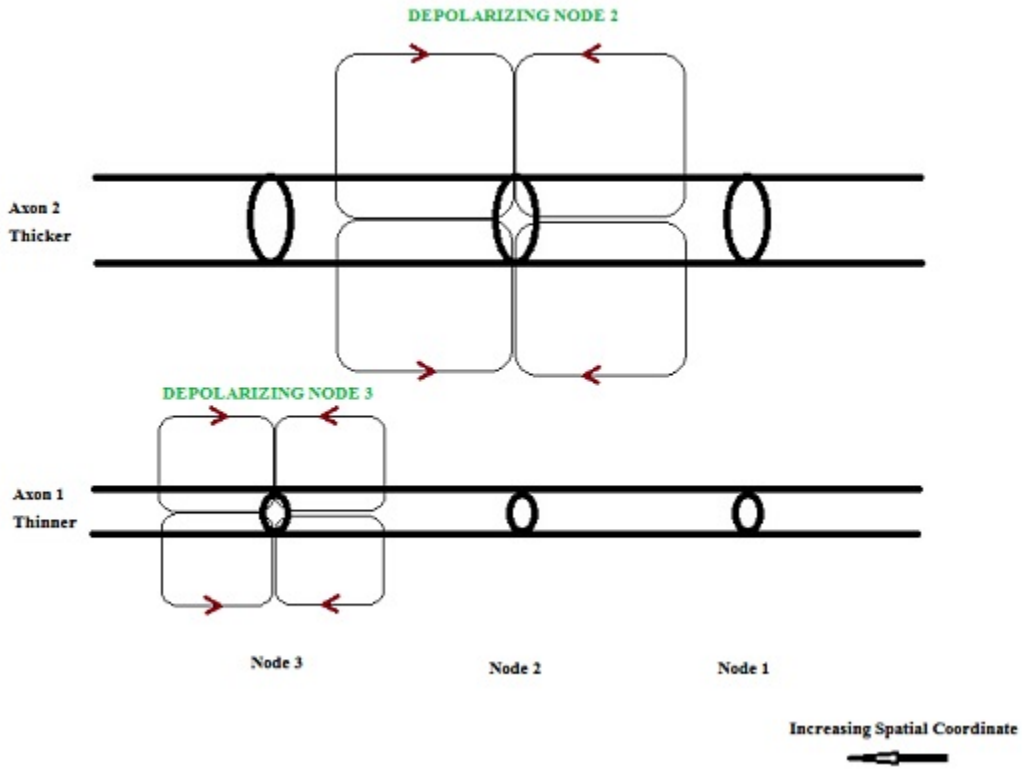

Figure 6.2: Mechanism of electric field mediated synchronization.

same position. As a result there is constructive superposition and the extracellular medium now injects a negative current into node 3 of axon 2.

This negative current gets input into node 3 of axon 2. There it causes a hyperpolarization. Thus any diffusion-carried depolarization would take more positive ions to trigger node 3 on axon 2. The conclusion is that the action potential on axon 2 has slowed down. In this way, axon 2's action potential will start hopping with the a velocity closer to the one on axon 1. None of this would occur if the action potentials were only slightly more separated in phase. This is because if axon 1's node 3 is repolarizing when axon 2's node 2 is depolarizing, the fields would oppose each other and cancel out their interactive effect at node 3 of axon 2. So axon 2's action potential would not slow down. Thus there is a threshold separation for interaction and if the two action potentials are within this separation, then they synchronize to a stable velocity. In this context we can ask, "Why will there be a stable velocity?" This is because if both the action potentials are on facing

nodes of Ranvier and both are in phase and both are depolarizing, their fields would again cancel and there will be no more interaction, until they begin to fall out of step, when the interaction will resume as discussed above. This is the origin of synchronization, which the field picture has so clearly illuminated for us. Compare this simple explanation with the qualitative analysis presented in Section 8.3.2 of [35] which is highly complex, involving fourth order derivatives and their analysis. Yet the essential prediction of synchronization with stable points is the same.

In addition, the field picture has avoided the assumption that Reutskiy et. al [5] made of the lack of potential gradients in the transverse plane. All we need to do is to place the axons in the extracellular medium and then initiate action potentials on one or several of them and they would tend to synchronize (if the field permits), while the extracellular field itself will have all sorts of directional gradients.

6.3 Future Work and Conclusion of Dissertation

Important future work would involve converting this qualitative analysis into a quantitative one and then trying to simulate the resultant equation. This would involve doing everything in vector analysis terms. The analysis would involve studying when do dipole fields add constructively and when do they add destructively in a situation with alternating field directions.

The field will also decay with distance, so we would be able to exactly quantify when the interaction will be strong enough to cause synchronization and when not. In general, the distance dependence of the interaction will become much clearer. Further, the field approach would allow axons to be immersed in each other's fields in arbitrary directions, alignments and tortuosities, and yet we would be able to determine effects such as synchronization by merely studying the field intensities and directions.

Thus in this chapter we bring to an end our entire dissertation by reaching the conclusion that the field mediated synchronization approach is to be favored over the limited, but still illuminating, current mediated synchronization and interaction picture of Chapters 2 and 3. The field was studied in Chapter 4 in terms of its magnitude and direction by the volume conduction and dipole

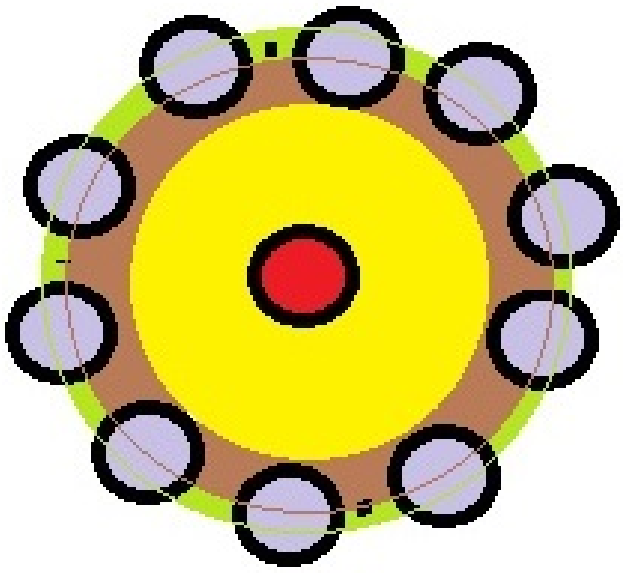

Figure 6.3: Tight packing of axons.

field in free-space approaches. There the magnitudes were found to be significant and the directions were noted. Here in this chapter we showed how the directions actually make it clear when synchronization will take place and when not, in agreement with the results of current-mediated synchronization such as those depicted in Fig. 2.16 or those considered in Chapter 8 of Scott's book. Synchronization in the field mediated setup as expounded in this present chapter (Chapter 6) can be regarded as a prediction of our studies, which needs to be tested via simulations, in future work.

To summarize and reiterate, fields produce currents and currents can generate fields too. In Chapter 2 and 3 we ignored these points. However in Chapter 4, we computed first the field produced by the node of Ranvier's ion channels from the current flowing in those channels. Next we computed the field based on the electric dipole that would result from this current. We found the two peak field strengths to be within a couple of orders of magnitude of each other and of the Hales-Pockett [50] value of about 10^8 V/m. Fig. 6.3 shows an axon in tight packing with various layers of materials around it that the electric field generated by it would have to pass through to reach other axons. These strengths were significant enough to cause about a 100 mV drop on an

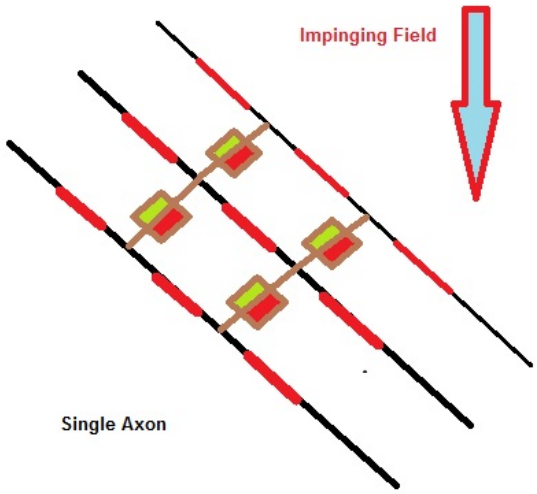

Figure 6.4: Interaction between an axon and the field of a neighboring axon's node of Ranvier.

axon placed nearby. Multiplied by the conductance of the membrane of the neighboring axon's node, this 100 mV drop can easily generate a couple of pico Amperes of sodium current through open sodium channels at that node since in Hilles book [18], about a 40 mV step is required to open the channels. Fig. 6.4 shows an electric field impinging on an axon. This mechanism of depolarizing the neighboring nodes was discussed in this chapter as causing interaction between the two axons in such a way that they will tend to synchronize in their velocity of propagation. Thus in the later chapters of this dissertation we have presented a generalization of the picture of axon-axon interaction that is prevalent today, and this picture needs to be mathematically modeled and then simulated to verify the prediction of synchronization[1].

Overall, this dissertation principally shows the following:

1. (In Chapter 1:) The study of nerve tracts and their self-interaction is well-motivated,

2. (In Chapter 2:) Nerve tracts are three dimensional and their specific geometry impacts ephaptic coupling,

3. (In Chapter 3:) There is a well developed theory for ephaptic synchronization of axons,

[1]Appendix C provides some initial ideas on implementing this simulation.

4. (In Chapter 4:) The node of Ranvier of an axon generates significant electric fields,

5. (In Chapter 5:) Nerve tracts may be considered as data storage channels, and

6. (In Chapter 6:) Nodal electric fields can lead to coupling between axons in a tract.

EPILOGUE

We began this dissertation with the hope of imparting to the reader some appreciation for the marvelous organ-system in the cranium and spinal column and an insight into his or her own mind. Towards this end, we studied ephaptic coupling in axon tracts and investigated field mediated interaction between axons. We saw that the field mediated setting, which generalizes ephaptic coupling, also allows for synchronization between axons.

Synchronization between axons in a tract may have been linked to amplification of the input entropy to the tract [34] in the time coding case. Since we understand how the electric field leads to synchronization, we can say that it is the tract electric field which bears the information that is amplified by coupling and "distributes" it over the entire synchronous field by the simple process of superposition of fields and the resultant field driven currents acting back on the axons which generate the fields in the first place. This feedback was noted by Koch and Anastassiou in their paper [6]. However, they stopped short of explaining synchronization using this (field-axon) feedback mechanism.

A synchronous field fires at a single particular rhythm across the axon tract. Our states of awareness may be related to different such rhythms (though brain-wide, not just tract-wide). Thus, by studying tracts, we may have some insight into how our brain's electric fields process information in synchronous states which we are subjectively aware of, such as those corresponding to alpha, beta and delta rhythms of EEG.

Since all these states are processing information by virtue of the synchronization taking place during them, we may conclude that regardless of whether we are conscious of it or not, we are processing information in our brains' electric fields. Ohm's law and the superposition principle seem to acquire an added importance in light of this conclusion.

REFERENCES

[1] Patrick Olivelle. *The Early Upanishads: Annotated Text and Translation*. Oxford University Press, 1998.

[2] Paul L Nunez and Ramesh Srinivasan. *Electric fields of the brain: the neurophysics of EEG*. Oxford University Press, USA, 2006.

[3] Stephen Waxman. *Multiple sclerosis as a neuronal disease*. Academic Press, 2005.

[4] Nanna Figved, Kjell-Morten Myhr, Jan-Petter Larsen, and Dag Aarsland. Caregiver burden in multiple sclerosis: the impact of neuropsychiatric symptoms. *Journal of Neurology, Neurosurgery & Psychiatry*, 78(10):1097–1102, 2007.

[5] S Reutskiy, Enrico Rossoni, and Brunello Tirozzi. Conduction in bundles of demyelinated nerve fibers: computer simulation. *Biological cybernetics*, 89(6):439–448, 2003.

[6] Costas A Anastassiou and Christof Koch. Ephaptic coupling to endogenous electric field activity: why bother? *Current opinion in neurobiology*, 31:95–103, 2015.

[7] Julian Schwinger, Lester L DeRaad Jr, and Kimball A Milton-Wu-yang Tsai. *Electrodynamics*. Perseus Books, Reading, MA, 1998.

[8] A Arvanitaki. Effects evoked in an axon by the activity of a contiguous one. *Journal of neurophysiology*, 5(2):89–108, 1942.

[9] VS Markin. Electrical interaction of parallel non-myelinated nerve fibres. 1. change in excitability of adjacent fibre. *BIOPHYSICS-USSR*, 15(1):122, 1970.

[10] Alan L Hodgkin and Andrew F Huxley. A quantitative description of membrane current and its application to conduction and excitation in nerve. *The Journal of physiology*, 117(4):500, 1952.

[11] VS Markin. Electrical interaction of parallel non-myelinated nerve fibres. 2. collective conduction of impulses. *BIOPHYSICS-USSR*, 15(4):713, 1970.

[12] VS Markin. Electrical interaction of parallel non-myelinated nerve fibresiii. interaction in bundles. *Biophysics*, 18:324–332, 1973.

[13] JC Eilbeck, SD Luzader, and AC Scott. Pulse evolution on coupled nerve fibres. *Bulletin of mathematical biology*, 43(4):389–400, 1981.

[14] B Frankenhaeuser and AF Huxley. The action potential in the myelinated nerve fibre of xenopus laevis as computed on the basis of voltage clamp data. *The Journal of Physiology*, 171(2):302, 1964.

[15] Costas A Anastassiou, Sean M Montgomery, Mauricio Barahona, György Buzsáki, and Christof Koch. The effect of spatially inhomogeneous extracellular electric fields on neurons. *Journal of Neuroscience*, 30(5):1925–1936, 2010.

[16] Dominique Debanne, Emilie Campanac, Andrzej Bialowas, Edmond Carlier, and Gisèle Alcaraz. Axon physiology. *Physiological reviews*, 91(2):555–602, 2011.

[17] G Bard Ermentrout and David H Terman. *Mathematical foundations of neuroscience*, volume 35. Springer Science & Business Media, 2010.

[18] Bertil Hille et al. *Ion channels of excitable membranes*, volume 507. Sinauer Sunderland, MA, 2001.

[19] Robert Plonsey and Roger C Barr. *Bioelectricity: a quantitative approach*. Springer Science & Business Media, 2007.

[20] B Frankenhaeuser. Quantitative description of sodium currents in myelinated nerve fibres of xenopus laevis. *The Journal of physiology*, 151(3):491, 1960.

[21] Jane Cronin. *Mathematical aspects of Hodgkin-Huxley neural theory*, volume 7. Cambridge University Press, 1987.

[22] Joseph B Patlak and Maurico Ortiz. Two modes of gating during late na+ channel currents in frog sartorius muscle. *The Journal of general physiology*, 87(2):305–326, 1986.

[23] Humberto R Maturana. The fine anatomy of the optic nerve of anurans an electron microscope study. *The Journal of biophysical and biochemical cytology*, 7(1):107–120, 1960.

[24] Stephen G Waxman and J Murdoch Ritchie. Organization of ion channels in the myelinated nerve fiber. *Science*, 228(4707):1502–1507, 1985.

[25] Humberto R Maturana. Number of fibres in the optic nerve and the number of ganglion cells in the retina of anurans. *Nature*, 183(4672):1406–1407, 1959.

[26] Stephen G Waxman and Michael H Brill. Conduction through demyelinated plaques in multiple sclerosis: computer simulations of facilitation by short internodes. *Journal of Neurology, Neurosurgery & Psychiatry*, 41(5):408–416, 1978.

[27] RK Nagle, EB Saff, and AD Snider. *Fundamentals of Differential Equations and Boundary Value Problems*. Pearson, 7th edition, 2017.

[28] JB Hursh. Conduction velocity and diameter of nerve fibers. *American Journal of Physiology–Legacy Content*, 127(1):131–139, 1939.

[29] Alwyn C. Scott. *Neuroscience: A Mathematical Primer*. Springer-Verlag, Inc., New York, 2002.

[30] Anna Corradi, Laura Croci, Vania Broccoli, Silvia Zecchini, Stefano Previtali, Wolfgang Wurst, Stefano Amadio, Roberto Maggi, Angelo Quattrini, and G Giacomo Consalez. Hypogonadotropic hypogonadism and peripheral neuropathy in ebf2-null mice. *Development*, 130(2):401–410, 2003.

[31] Leroy T Brown. Projections and termination of the corticospinal tract in rodents. *Experimental brain research*, 13(4):432–450, 1971.

[32] Stephen Douglas Luzader. *Neurophysics of parallel nerve fibers*, volume 1. University of Wisconsin–Madison., 1979.

[33] SJW Lisney and Carolyn M Pover. Coupling between fibres involved in sensory nerve neuromata in cats. *Journal of the neurological sciences*, 59(2):255–264, 1983.

[34] Aman Chawla and Salvatore D Morgera. Ephaptic synchronization as a mechanism for selective amplification of stimuli. *BMC Neuroscience*, 15(Suppl 1):P87, 2014.

[35] Alwyn Scott. *Neuroscience: A mathematical primer*. Springer Science & Business Media, 2002.

[36] Colin D McCaig and Min Zhao. Physiological electrical fields modify cell behaviour. *Bioessays*, 19(9):819–826, 1997.

[37] Luigi Galvani and Giovanni Aldini. *De Viribus Electricitatis In Motu Musculari Comentarius Cum Joannis Aldini Dissertatione Et Notis; Accesserunt Epistolae ad animalis electricitatis theoriam pertinentes*. Apud Societatem Typographicam, 1792.

[38] Frederic A Gibbs, Hallowell Davis, and William G Lennox. The electro encephalogram in epilepsy and in conditions of impaired consciousness. *American Journal of EEG Technology*, 8(2):59–73, 1968.

[39] Gary R Holt and Christof Koch. Electrical interactions via the extracellular potential near cell bodies. *Journal of computational neuroscience*, 6(2):169–184, 1999.

[40] Bradley J Roth and JP Wikswo. The magnetic field of a single axon. a comparison of theory and experiment. *Biophysical journal*, 48(1):93–109, 1985.

[41] Bradley J Roth and John P Wikswo. The electrical potential and the magnetic field of an axon in a nerve bundle. *Mathematical biosciences*, 76(1):37–57, 1985.

[42] Colin G. Hales, David B. Grayden, and Harry Quiney. The electric field system of a macular ion channel plaque. *Proceedings of the Annual International Conference of the IEEE Engineering in Medicine and Biology Society, EMBS*, pages 294–297, 2011.

[43] Kenneth W Horch and Gurpreet S Dhillon. *Neuroprosthetics: theory and practice*, volume 2. World Scientific, 2004.

[44] Robert Plonsey and Dennis B Heppner. Considerations of quasi-stationarity in electrophysiological systems. *The Bulletin of mathematical biophysics*, 29(4):657–664, 1967.

[45] Julian Schwinger, Lester L DeRaad Jr, Kimball Milton, and Wu-yang Tsai. *Classical electrodynamics*. Westview Press, 1998.

[46] Harry Moritz Schey. *Div, grad, curl, and all that: an informal text on vector calculus*. WW Norton, 2005.

[47] David J Griffiths. *Introduction to electrodynamics*. AAPT, 2005.

[48] David C Gadsby. Ion channels versus ion pumps: the principal difference, in principle. *Nature reviews Molecular cell biology*, 10(5):344–352, 2009.

[49] J David Jackson. *Electrodynamics*. Wiley Online Library, 1975.

[50] Colin G Hales and Susan Pockett. The relationship between local field potentials (lfps) and the electromagnetic fields that give rise to them. *Frontiers in systems neuroscience*, 8:233, 2014.

[51] Richard B Borgens, Andrew R Blight, DJ Murphy, and Lygia Stewart. Transected dorsal column axons within the guinea pig spinal cord regenerate in the presence of an applied electric field. *Journal of Comparative Neurology*, 250(2):168–180, 1986.

[52] Sheldon Jay Axler. *Linear algebra done right*, volume 2. Springer, 1997.

[53] Christoph Adami. *Introduction to artificial life*, volume 1. Springer Science & Business Media, 1998.

[54] Pramod Viswanath and David N. C. Tse. Sum capacity of the vector gaussian broadcast channel and uplink-downlink duality. *IEEE Transactions on Information Theory*, 49(8):1912–1921, 2003.

[55] Daniel Pérez Palomar and Sergio Verdú. Gradient of mutual information in linear vector gaussian channels. *IEEE Transactions on Information Theory*, 52(1):141–154, 2006.

[56] Wei Yu and John M Cioffi. Sum capacity of gaussian vector broadcast channels. *IEEE Transactions on information theory*, 50(9):1875–1892, 2004.

[57] Sriram Vishwanath and Syed Ali Jafar. On the capacity of vector gaussian interference channels. In *Information Theory Workshop, 2004. IEEE*, pages 365–369. IEEE, 2004.

[58] Michael Spivak. *A Comprehensive Introduction to Differential Geometry*. Publish or Perish, Inc., University of Tokyo Press, 1981.

[59] Robert Susil, Dejan Šemrov, and Damijan Miklavčič. Electric field-induced transmembrane potential depends on cell density and organizatio. *Electro-and magnetobiology*, 17(3):391–399, 1998.

[60] S Binczak, JC Eilbeck, and Alwyn C Scott. Ephaptic coupling of myelinated nerve fibers. *Physica D: Nonlinear Phenomena*, 148(1):159–174, 2001.

APPENDIX A THE EPHAPTIC GEOMETRY PROGRAM

A.1 Outline of our Program

In the following we give an outline of our MATLAB program. Items in italics are names of methods or m-files.

- *Mainaxon* calls *packagedCNN* while inputting the parameters
- *packagedCNN* creates a bundle (structure) and an array of axons (each a structure), returning this array
- *bUndle* holds the global, tract-wide parameters
- *aXon* array holds N axons
- each axon holds its local parameters including its voltage as a function of position and time as well as ionic and stimulation currents
- the methods *activationupdate* and *ionicupdate* are called to update the activation/inactivation variables m, n, h and p and the ionic currents respectively
- a block tridiagonal matrix is created holding the coefficients that give the sequentially next time instant value of the voltages on the basis of the present value of the voltage and currents.
- *triblocksolve* is used to solve this block tridiagonal system
- the solution is updated into the axons
- when this is completed for all positions and times, the axon array is ready to be returned.

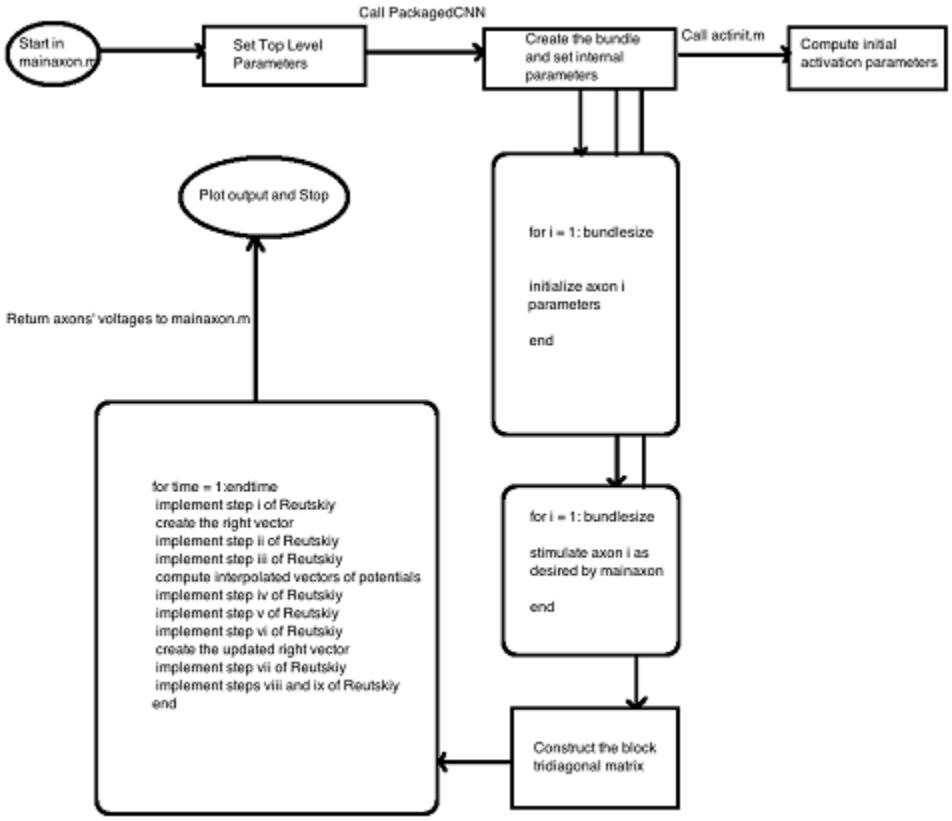

Figure A.1: Flowchart of our implementation.

The flowchart representing this program is depicted in Fig. A.1. The program structure is somewhat similar to that used by Reutskiy et. al. [5]. The main modification comes in first when we wish to consider the case of two fibers of different diameters. For this, we include the modifications mentioned in Section 2.5.2 in the main method, before calling the central routine. That is, the modified diameters, capacitances and conductances are input into the central routine as parameters. The central routine itself gets modified particularly in the parameters that go into the tridiagonal matrix. The rest of the code remains unchanged. To incorporate geometry, we modify again the parameters that go into the tridiagonal matrix, making them now dependent upon the geometry.

A.2 Values of Constants Used in Our Program

Table A.1 lists the values of the constants and their corresponding units that are used in the final version of our program.

A.3 Details of Implementation

We implemented the algorithm presented in the appendix of [5] in the mathematical programming software MATLAB®. An outline of our method-oriented implementation can be found in Appendix A.1. Despite the close parallels, there are, however, also some differences. In particular, we found that the equation governing the parameter β_h used by [5] is different from the one presented in [20]. This difference led to instabilities in our implementation output. This prompted a thorough investigation of all the parameters, their governing equations and related constants. The final list of constants used is presented in Appendix A.2.

With this modification, we were able to consistently obtain stable action potential output from stimulated fibers as well as coupled ones. Fig. A.2 shows a single action potential generated by our program when there was a single fiber in the tract. For larger number of fibers $N \geqslant 2$, the output showed synchronization phenomena in line with that expected based on the figures shown in [5]. From the next two Figs. A.3 and A.4, it is clear that the action potential conduction velocity depends crucially on the extracellular resistance. It may be easily seen that setting the extracellular

Table A.1: List of constants and their values.

Constant	Value	Note
d	$1e-3$	fiber diameter in centimeters
ell	$2.5e-4$	length of a Ranvier node in centimeters
L	$.2$	length of myelinated internode in centimeters
$delX$	$\frac{L}{10}$	length of a mesh point
$delT$	$2e-6$	duration of a time unit in seconds
$temperature$	20	degrees Celsius
rf	$1.27e8$	fiber resistance per unit length in Ohm per centimeter
c_m	$1.87e-11$	myelin capacitance per unit length in Farad per centimeter
g_m	$5.6e-9$	myelin conductance per unit length in per Ohm-centimeter
c_{nd}	$3.14e-9$	nodal capacitance per unit length in Farad per centimeter
A_{α_m}	$3.6e5$	per volt-s
A_{α_h}	$1e5$	per volt-s
A_{α_n}	$2e4$	per volt-s
A_{α_p}	$6e3$	per volt-s
A_{β_h}	$4.5e3$	per s
A_{β_m}	$4e5$	per volt-s
A_{β_n}	$5e4$	per volt-s
A_{β_p}	$9e4$	per volt-s
B_{α_h}	$-1e-2$	volts
B_{α_m}	$2.2e-2$	volts
B_{α_n}	$3.5e-2$	volts
B_{α_p}	$4e-2$	volts
B_{β_h}	$4.5e-2$	volts
B_{β_m}	$1.3e-2$	volts
B_{β_n}	$1e-2$	volts
B_{β_p}	$-2.5e-2$	volts
C_{α_h}	$6e-3$	volts
C_{α_m}	$3e-3$	volts
C_{α_n}	$1e-2$	volts
C_{α_p}	$1e-2$	volts

Table A.1 (continued).

Constant	Value	Note
C_{β_h}	$1e-2$	volts
C_{β_m}	$2e-2$	volts
C_{β_n}	$1e-2$	volts
C_{β_p}	$2e-2$	volts

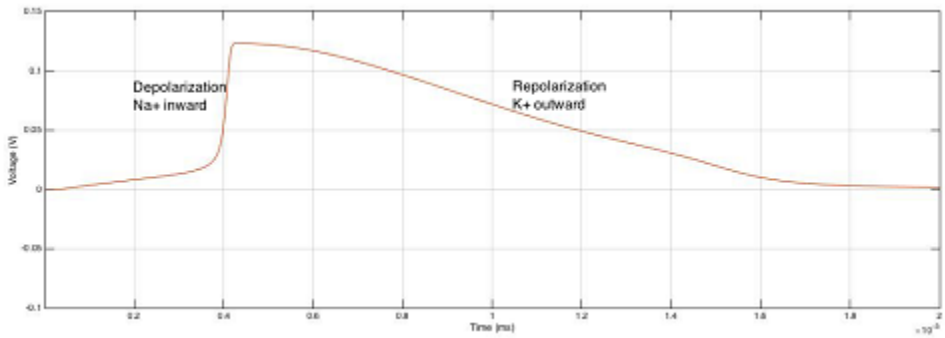

Figure A.2: Single action potential on single stimulated axon, showing the depolarization and repolarization phases. The x-axis is time in milliseconds and the y-axis is voltage in volts.

resistance r_0 to zero is a good way to zero out the coupling constant. The optimal situation, however, would be to zero out the coupling coefficient while maintaining the same unchanged conduction velocity, a point which remains to be studied in future work.

Here we would like to point out to the reader that the simulations went through several stages to ensure correctness. For example, we now introduce three figures (A.5, A.6 and A.7) which show synchronization as it was originally recorded (computer-experimentally) in a tract of three identical axons on December 1, 2015, when only two were stimulated with delay. Here the simulation program was at about 60 percent of its final development. The figures are space-time representations of axonal voltages, and illustrate three phenomena: synchronization, merger of the stimulated spike trains, and thirdly, disappearance of the synchronized trains and emergence of an antidromic spike train on the third axon. Phenomena such as these kept the authors fascinated and excited enough to continue exploring the parameter spaces in the program, ultimately leading to the final version.

We would like to make some remarks relating to these three figures:

1. All three figures show traces of the presence of action potentials on the other axons. Thus in

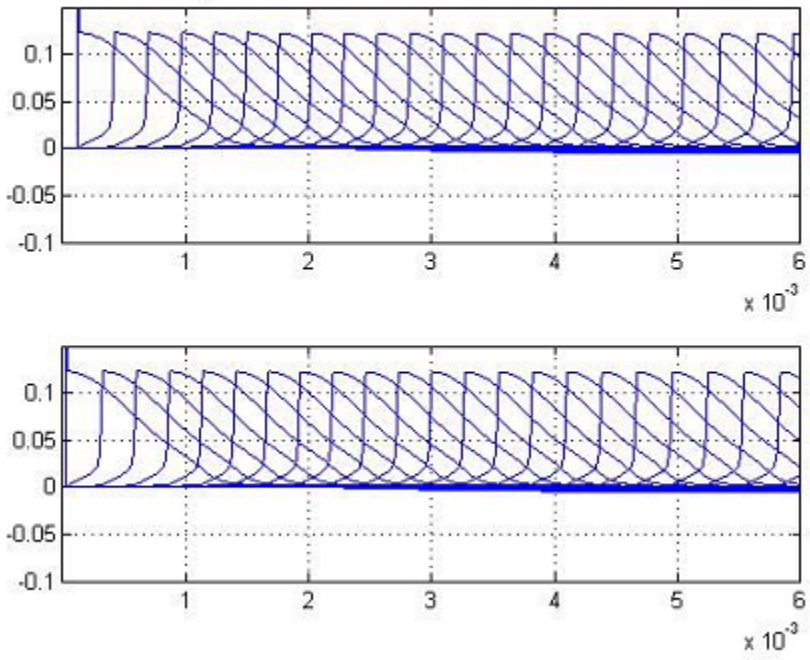

Figure A.3: Voltage vs time at the Ranvier nodes of axons 1 and 2 under 0 extracellular resistance condition. Axon 1 was stimulated after axon 2. Due to no coupling, fixed by setting extracellular resistance to 0, we see lack of synchronization. The value of $r0$ used was 0 and rf was $1.27e8$ in Ohms per centimeter. The x-axis is time in seconds and the y-axis is voltage in volts.

any figure, we can note deep-blue footprints of the other fibers.

2. This is convenient, for on any figure we can study the convergence of the tracks of the action potentials on axons 1 and 2 and the antidromic or post-synchronization emergence of a track on axon 3.

3. Axon 3 was not stimulated, but displays a post-synchronization antidromic action potential.

4. Action potentials on axons 1 and 2 essentially become antidromic subthreshold phenomena after synchronization.

A.4 Actual Code

In this section we include for illustrative purposes the central routine which is called by the main method in order to compute the voltages on the axons.

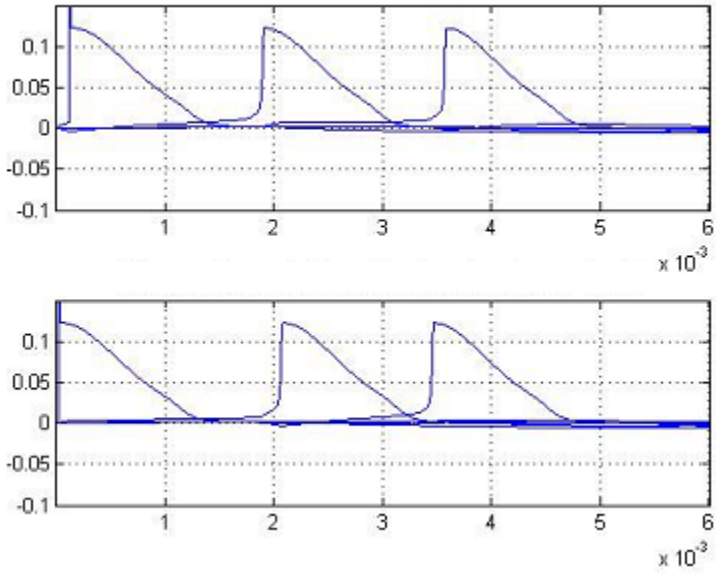

Figure A.4: Voltage vs time at the Ranvier nodes of axons 1 and 2, when axon 1 was stimulated after axon 2. Due to ephaptic coupling, it is visible that the APs on axon 1 speed up to catch up to the APs on axon 2 in a dramatic demonstration of synchronization. The average speed of the APs is however much slower than in the uncoupled case of the previous figure. The values of $r0$ and rf were $5 \times 1.27e8$ Ohms per centimeter and $1.27e8$ Ohms per centimeter respectively. The x-axis is time in seconds, the y-axis is voltage in volts.

A.4.1 packagedCNN.m

```
%%%%%%%%%%%%%%%%%%%%%%%%%%%%%%%%
%%% Author: Aman Chawla     %%
%%% Date: September 1, 2015 %%
%%% Rev: October 21, 2015%%
%%% Rev: November 1, 2015 (double stimulation) %%
%%% Rev: Nov 3, 2015 (single stimulation) %%
%%% Rev: Dec 27, 2015 %%%
%%%%%%%%%%%%%%%%%%%%%%%%%%%%%%%%
function axon = packagedCNNJan20_2017CV(noiseon, N, d, ell, L,
   delT, timesteps, endlength, temperature, Ranvier_array, r0, cm
   , gm, cnd, gnd, rf, InjectionDuration, injectnumber1, stimpos1
```

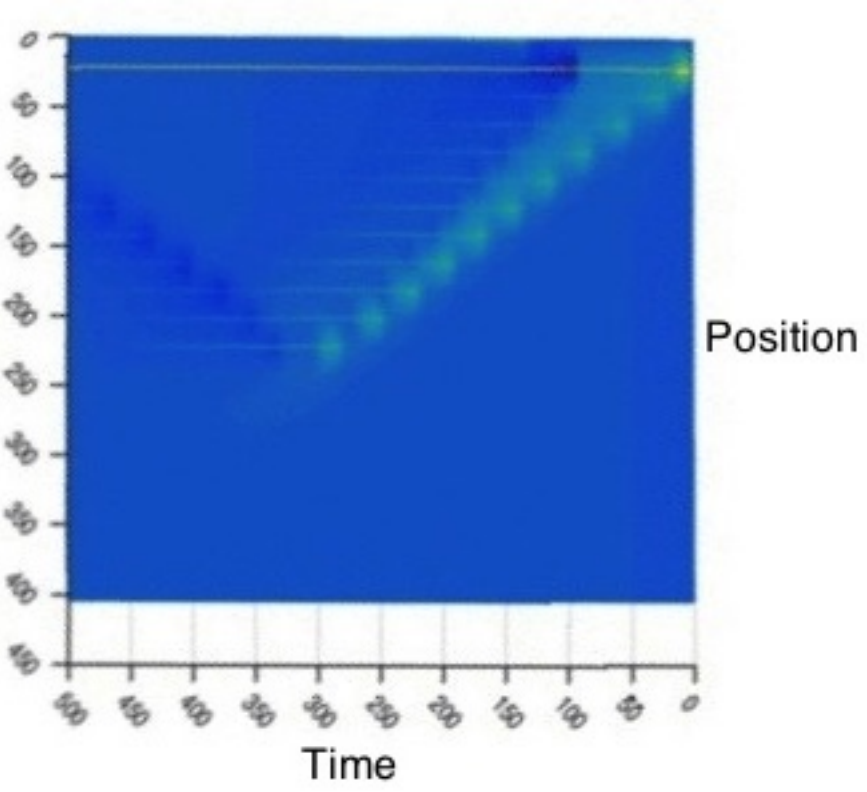

Figure A.5: Axon 1, stimulated first. This original record is a space-time projection of the voltage-space-time graph. It shows a yellow-green track or world-line of the action potential. The yellow-green track is seen to end abruptly at time between 300 and 350 and position between 200 and 250. The x-axis is time in time-steps and the y-axis is position in position-steps.

```
   , delaydelta, injectnumber2, stimpos2, delaydelta2,
   injectnumber3, stimpos3, delaydelta3, injectnumber4, stimpos4,
    Eonoff, Estrength, K)


bundle1 = bUndle; % create bundle1 as a bundle array
bundle1.N = N;  % Number of axons in bundle
bundle1.d = d;
bundle1.ell = ell;
bundle1.L = L;
bundle1.delX = bundle1.L/10;
```

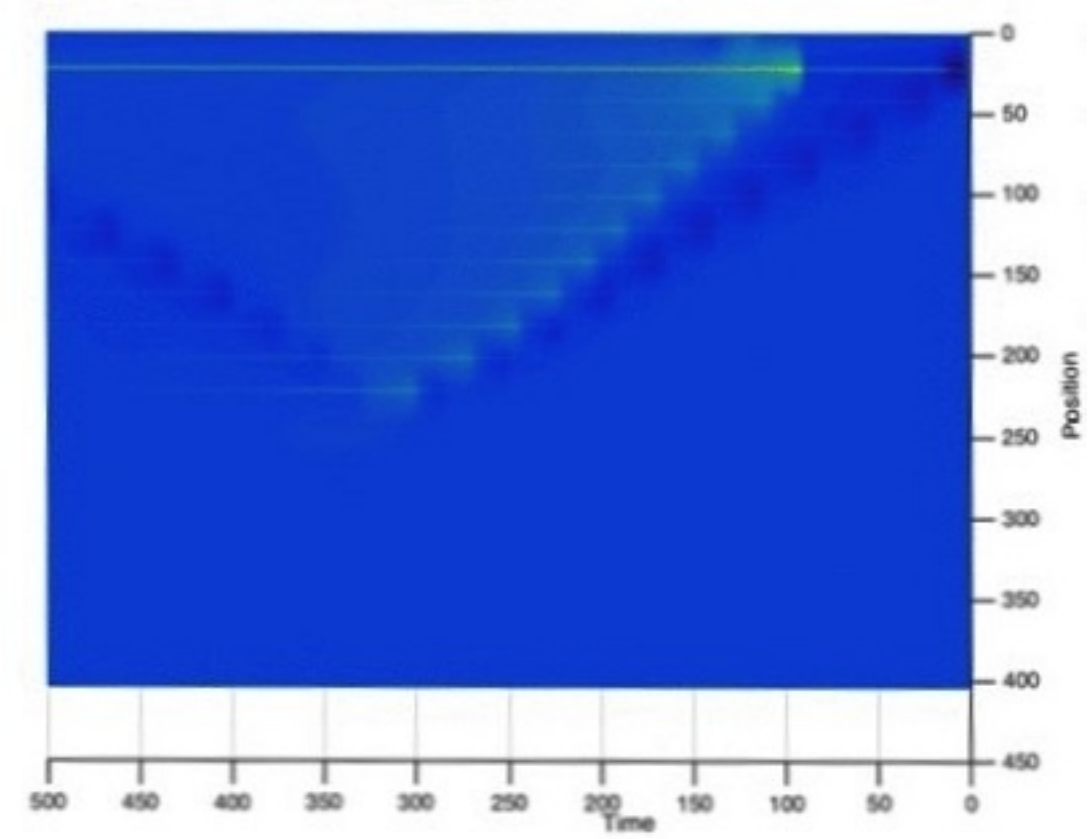

Figure A.6: Axon 2, stimulated after axon 1. This original record is again a space-time projection showing the track or world-line of the action potential on axon 2, in yellow-green. The world line ends abruptly at time between 300 and 350 and position between 200 and 250. The x-axis, running from right to left is time in time-steps and the y-axis, running from top to bottom is position in position-steps.

```
bundle1.delT = delT;

bundle1.timesteps = timesteps;

bundle1.duration = bundle1.timesteps*bundle1.delT;

bundle1.endlength = endlength;

bundle1.temperature = temperature; % temperature in degrees
   Celsius

bundle1.Ranvier = Ranvier_array;

LTminus1 = bundle1.timesteps;

bundle1.K = K;

LYY = LTminus1;    % Both symbols are used in the code
```

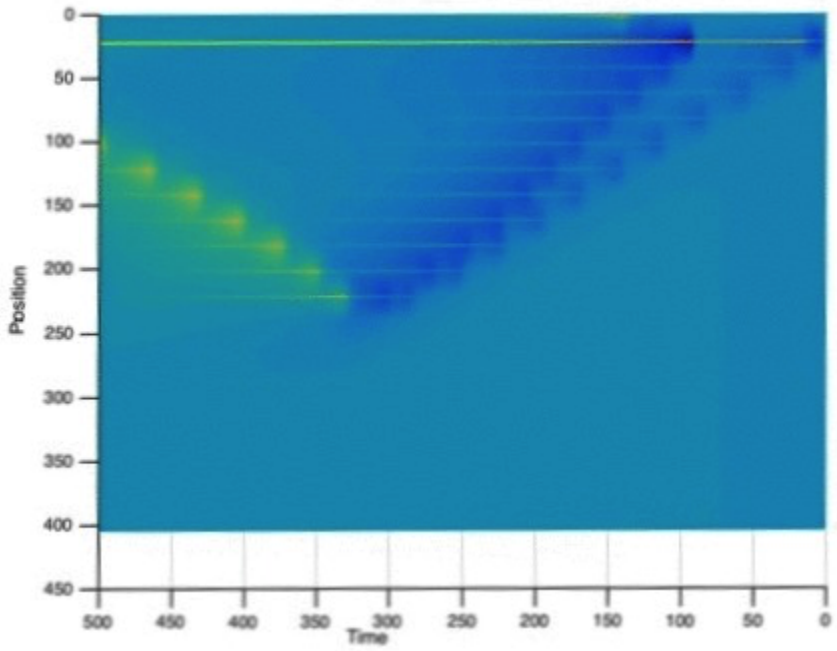

Figure A.7: Axon 3, not stimulated. In this third original record, there is no action potential visible until time between 300 and 350 and position between 200 and 250, when a yellow-green world line starts antidromically moving towards position 100. The x-axis, running from right to left is time in time-steps and the y-axis, running from top to bottom is position in position-steps.

```
bundle1.r0 = r0;  % interfiber medium resistance
bundle1.rf = rf;  % Ohm/cm


alpha_0 = bundle1.r0/bundle1.rf ;
alpha_N = alpha_0/(1 + bundle1.N*alpha_0);


bundle1.cm = cm;  % F/cm (both)
bundle1.gm = gm;  % per Ohm-cm (both)
bundle1.cnd = cnd; % F/cm (from Waxman - Reutskiy has wrong
   dimensions)
bundle1.gnd = gnd;   % Not used in Reutskiy, but included in code
    here
```

```
egm = exp(-bundle1.gm*bundle1.delT/bundle1.cm);
egnd = exp(-bundle1.gnd*bundle1.delT/bundle1.cnd);


bundle1.injectnumber = injectnumber1; % axon to be injected in
   the bundle.


Q = 3^((bundle1.temperature-20)/10);

bundle1.F = 96485; %Coulombs per mole
bundle1.R = 8.3145; %Joules per Kelvin - mole
T_ab = bundle1.temperature+273.15; %Kelvin temperature
gamma = bundle1.F./(bundle1.R*T_ab); % per volt

% Specify the ionic concentrations inside and outside
bundle1.Nao = 114.5e-6; % moles per cm^3
bundle1.Nai = 13.74e-6;
bundle1.Ko = 2.5e-6;
bundle1.Ki = 120e-6;

% Sodium Nernst potential
NaNernstPot  = (1/gamma)*log(bundle1.Nao/bundle1.Nai);



% The above, so far, are the common parameters.
```

```
 factor = 4;
    InjectionIntensity = factor*(-1e-9/bundle1.ell); % A/cm
    CoulombsInjected = InjectionIntensity*bundle1.ell*
       InjectionDuration;
    E_rest = -70e-3; % volts
    V_l = -0.026*3.5; % volts. adjusted so that the initial ionic
        current (unstimulated condition) is 0
    g_l = 30.3e-6; % S per cm^2
    P_Na = 0.008; P_p = 0.00054; P_K = 0.0012; % cm/s
    % compute alphas and betas starting values
[alpham, alphan, alphah, alphap, betam, betan, betah, betap] =
   actinit(E_rest);
 % create axon objects. axon is an array of N axons.
    axon = aXon;

     E_rest =-70e-3;

 for i = 1:bundle1.N % axon index
    mynoiseon = 0;

    axon(i).number = i;
    axon(i).stimpos = stimpos1;

%     % allocate space
    axon(i).J_ex = zeros(bundle1.endlength, LTminus1);

    % put starting values
```

```
axon(i).E(1:bundle1.endlength,1) = E_rest.*ones(bundle1.
   endlength,1); % since V = E - E_r
axon(i).V(1:bundle1.endlength,1) =  0.*ones(bundle1.endlength
   ,1);


axon(i).m(1:bundle1.endlength,1) = (alpham/(alpham+betam));
axon(i).n(1:bundle1.endlength,1) = (alphan/(alphan+betan));
axon(i).h(1:bundle1.endlength,1) = (alphah/(alphah+betah));
axon(i).p(1:bundle1.endlength,1) = (alphap/(alphap+betap));

axon(i).Zfactor(1:bundle1.endlength,1)=exp(-gamma.*axon(i).E
   (1:bundle1.endlength,1));
axon(i).Z_Na(1:bundle1.endlength,1) = gamma*bundle1.F.*axon(i
   ).E(1:bundle1.endlength,1).*((bundle1.Nao.*axon(i).Zfactor
   (1:bundle1.endlength,1) - bundle1.Nai)./(1-axon(i).Zfactor
   (1:bundle1.endlength,1)));
axon(i).Z_K(1:bundle1.endlength,1) = gamma*bundle1.F.*axon(i)
   .E(1:bundle1.endlength,1).*((bundle1.Ko.*axon(i).Zfactor
   (1:bundle1.endlength,1) - bundle1.Ki)./(1-axon(i).Zfactor
   (1:bundle1.endlength,1)));


[axon(i).J_ion(1:bundle1.endlength,1), axon(i).J_Na(1:bundle1
   .endlength,1), axon(i).J_K(1:bundle1.endlength,1), axon(i)
   .J_p(1:bundle1.endlength,1), axon(i).J_l(1:bundle1.
   endlength,1)] = ionicupdate(noiseon,axon(i).m(1:bundle1.
   endlength,1),axon(i).n(1:bundle1.endlength,1),axon(i).h(1:
```

```
        bundle1.endlength,1),axon(i).p(1:bundle1.endlength,1),axon
        (i).Z_K(1:bundle1.endlength,1),axon(i).Z_Na(1:bundle1.
        endlength,1),V_l,axon(i).E(1:bundle1.endlength,1),bundle1.
        d, E_rest);

 end

 % Prepare for current injection of a sequence of inputs.
injectnumberarray = [injectnumber1, injectnumber2, injectnumber3,
    injectnumber4];
stimposarray = [stimpos1, stimpos2, stimpos3, stimpos4];
delaydeltarray = [delaydelta, delaydelta2, delaydelta3];
if bundle1.N == 1
    axon(1).stimpos = stimposarray(1);
    axon(injectnumberarray(1)).J_ex(axon(injectnumberarray(1)).
       stimpos, 10:floor(InjectionDuration/bundle1.delT)+10) =
       factor*InjectionIntensity;
    axon(injectnumberarray(1)).J_ex(axon(injectnumberarray(1)).
       stimpos, 10+delaydelta:delaydelta+floor(InjectionDuration/
       bundle1.delT)+10) = 2*factor*InjectionIntensity;
    axon(injectnumberarray(1)).J_ex(axon(injectnumberarray(1)).
       stimpos, 10+delaydelta2:delaydelta2+floor(
       InjectionDuration/bundle1.delT)+10) = 2*factor*
       InjectionIntensity;
    axon(injectnumberarray(1)).J_ex(axon(injectnumberarray(1)).
       stimpos, 10+delaydelta3:delaydelta3+floor(
       InjectionDuration/bundle1.delT)+10) = 2*factor*
       InjectionIntensity;
```

```
end

    for my_count = 1:bundle1.N
    axon(injectnumberarray(my_count)).stimpos = stimposarray(
       my_count);

 % inject current
    if my_count >=2
        my_count
    axon(injectnumberarray(my_count)).J_ex(axon(injectnumberarray
       (my_count)).stimpos, 10+delaydeltarray(my_count-1):
       delaydeltarray(my_count-1)+floor(InjectionDuration/bundle1
       .delT)+10) = factor*InjectionIntensity;
    else
    axon(injectnumberarray(my_count)).J_ex(axon(injectnumberarray
       (my_count)).stimpos, 10:floor(InjectionDuration/bundle1.
       delT)+10) = factor*InjectionIntensity;
    end
end

 % Prepare to apply field
        V_app = 12; % Volts DC
        R_T1 = -1*V_app/(Estrength/bundle1.ell); % Ohms
        R_12 = -1*V_app/(Estrength/bundle1.ell); % Ohms
        R_23 = -1*V_app/(Estrength/bundle1.ell); % Ohms
        R_34 = -1*V_app/(Estrength/bundle1.ell); % Ohms

        % Apply field
```

```
        axon(injectnumber1).J_ex = axon(injectnumber1).J_ex +
           Eonoff.*(V_app/R_T1);
        axon(injectnumber2).J_ex = axon(injectnumber2).J_ex +
           Eonoff.*(V_app/R_12);
        axon(injectnumber3).J_ex = axon(injectnumber3).J_ex +
           Eonoff.*(V_app/R_23);
        axon(injectnumber4).J_ex = axon(injectnumber4).J_ex +
           Eonoff.*(V_app/R_34);




         % BLOCK tridiagonal matrix for internodal segments

         a = (alpha_N-1)/(2*bundle1.rf*(bundle1.delX)^2);
         b = bundle1.cm/bundle1.delT + (1-alpha_N)/(bundle1.rf*(
            bundle1.delX)^2) + bundle1.gm/2;
         c = a;
         ee = alpha_N/(2*bundle1.rf*(bundle1.delX)^2);
         % create the Amd subblock

      B = diag(b.*ones(bundle1.N, 1)) + ((-2*ee).*ones(bundle1.N,
         bundle1.N)-diag((-2*ee).*ones(bundle1.N,1)));
% repair B
for i = 1:N
    for j = 1:N
        if i==j
```

```
            B(i,j) = (B(i,j)- (bundle1.cm/bundle1.delT) - (1/(
               bundle1.rf*(bundle1.delX)^2)) - (bundle1.gm/2))*K(
               i,j) + (bundle1.cm/bundle1.delT + (1/(bundle1.rf*(
               bundle1.delX)^2)) + bundle1.gm/2);
        else
            B(i,j) = B(i,j)*K(i,j);
        end
    end
end


         % create the Asubd subblock

             A = diag(a.*ones(bundle1.N, 1)) + ((ee).*ones(
                bundle1.N, bundle1.N)-diag((ee).*ones(bundle1.N
                ,1)));

            %repair A
            for i = 1:N
               for j = 1:N
                   if i==j
                       A(i,j) = (A(i,j) + (1/(2*bundle1.rf*(
                          bundle1.delX)^2)))*K(i,j) - (1/(2*
                          bundle1.rf*(bundle1.delX)^2));
                   else
                       A(i,j) = A(i,j)*K(i,j);
                   end
               end
```

```
    end



% create the Asupd subblock

    C = diag(c.*ones(bundle1.N, 1)) + ((ee).*ones(
       bundle1.N, bundle1.N)-diag((ee).*ones(bundle1.N
       ,1)));


    % repair C

    for i = 1:N
        for j = 1:N
            if i == j
              C(i,j) = (C(i,j) + (1/(2*bundle1.rf*(
                 bundle1.delX)^2)))*K(i,j) - (1/(2*
                 bundle1.rf*(bundle1.delX)^2));
            else
                C(i,j) = C(i,j)*K(i,j);
            end
        end
    end

% construct the block tridiagonal matrix
leftmatrix = blktridiag(B, A, C, bundle1.endlength);
```

```
% Repair Ranvier-node parameters



 b_nd = bundle1.cnd/bundle1.delT + (1-alpha_N)/(bundle1.
    rf*(bundle1.delX)^2);
a_nd = a;
 c_nd = c;
 e_nd = ee;


 % create the Amd subblock

    B_nd = diag(b_nd.*ones(bundle1.N, 1)) + ((-2*e_nd).*
       ones(bundle1.N, bundle1.N)-diag((-2*e_nd).*ones(
       bundle1.N,1)));

 % Repair B_nd
 for i = 1:N
     for j = 1:N
         if i==j
             B_nd(i,j) = (B_nd(i,j) - (bundle1.cnd/
                bundle1.delT) -(1/(bundle1.rf*(bundle1.
                delX)^2)))*K(i,j) + ((bundle1.cnd/bundle1
                .delT) + (1/(bundle1.rf*(bundle1.delX)^2)
                ));
```

```
        else
            B_nd(i,j) = B_nd(i,j)*K(i,j);
        end
    end
end

% create the Asubd subblock
A_nd = A;

% create the Asupd subblock

C_nd = C;

   for i = 2:bundle1.endlength % The first position
      should not be a node
       if ismember(i, bundle1.Ranvier)
           leftmatrix(((i-1)*bundle1.N)+1:i*bundle1.N,((
              i-1)*bundle1.N)-bundle1.N+1:((i-1)*bundle1
              .N)) = A_nd;
           leftmatrix(((i-1)*bundle1.N)+1:i*bundle1.N,((
              i-1)*bundle1.N)+1:i*bundle1.N) = B_nd;
           leftmatrix(((i-1)*bundle1.N)+1:i*bundle1.N,(i
              *bundle1.N)+1:((i+1)*bundle1.N)) = C_nd;
       else % do nothing
       end
   end
```

```
            bundle1.a = a;
            bundle1.b = b;
            bundle1.c = c;
            bundle1.ee = ee;
            bundle1.b_nd = b_nd;
% Begin time stepping
   for time = 1:(LTminus1-1)  %Recall initial value of V_1 is set
       to zero.
       t=time; % Both notations are used
      disp(t)
   % Step (i) of Reutskiy algorithm
           for i = 1:bundle1.endlength
        for j=1:bundle1.N
            if ismember(i,bundle1.Ranvier)
       % Update the ionic current

            axon(j).E(i,t) = axon(j).V(i,t) + E_rest;
            axon(j).Zfactor(i,t)=exp(-gamma*axon(j).E(i,t));
            axon(j).Z_Na(i,t) = gamma*bundle1.F*axon(j).E(i,t)*((
               bundle1.Nao*axon(j).Zfactor(i,t) - bundle1.Nai)
               /(1-axon(j).Zfactor(i,t)));

            axon(j).Z_K(i,t) = gamma*bundle1.F*axon(j).E(i,t)*((
               bundle1.Ko*axon(j).Zfactor(i,t) - bundle1.Ki)/(1-
               axon(j).Zfactor(i,t)));
            [axon(j).J_ion(i,t), axon(j).J_Na(i,t), axon(j).J_K(i
               ,t), axon(j).J_p(i,t), axon(j).J_l(i,t)]  =
               ionicupdate(noiseon,axon(j).m(i,t),axon(j).n(i,t),
```

```
        axon(j).h(i,t),axon(j).p(i,t),axon(j).Z_K(i,t),
        axon(j).Z_Na(i,t),V_l,(axon(j).V(i,t)+E_rest),
        bundle1.d, E_rest);

    end
  end
   end


    % Create the right vector
     dee = bundle1.cm/bundle1.delT - (1-alpha_N)/(bundle1
        .rf*((bundle1.delX)^2)) - (bundle1.gm/2);
    dee_nd = bundle1.cnd/bundle1.delT + (alpha_N - 1)/(
        bundle1.rf*(bundle1.delX)^2);
    Dd = rightcreateReutskiy1(axon, bundle1, dee, dee_nd,
        t);


     % Step (ii) of Reutskiy algorithm.
axon = ReutskiyStep2or7(leftmatrix, Dd, bundle1, axon, time
   ,0);

 % Step (iii) of Reutskiy algorithm


 % Compute the interpolated vectors of the potentials.
 for axnum = 1:bundle1.N
```

```
axon(axnum).Vcoeff(:,time) = 0.5.*(axon(axnum).V(:,time+1)
    + axon(axnum).V(:,time));
end



% Step (iv) of Reutskiy algorithm
 for i = 1:bundle1.endlength
 for j=1:bundle1.N

     % execute the Ranvier nodal code
     %  Update the concentrations m, n, h, p

     [mnew, nnew, hnew, pnew] = activationupdate(axon(j).m
        (i,t), axon(j).n(i,t), axon(j).h(i,t), axon(j).p(i
        ,t), (axon(j).Vcoeff(i,t)), Q, bundle1.delT);

     axon(j).m(i,t+1) = mnew;
     axon(j).n(i,t+1) = nnew;
     axon(j).h(i,t+1) = hnew;
     axon(j).p(i,t+1) = pnew;
     end % Finish with Ranvier nodes
% Skip myelin nodes
 end



 % Step (v) of Reutskiy algorithm
```

```
% Compute the interpolated vectors of the activation
   variables.
for axnum = 1:bundle1.N
axon(axnum).mcoeff(:,time) = 0.5.*(axon(axnum).m(:,time+1)
    + axon(axnum).m(:,time));
axon(axnum).ncoeff(:,time) = 0.5.*(axon(axnum).n(:,time+1)
    + axon(axnum).n(:,time));
axon(axnum).hcoeff(:,time) = 0.5.*(axon(axnum).h(:,time+1)
    + axon(axnum).h(:,time));
axon(axnum).pcoeff(:,time) = 0.5.*(axon(axnum).p(:,time+1)
    + axon(axnum).p(:,time));

end


% Step (vi) of Reutskiy algorithm



  for i = 1:bundle1.endlength
 for j=1:bundle1.N

% Update the ionic-coeff current

     axon(j).Ecoeff(i,t) = axon(j).Vcoeff(i,t) + E_rest;
```

```
    axon(j).Zfactorcoeff(i,t)=exp(-gamma*axon(j).Ecoeff(i
       ,t));
    axon(j).Z_Nacoeff(i,t) = gamma*bundle1.F*axon(j).
       Ecoeff(i,t)*((bundle1.Nao*axon(j).Zfactorcoeff(i,t
       ) - bundle1.Nai)/(1-axon(j).Zfactorcoeff(i,t)));

    axon(j).Z_Kcoeff(i,t) = gamma*bundle1.F*axon(j).
       Ecoeff(i,t)*((bundle1.Ko*axon(j).Zfactorcoeff(i,t)
        - bundle1.Ki)/(1-axon(j).Zfactorcoeff(i,t)));

    axnum = j;
    [axon(axnum).J_ioncoeff(i,time), axon(axnum).
       J_Nacoeff(i,time), axon(axnum).J_Kcoeff(i,time),
       axon(axnum).J_pcoeff(i,time), axon(axnum).J_lcoeff
       (i,time)] = ionicupdate(noiseon,axon(axnum).mcoeff
       (i,time),axon(axnum).ncoeff(i,time),axon(axnum).
       hcoeff(i,time),axon(axnum).pcoeff(i,time),axon(
       axnum).Z_Kcoeff(i,time),axon(axnum).Z_Nacoeff(i,
       time),V_l,(axon(axnum).Ecoeff(i,time)),bundle1.d,
       E_rest);


end
 end


    % Create the right vector
```

```
      Ddcoeff = rightcreateReutskiy6(axon, bundle1, dee,
         dee_nd, t);


      % Step (vii) of Reutskiy algorithm
      axon = ReutskiyStep2or7(leftmatrix, Ddcoeff, bundle1
         , axon, time,1);



% step (viii) of Reutskiy algorithm
 % Compute the interpolated vectors of the potentials.
for axnum = 1:bundle1.N
axon(axnum).Vcoeff(:,time) = 0.5.*(axon(axnum).V(:,time+1)
    + axon(axnum).V(:,time));
end

% Step (ix) of Reutskiy algorithm

for i = 1:bundle1.endlength
 for j=1:bundle1.N
     if ismember(i,bundle1.Ranvier)
     % execute the Ranvier nodal code
     %  Update the concentrations m, n, h, p
```

```
            [axon(j).m(i,t+1), axon(j).n(i,t+1), axon(j).h(i,t+1)
               , axon(j).p(i,t+1)] = activationupdate(axon(j).m(i
               ,t), axon(j).n(i,t), axon(j).h(i,t), axon(j).p(i,t
               ), (axon(j).Vcoeff(i,t)), Q, bundle1.delT);


            end % Finish with Ranvier nodes
    end    % Skip myelin nodes
       end


end
```

APPENDIX B THE E-FIELD SIMULATOR

In this appendix the reader will find sections of the simulation program. The sections are chosen since they illustrate how we zoom out from channel to ring on a node to entire axon. Each file contains a call to the respective zoomed-in file. The program is self-explanatory.

B.1 Channelefield.m

```
function [Efieldx, Efieldy, Efieldz] = channelefield(rprimeplus,
   thetaprimeplus, phiprimeplus, rprimeminus, thetaprimeminus,
   phiprimeminus, r, theta, phi, choice)

deltaqdoubleprime = 12e-6; % known charge transferred through
   channel in cgs units (statCoulombs).
rnor = 0.5e-6*100; % radius of node of ranvier in cgs units
d = 1e-9*100; %thickness of cell membrane at node in cgs units
g = rnor/1000000; % arbitrary dumbell radius in cgs units
s = d+(3*g/4); % separation of dipolar charges in cgs units

rminusprimemag = rprimeminus;
rplusprimemag = rprimeplus;
fieldposmag = r;

phiprimeplus = phiprimeplus;
phiprimeminus = phiprimeminus;
```

```
thetaminusprime = thetaprimeminus;

% Find the required angle
rminusprimedotr = r*rminusprimemag*(sin(phi)*sin(phiprimeminus)*
   cos(theta - thetaminusprime) + cos(phi)*cos(phiprimeminus));

reqangle = acos(rminusprimedotr/(rminusprimemag*r)); % assuming r
    is nonnegative.


[rminusprimex, rminusprimey, rminusprimez] = spher2cart(
   rprimeminus, thetaprimeminus, phiprimeminus)
[rplusprimex, rplusprimey, rplusprimez] = spher2cart(rprimeplus,
   thetaprimeplus, phiprimeplus);
[x,y,z] = spher2cart(r, theta, phi)

G = [x,y,z]-[rminusprimex, rminusprimey, rminusprimez];
[rminusr, rminustheta, rminusphi] = cart2spher(G(1), G(2), G(3));
rminusmag = sqrt(rminusprimemag^2 + fieldposmag^2 - 2*fieldposmag
   *rminusprimemag^2*cos(reqangle));

% Thus we can find the unit vector n

N = (1/rminusmag).*G;
if choice == 1
% Alternate dipole moment method
rprimemag = 0.5*(rplusprimemag + rminusprimemag);
thetaprime = 0.5*(thetaprimeplus + thetaprimeminus);
```

```
phiprime = 0.5*(phiprimeplus + phiprimeminus);
f = rprimemag*cos(thetaprime);
[AA, BB, CC] = spher2cart(rprimemag, thetaprime, phiprime)
[DD, EE, FF] =  spher2cart(f, 0, 0)
II = [AA, BB, CC]-[DD, EE, FF];
requnit = sqrt(II(1)^2 + II(2)^2 + II(3)^2);
% Thus
P = (deltaqdoubleprime/requnit).*[II(1), II(2), II(3)];



else
% Find the dipole moment
P = deltaqdoubleprime.*([rplusprimex, rplusprimey, rplusprimez] -
    [rminusprimex, rminusprimey, rminusprimez]);
end
% Find the dot product of unit vector n with the dipole moment
ndotp = P(1)*N(1) + P(2)*N(2) + P(3)*N(3);

% Find the denominator

DEN = [x, y, z] - 0.5.*([rminusprimex, rminusprimey, rminusprimez
   ] + [rplusprimex, rplusprimey, rplusprimez])
%magnitude of denominator
magden = sqrt(DEN(1)^2 + DEN(2)^2 + DEN(3)^2);
denfinal = magden^3;

% find the field
Efield = (3*ndotp.*N - P)./denfinal;
```

```
Efieldx = Efield(1);
Efieldy = Efield(2);
Efieldz = Efield(3);
```

B.2 Ringefield.m

```
function [Efieldx, Efieldy, Efieldz] = ringefield(rprime,
   thetaprime, r, theta, phi, choice)
deltaqdoubleprime = 12e-6; % known charge transferred through
   channel in cgs units
rnor = 0.5e-6*1e2; % radius of node of ranvier in cgs units
d = 1e-9*1e2; %thickness of cell membrane at node in cgs units
g = rnor/1000000; % arbitrary dumbell radius in cgs units
s = d+(3*g/4); % separation of dipolar charges in cgs units



rprimemag = abs(rprime);
f = rprimemag*cos(thetaprime);



rprimeplusmag = sqrt(f^2 + (rnor + s/2)^2);
thetaprimeplus = atan((rnor + s/2)/f);
thetaprimeminus = atan((rnor-s/2)/f);

rprimeminusmag = sqrt(f^2 + (rnor -s/2)^2);
```

```
Summedx = 0;
Summedy = 0;
Summedz = 0;


for phiprimeplus = 2*pi/16:(2*pi/16):32*pi/16


[myEfieldx, myEfieldy, myEfieldz] = channelefield(rprimeplusmag,
   thetaprimeplus, phiprimeplus, rprimeminusmag, thetaprimeminus,
    phiprimeplus-pi/8, r, theta, phi, choice);

Summedx = Summedx + myEfieldx;
Summedy = Summedy + myEfieldy;
Summedz = Summedz + myEfieldz;
end

Efieldx = Summedx;
Efieldy = Summedy;
Efieldz = Summedz;
```

B.3 Axonefield.m

```
function [Efieldx, Efieldy, Efieldz] = axonefield(numnodes, r,
   theta, phi, choice, offsetrmag, offsettheta)

internodallength = 50e-6*100;%50e-6*100;
```

```
rnor = 0.5e-6*1e2; % radius of node of ranvier in cgs units
d = 1e-9*1e2; %thickness of cell membrane at node in cgs units
g = rnor/1000000; % arbitrary dumbell radius in cgs units
s = d+(3*g/4); % separation of dipolar charges in cgs units

Summedx = 0;
Summedy = 0;
Summedz = 0;

for f = internodallength:internodallength:numnodes*
   internodallength
    thetaprime = atan(rnor/f)+offsettheta;
    rprime = sqrt(f^2 + rnor^2)+offsetrmag;



    [Efieldx, Efieldy, Efieldz] = ringefield(rprime, thetaprime,
       r, theta, phi, choice);

    %if f == 5*internodallength % there is only one node in an
       axon of ''length'' 10 nodes
    Summedx = Summedx + Efieldx;
    Summedy = Summedy  + Efieldy;
    Summedz = Summedz + Efieldz;
    %end
end

Efieldx = Summedx;
```

```
Efieldy = Summedy;
Efieldz = Summedz;
```

APPENDIX C IMPLEMENTING RUDIMENTARY FIELD-MEDIATED SYNCHRONIZATION OF AXONS

To see if an ion-channel ring's e-field, and hence axonal e-field, leads to synchronization, we sketch our approach in this appendix.

Since the current density corresponding to a field is known to follow $\vec{J} = \sigma\vec{E}$ and the law of superposition [44], we can compute this current density and then superpose it on the ionic current density and injected current density already present at a given node to get the net current density at that node. This amounts to the addition of a single term to the nodal Generalized Ephaptic Equation (2.11) .

More specifically, for the following suppose we have only two axons. For each node on axon 1, we must write an algorithm that computes, at each time instant the e-field magnitude at every node on the neighboring axon, axon 2. The correct geometry, mainly distances to every other node on the adjoining axon, must be incorporated. This gives the current density at those nodes due to this node at the current time. Treating this current density as a stimulation current input to those nodes and injecting it at the present time, we compute this current density for each time, from each node to every other neighboring-axon node - this is likely to be a $n \times n$ matrix where n is the number of nodes on each axon and each entry of the matrix will be an array of two numbers, one representing the stimulating current generated by this node at the other node and the other representing the stimulation received from the other node by this node. For the case of geometrical symmetry, these numbers may be the same. We call this matrix $L(t)$.

Finally we run the program we have for ephaptic synchronization of $N = 2$ axons, presented in chapter 2, suitably modified to incorporate the L-matrix values for each time step via the Generalized Ephaptic Equation. In this methodology however, the injection of a current at the distant node may be too simplistic a description of actual events. So as a second attempt, we pro-

pose to include the following detail to the injection mechanism. On the emission side we proposed to model the axon tract under tight packing as a single myelinated axon, surrounded by a ring of axons which, due to the tight packing, form an annular layer of myelin followed by an annular layer of axoplasm. Between the central axon and the myelin layer is a layer of extracellular space. This is illustrated in Fig. 6.3.

On the reception side, we propose to convert the Hodgkin Huxley one dimensional axon model into a three dimensional one by simply revolving the extracellular arm of a two-arm circuit (the usual circuit which generates the cable equation) around the intracellular arm. Depending on the direction from which the neighboring node's field is incident, as illustrated in Fig. 6.4, it will impinge on one extracellular arm before its opposite arm on the opposite side of the axon. Therefore a potential difference will be setup. This additional potential difference will then drive ions as per their signs, into or out of the axoplasm. This is akin to a time varying voltage source added in parallel with the nodal capacitance and conductance. The resulting dynamics of the cable equation will be modified from the usual dynamics.

In particular, since the time variation will capture the presence of action potentials on the source axon, this is a new form of coupling between action potentials on two axons within a tract and can be studied by means of simulations. This field-based coupling was outlined in Chapter 6.

APPENDIX D COPYRIGHT PERMISSIONS

D.1 Permission for Figure 2.6

This section presents the permission for Fig. 2.6.

5/13/2017 University of South Florida Mail - Permission to use figure in dissertation

USF

Aman Chawla <amanchawla@mail.usf.edu>

Permission to use figure in dissertation

RUP Permissions <permissions@mail.rockefeller.edu> Thu, Apr 21, 2016 at 9:36 PM
To: Aman Chawla <amanchawla@mail.usf.edu>

Dear Aman,

Thank you for writing. You may reuse the figure in the manner described in your request. Please note, the original article must be accompanied with full citation:

©1986 Patlak and Ortiz. The Journal of General Physiology. 87:305-326. doi:10.1085/jgp.87.2.305

With best wishes as you complete your dissertation,
Suzanne O'Donnell
RUP Permissions Department

On 4/19/2016 9:45 PM, Aman Chawla wrote:

> Dear Ms. Suzanne O'Donnell,
>
> I'm a doctoral candidate at the University of South Florida. I wish to include a figure from the following source in my doctoral dissertation:
>
> Patlak, J. B., & Ortiz, Maurico (1986). Two modes of gating during late Na+ channel currents in frog sartorius muscle. *The Journal of general physiology, 87*(2), 305-326.
>
> The relevant figure is Figure 3 on page 311.
>
> Please let me know the copyright policy for reusing this material in a chapter in my dissertation. All USF dissertations are published via ProQuest Dissertation Publishing and also made available online at USF Scholar Commons.
>
> Sincerely,
>
> Aman Chawla

D.2 Permission for Figure 2.15

This section presents the permission for Fig. 2.15.

Development

Order detail ID:	70585340
Order License Id:	4136590504123
ISSN:	1477-9129
Publication Type:	e-Journal
Volume:	
Issue:	
Start page:	
Publisher:	COMPANY OF BIOLOGISTS,
Author/Editor:	Company of Biologists

Permission Status: Granted

Permission type: Republish or display content
Type of use: Republish in a thesis/dissertation

Requestor type	Academic institution
Format	Print, Electronic
Portion	image/photo
Number of images/photos requested	1
Title or numeric reference of the portion(s)	Figure 7A, page 407
Title of the article or chapter the portion is from	Hypogonadotropic hypogonadism and peripheral neuropathy in Ebf2-null mice
Editor of portion(s)	N/A
Author of portion(s)	Anna Corradi, Laura Croci, Vania Broccoli, Silvia Zecchini, Stefano Previtali, Wolfgang Wurst, Stefano Amadio, Roberto Maggi, Angelo Quattrini, G. Giacomo Consalez
Volume of serial or monograph	130
Issue, if republishing an article from a serial	2
Page range of portion	401 - 410
Publication date of portion	January 15, 2003
Rights for	Main product
Duration of use	Life of current and all future editions
Creation of copies for the disabled	no
With minor editing privileges	no

For distribution to	Worldwide
In the following language(s)	Original language of publication
With incidental promotional use	no
Lifetime unit quantity of new product	Up to 499
Made available in the following markets	Education
The requesting person/organization	Aman Chawla/University of South Florida
Order reference number	
Author/Editor	Aman Chawla
The standard identifier of New Work	N/A
The proposed price	N/A

Title of New Work	On Axon-Axon Interaction via Currents and Fields
Publisher of New Work	University of South Florida
Expected publication date	Aug 2017
Estimated size (pages)	140

D.3 Permission for Figure 4.4

This section presents the permission for Fig. 4.4.

NATURE PUBLISHING GROUP LICENSE TERMS AND CONDITIONS

May 13, 2017

This Agreement between Aman Chawla ("You") and Nature Publishing Group ("Nature Publishing Group") consists of your license details and the terms and conditions provided by Nature Publishing Group and Copyright Clearance Center.

License Number	4102661132730
License date	
Licensed Content Publisher	Nature Publishing Group
Licensed Content Publication	Nature Reviews Molecular Cell Biology
Licensed Content Title	Ion channels versus ion pumps: the principal difference, in principle
Licensed Content Author	David C. Gadsby
Licensed Content Date	May 1, 2009
Licensed Content Volume	10
Licensed Content Issue	5
Type of Use	reuse in a dissertation / thesis
Requestor type	academic/educational
Format	print and electronic
Portion	figures/tables/illustrations
Number of figures/tables/illustrations	1
High-res required	no
Figures	Figure 1 Ion channels versus ion pumps | In principle
Author of this NPG article	no
Your reference number	
Title of your thesis / dissertation	On axon-axon interaction via currents and fields
Expected completion date	Jul 2017
Estimated size (number of pages)	120

Total 0.00 USD

Terms and Conditions

Terms and Conditions for Permissions

Nature Publishing Group hereby grants you a non-exclusive license to reproduce this material for this purpose, and for no other use,subject to the conditions below:

1. NPG warrants that it has, to the best of its knowledge, the rights to license reuse of this material. However, you should ensure that the material you are requesting is original to Nature Publishing Group and does not carry the copyright of another entity (as credited in the published version). If the credit line on any part of the material you have requested indicates that it was reprinted or adapted by NPG with permission from another source, then you should also seek permission from that source to reuse the material.

2. Permission granted free of charge for material in print is also usually granted for any electronic version of that work, provided that the material is incidental to the work as a whole and that the electronic version is essentially equivalent to, or substitutes for, the print version.Where print permission has been granted for a fee, separate permission must be obtained for any additional, electronic re-use (unless, as in the case of a full paper, this has already been accounted for during your initial request in the calculation of a print run).NB: In all cases, web-based use of full-text articles must be authorized separately through the 'Use on a Web Site' option when requesting permission.

3. Permission granted for a first edition does not apply to second and subsequent editions and for editions in other languages (except for signatories to the STM Permissions Guidelines, or where the first edition permission was granted for free).

4. Nature Publishing Group's permission must be acknowledged next to the figure, table or abstract in print. In electronic form, this acknowledgement must be visible at the same time as the figure/table/abstract, and must be hyperlinked to the journal's homepage.

5. The credit line should read:
   Reprinted by permission from Macmillan Publishers Ltd: [JOURNAL NAME] (reference citation), copyright (year of publication)
   For AOP papers, the credit line should read:
   Reprinted by permission from Macmillan Publishers Ltd: [JOURNAL NAME], advance online publication, day month year (doi: 10.1038/sj.[JOURNAL ACRONYM].XXXXX)

   Note: For republication from the *British Journal of Cancer*, the following credit lines apply.
   Reprinted by permission from Macmillan Publishers Ltd on behalf of Cancer Research UK: [JOURNAL NAME] (reference citation), copyright (year of publication)For AOP papers, the credit line should read:
   Reprinted by permission from Macmillan Publishers Ltd on behalf of Cancer Research UK: [JOURNAL NAME], advance online publication, day month year (doi: 10.1038/sj.[JOURNAL ACRONYM].XXXXX)

6. Adaptations of single figures do not require NPG approval. However, the adaptation should be credited as follows:

   Adapted by permission from Macmillan Publishers Ltd: [JOURNAL NAME] (reference citation), copyright (year of publication)

   Note: For adaptation from the *British Journal of Cancer*, the following credit line applies.
   Adapted by permission from Macmillan Publishers Ltd on behalf of Cancer Research UK: [JOURNAL NAME] (reference citation), copyright (year of publication)

7. Translations of 401 words up to a whole article require NPG approval. Please visit http://www.macmillanmedicalcommunications.com for more information.Translations of up to a 400 words do not require NPG approval. The translation should be credited as follows:

Translated by permission from Macmillan Publishers Ltd: [JOURNAL NAME] (reference citation), copyright (year of publication).

Note: For translation from the *British Journal of Cancer*, the following credit line applies.
Translated by permission from Macmillan Publishers Ltd on behalf of Cancer Research UK: [JOURNAL NAME] (reference citation), copyright (year of publication)

We are certain that all parties will benefit from this agreement and wish you the best in the use of this material. Thank you.
Special Terms:
v1.1

Questions? customercare@copyright.com or +1-855-239-3415 (toll free in the US) or +1-978-646-2777.